



PONTIFICIA UNIVERSIDAD CATOLICA DE CHILE
SCHOOL OF ENGINEERING

**OPTIMAL PRECONDITIONERS FOR
SOLVING TWO-DIMENSIONAL
FRACTURES AND SCREENS USING
BOUNDARY ELEMENTS.**

CAROLINA ALEJANDRA URZÚA TORRES

Thesis submitted to the Office of Research and Graduate Studies
in partial fulfillment of the requirements for the degree of
Master of Science in Engineering

Advisor:

CARLOS JEREZ HANCKES

Santiago de Chile, January 2014

© MMXIV, CAROLINA A. URZÚA TORRES



PONTIFICIA UNIVERSIDAD CATOLICA DE CHILE
SCHOOL OF ENGINEERING

**OPTIMAL PRECONDITIONERS FOR
SOLVING TWO-DIMENSIONAL
FRACTURES AND SCREENS USING
BOUNDARY ELEMENTS.**

CAROLINA ALEJANDRA URZÚA TORRES

Members of the Committee:

CARLOS JEREZ HANCKES

ESTEBAN SÁEZ ROBERT

NORBERT HEUER

MARIO DURÁN TORO

Thesis submitted to the Office of Research and Graduate Studies
in partial fulfillment of the requirements for the degree of
Master of Science in Engineering

Santiago de Chile, January 2014

© MMXIV, CAROLINA A. URZÚA TORRES

*A la memoria de mi Tata Julio,
quien me contagió su pasión por las
matemáticas, la música, la
tecnología y los postres.*

ACKNOWLEDGEMENTS

I would like to express my deepest gratitude to all those who provided me the possibility to complete this thesis. A special appreciation I give to my supervisor, Professor Carlos Jerez Hanckes, who was the first one to encourage me to research and accepted the challenge of having me as his master student. I will never forget his insightful comments about research and life. I wish him to continue growing as a Professor, as I am certain he will accomplish even more.

I will also like to mention my committee: Professor Durán, Professor Heuer, and Professor Saez. Without their help and comments this dissertation would not have been possible. I know the whole process was particularly non-typical since I was away at the beginning. This makes me particularly grateful for all the support and understanding they all gave me.

I have no words to express my gratitude to Professor Hiptmair. He first honored me by inviting me as a visiting student at ETH. During my visit, he dedicatedly guided me through writing our joint paper and improving this thesis. I owe him so much already and I look forward to learn even more from him.

Last but not least, I would like to thank my family and friends, who have supported me throughout the entire process. Thanks to Fifi, Tanky, Cesar, Vignin, Priss, Pollin, Pedro and Paula. I could have never asked for better friends than you.

Thanks to my Dad for teaching me how to be strong and never give up. Thanks to my Mom for allowing me to be creative and teaching me to be myself and believe in my dreams. Thanks to my grandparents for all their love, care, and understanding.

I cannot end my acknowledgements without mentioning Ignacio. I don't know whatever comes our way, but I know I would not have made it to this point without you. You taught me to be patient and reminded me of my love for small things and details: Two key ingredients to become a good researcher.

TABLE OF CONTENTS

ACKNOWLEDGEMENTS	iv
LIST OF FIGURES	viii
LIST OF TABLES	x
ABSTRACT	xii
RESUMEN	xiii
1. Introduction	1
Operator preconditioning	4
Outline	5
2. Theory and Notation	7
2.1. Boundary Integral Operators (BIO)	7
2.1.1. Sobolev spaces	7
2.1.2. Boundary integral operators on a segment	8
2.1.3. (Augmented) boundary integral equations	9
2.1.4. Generalizations	11
2.2. Boundary Element Spaces	15
2.2.1. Primal and dual meshes	15
2.2.2. Dual pairs of spaces	15
2.3. Stability of Discrete Duality Pairings	19
2.3.1. Assumptions on mesh geometry	19
2.3.2. Stability Results	21
2.3.3. Local mesh conditions	25
3. Implementation	28
3.1. Quadrature	28
3.2. Trial and Test Spaces	29

3.3.	Boundary Integral Operator's implementation	29
3.3.1.	Weakly singular operator	29
3.3.2.	Hypersingular operator	31
3.3.3.	Modified weakly singular operator	31
3.3.4.	Modified hypersingular operator	32
3.4.	Calderón-type Identities and Strong Formulations	33
3.5.	Tensors for the Augmented Operators	34
3.6.	Dual Parity Operators	35
3.6.1.	$X := \tilde{H}^{-1/2}(\Gamma), Y := H^{1/2}(\Gamma)$ (Case A)	35
3.6.2.	$X := \tilde{H}^{1/2}(\Gamma), Y := H^{-1/2}(\Gamma)$ (Case B)	36
3.6.3.	$X := H^{-1/2}(\Gamma), Y := \tilde{H}^{1/2}(\Gamma)$ (Case C)	36
3.6.4.	$X := H^{1/2}(\Gamma), Y := \tilde{H}^{-1/2}(\Gamma)$ (Case D)	37
3.7.	Helmholtz Equation Integral Operators Implementation	37
3.8.	Norms	39
4.	Numerical Experiments	40
4.1.	Calderón-type Identities	40
4.1.1.	Weakly singular operator	41
4.1.2.	Hypersingular operator	42
4.1.3.	Modified weakly singular operator	44
4.1.4.	Modified hypersingular operator	45
4.2.	Preconditioning	46
4.2.1.	Weakly singular operator (Case A, row 1 of Table 2.2)	47
4.2.2.	Hypersingular operator (Case B, row 2 of Table 2.2)	49
4.2.3.	Modified weakly singular operator (Case C, row 3 of Table 2.2)	51
4.2.4.	Modified hypersingular operator (Case D, row 4 of Table 2.2)	51
4.2.5.	Boundary integral operators for Helmholtz equation	52
5.	Conclusions and Future Research	55
APPENDIX A.	Chebyshev Polynomials and Properties.	56

APPENDIX B. Proof of Theorem 2.3	60
APPENDIX C. Stability results for case B.	65
C.1. Proof of Lemma 2.1	65
C.2. Proof of Proposition 2.2	67
References	73

LIST OF FIGURES

2.1	Plot of kernel δk associated with $a_{\bar{v}} - a_{\bar{v},c}$ for $s(t) = \begin{pmatrix} \sin(t) \\ \cos(t) \end{pmatrix}$ (arc curve, left) and $s(t) = \frac{t+0.01}{\sqrt{2}} \begin{pmatrix} \cos(\log(\frac{t+0.01}{\sqrt{2}})) \\ \sin(\log(\frac{t+0.01}{\sqrt{2}})) \end{pmatrix}$ (spiral, right). The kernels are piecewise smooth and continuous.	13
2.2	Case A: $X := \tilde{H}^{-1/2}$, $Y := H^{1/2}$, piecewise constant basis functions q_j for $X_h := \mathcal{S}^{-1,0}(\Gamma_h)$ in blue, piecewise linear basis functions (“tent functions”) b_j for $Y_h := \bar{\mathcal{S}}^{0,1}(\hat{\Gamma}_h)$ in red/green. Note the extended “ramp functions” (in green) supported in the two leftmost and rightmost intervals of the dual mesh.	16
2.3	Case B: $X := \tilde{H}^{1/2}$, $Y := H^{-1/2}$, piecewise linear basis functions (“tent functions”) b_j for $X_h := \mathcal{S}_0^{0,1}(\Gamma_h)$ in blue, piecewise constant basis functions q_j for $Y_h := \bar{\mathcal{S}}^{-1,0}(\hat{\Gamma}_h)$ in red/green. Note the extended “characteristic functions” (in green) for the two leftmost and rightmost intervals of the dual mesh.	17
2.4	Case C: $X := H^{-1/2}$, $Y := \tilde{H}^{1/2}$, piecewise constant basis functions q_j for $X_h := \mathcal{S}^{-1,0}(\Gamma_h)$ in blue, piecewise linear basis functions (“tent functions”) b_j for $Y_h := \mathcal{S}_0^{0,1}(\hat{\Gamma}_h)$ in red/green. Note that no basis functions are assigned to η_0 and η_N	17
2.5	Case D: $X := H^{1/2}$, $Y := \tilde{H}^{-1/2}$, piecewise linear basis functions (“tent functions”) b_j for $X_h := \mathcal{S}^{0,1}(\Gamma_h)$ in blue, basis functions q_j for $Y_h := \mathcal{S}^{-1,0}(\hat{\Gamma}_h)$, the characteristic functions of the dual mesh intervals, in red/green.	18
4.1	Plot of errors obtained by both methods for V_h . We use black to show the results when using a uniform mesh, blue for the Chebyshev mesh, and red for the algebraically graded mesh.	42
4.2	Plot of errors obtained by both methods for W_h . We use black to show the results when using a uniform mesh, blue for the Chebyshev mesh, and red for the algebraically graded mesh.	43

4.3	Plot of errors obtained by both methods for \bar{V}_h . We use black to show the results when using a uniform mesh, blue for the Chebyshev mesh, and red for the algebraically graded mesh.	44
4.4	Plot of errors obtained by both methods for \bar{W}_h . We use black to show the results when using a uniform mesh, blue for the Chebyshev mesh, and red for the algebraically graded mesh.	46
4.5	Plot of spectrum for V_h preconditioned by M_h (Case A, row 1 of Table 2.2) for our three meshes. We use black triangles to show the eigenvalues when using a uniform mesh, blue circles for the Chebychev mesh, and red squares for the algebraically graded mesh.	48
4.6	Plot of spectrum for W_h preconditioned by M_h (Case B, row 2 of Table 2.2) for our three meshes. We use black triangles to show the eigenvalues when using a uniform mesh, blue circles for the Chebychev mesh, and red squares for the algebraically graded mesh.	50
4.7	Plot of spectrum for \bar{V}_h preconditioned by M_h (Case C, row 3 of Table 2.2) for our three meshes. We use black triangles to show the eigenvalues when using a uniform mesh, blue circles for the Chebychev mesh, and red squares for the algebraicly graded mesh.	51
4.8	Plot of spectrum for \bar{W}_h preconditioned by M_h (Case D, row 4 of Table 2.2) for our three meshes. We use black triangles to show the eigenvalues when using a uniform mesh, blue circles for the Chebychev mesh, and red squares for the algebraicly graded mesh.	52
4.9	Helmholtz GMRES results when using an uniform mesh and wave number $k = 1$.	53
4.10	Helmholtz GMRES results when using an uniform mesh and wave number $k = 4$.	54
4.11	Helmholtz GMRES results when using an uniform mesh and wave number $k = 8$.	54

LIST OF TABLES

2.1	(Partial) summary of operator preconditioning strategy for variational boundary integral equations on an open curve \mathcal{C} . For notations see Theorem 1.1.	14
2.2	Summary of operator preconditioning strategy for variational boundary integral equations on the interval Γ . For notations see Theorem 1.1.	19
4.1	Errors obtained for V_h . The first part shows the error obtained by indirect solving ($\varphi_v = V_h \setminus \underline{g}_h$), while the second part exhibits our results when applying the inverse deduced from Proposition 2.2 to right hand side ($\varphi_d = \bar{W}_h^S \pi x$).	41
4.2	Errors slopes τ obtained for V_h when using algebraic mesh and different numbers of quadrature nodes Nq	42
4.3	Errors obtained for W_h . The first part shows the error obtained by indirect solving ($\varphi_v = W_h \setminus \underline{g}_h$), while the second part exhibits our results when applying the inverse deduced from Proposition 2.2 to right hand side ($\varphi_d = \bar{V}_h^S \pi$).	43
4.4	Errors obtained for \bar{V}_h . The first part shows the error obtained by indirect solving ($\varphi_v = \bar{V}_h \setminus \underline{g}_h$), while the second part exhibits our results when applying the inverse deduced from Proposition 2.2 to right hand side ($\varphi_d = W_h^S \pi x \sqrt{1 - x^2}$).	45
4.5	Errors obtained for \bar{W}_h . The first part shows the error obtained by indirect solving ($\varphi_v = \bar{W}_h \setminus \underline{g}_h$), while the second part exhibits our results when applying the inverse deduced from Proposition 2.2 to right hand side ($\varphi_d = V_h^S x / \sqrt{1 - x^2}$).	46
4.6	Performance of preconditioners for V_h (Case A, row 1 of Table 2.2).	49
4.7	Results for operator preconditioning of V_h (Case A) with different (regularized) discrete versions of the unmodified hypersingular operator W	49
4.8	Performance of preconditioners for for W_h (Case B, row 2 of Table 2.2).	50
4.9	Spectral condition numbers obtained for \bar{V}_h (Case C, row 3 of Table 2.2).	51
4.10	Spectral condition numbers obtained for \bar{W}_h (Case D, row 4 of Table 2.2).	52

4.11 GMRES iteration counts for Helmholtz operators using $k = 1, 4, 8$ as wave numbers. 53

ABSTRACT

An extensive range of problems in science and engineering involve two-dimensional crack, screen (Shestopalov, Smirnov, & Chernokozhin, 2000; Meixner, 1972; E. Stephan, 1987), or interface problems (Costabel & Dauge, 2002; Nicaise & Sändig, 1994a, 1994b; E. P. Stephan & Wendland, 1984). The simplest approach to model them is to consider the following problem for an open curve $\mathcal{C} \subset \mathbb{R}^2$,

$$-\Delta U = 0 \quad \text{in } \mathbb{R}^d \setminus \mathcal{C} \quad , \quad U = g \quad \text{or} \quad \frac{\partial U}{\partial \mathbf{n}} = h \quad \text{on } \mathcal{C} \quad , \quad (0.1)$$

plus decay conditions at ∞ , and with suitable boundary data g and h .

Boundary integral methods (BEM) are an attractive option to deal with the unboundedness of the domain and the decay conditions at ∞ . Unfortunately, the singular behaviour of the solutions causes the linear systems arising from the related integral operators to be numerically ill-conditioned. Therefore, iterative solvers require unreasonable computational work. This can be tackled by using suitable preconditioners (Hiptmair, 2006).

This thesis presents the numerical implementation of the Calderón-type identities deduced from Jerez-Hanckes and Nédélec (Jerez-Hanckes & Nédélec, 2011; Jerez-Hanckes & Nédélec, 2012) for an open interval. In addition, they are used to build optimal preconditioners for the associated integral operators arising from (0.1) and their extension to the Helmholtz equation. Finally, since the singularities of the solutions to the associated weakly singular operator behave as $1/\sqrt{d}$ where d is the distance to the endpoints, we can achieve more accuracy through local refinement around the two endpoints. Therefore, this work also extends preconditioning theory to non-uniform meshes.

Keywords: Calderón preconditioning, screen problems, fracture problems, boundary integral operators.

RESUMEN

Muchos problemas en ingeniería pueden ser formulados como problemas de fractura , pantalla (Shestopalov et al., 2000; Meixner, 1972; E. Stephan, 1987), o interfaz (Costabel & Dauge, 2002; Nicaise & Sändig, 1994a, 1994b; E. P. Stephan & Wendland, 1984) en dos dimensiones. La forma más simple de modelarlos es considerar el siguiente problema para una curva abierta $\mathcal{C} \subset \mathbb{R}^2$,

$$-\Delta U = 0 \quad \text{en } \mathbb{R}^2 \setminus \mathcal{C} \quad , \quad U = g \quad \text{o} \quad \frac{\partial U}{\partial \mathbf{n}} = h \quad \text{en } \mathcal{C} \quad , \quad (0.2)$$

más condiciones de decaimiento en ∞ y condiciones de borde g y h apropiadas.

El método de elementos de frontera (BEM) es una opción atractiva para lidiar con el carácter infinito del dominio y la condición de decaimiento. Desafortunadamente, el comportamiento singular de las soluciones hace que los operadores integrales asociados estén mal condicionados. Por lo tanto, la resolución mediante métodos iterativos requiere un alto costo computacional. Una forma de abordar esta dificultad y mejorar el condicionamiento de dichos operadores es utilizando preconditionadores (Hiptmair, 2006).

En esta tesis se presenta la implementación de las las identidades de tipo Calderón formuladas por Jerez-Hanckes y Nédélec (Jerez-Hanckes & Nédélec, 2011; Jerez-Hanckes & Nédélec, 2012) para intervalos abiertos. Adicionalmente, éstas se utilizan para construir preconditionadores óptimos para los operadores integrales asociados a (1.1) y su extensión a la ecuación de Helmholtz. Finalmente, dado que la singularidad de las soluciones se comporta como $\frac{1}{\sqrt{d}}$, donde d es la distancia a los bordes de la fractura, se puede obtener mayor precisión utilizando mallados que se refinan cerca de los bordes. Por esta razón el presente trabajo también muestra la extensión de la teoría de preconditionamiento a mallados no uniformes.

Keywords: Precondicionamiento tipo Calderón, Problemas de pantalla, problemas de fractura, operadores integrales de frontera.

1. INTRODUCTION

We want to describe the behaviour of an incident wave hitting an open curve $\mathcal{C} \subset \mathbb{R}^2$. For this, we assume an homogeneous and isotropic medium.

We split the solution u of the problem into two parts, $u = u_{inc} + u_{sc}$, where u_{sc} is the scattered part of the solution and u_{inc} is the incoming wave, which is assumed to be a planar wave. These hypotheses allow us to reduce the model problem from the Maxwell's equations to the Helmholtz equation.

For the sake of simplicity, we set the wave number k to be zero and consider the following Dirichlet and Neumann boundary value problems (BVPs) in the exterior of an open curve $\mathcal{C} \subset \mathbb{R}^2$,

$$-\Delta U = 0 \quad \text{in } \mathbb{R}^2 \setminus \bar{\mathcal{C}} \quad , \quad U = g \quad \text{or} \quad \frac{\partial U}{\partial \mathbf{n}} = f \quad \text{on } \mathcal{C} \quad , \quad (1.1)$$

plus appropriate decay conditions at ∞ , see (McLean, 2000, Thm. 8.9) and with suitable boundary data g or f . If \mathcal{C} is a regular Lipschitz curve, then (1.1) possesses a unique weak solution in $H_{loc}^1(\mathbb{R}^2 \setminus \bar{\mathcal{C}})$. Exterior BVPs like (1.1) play a central role in a number of mathematical models like crack models in elasticity (Gross & Seelig, 2011) or dimensionally reduced antenna models in electromagnetics (Shestopalov et al., 2000).

For the approximate numerical solution of boundary value problems like (1.1), posed on an unbounded homogeneous exterior domain, *boundary element methods* are an attractive option, because they respect the decay conditions at infinity and require a mesh on \mathcal{C} only. They exploit the possibility that (1.1) can be converted into *first-kind boundary integral equations* (BIEs) for the unknown jump of the complementary boundary data on \mathcal{C} . These boundary integral equations, their variational formulation in suitable Sobolev spaces, and boundary element Galerkin discretization have been studied thoroughly, prominently by E. Stephan and coworkers. Please refer to (E. Stephan, 1987; Wendland & Stephan, 1990; Ervin & Stephan, 1990; Tran, 1995), and the textbook (Sauter & Schwab, 2010, Sect. 3.5.3).

Since we face first-kind BIEs, the spectral condition numbers of the linear systems of equations arising from low-order Galerkin boundary element methods (BEM) for (1.1) using the customary locally supported basis functions will grow like $O(h^{-1})$, where h is the size of the smallest cell of the mesh, see (Sauter & Schwab, 2010, Sect. 4.5). Thus, effective preconditioning becomes indispensable when conjugate gradient type iterative solvers are used to compute BEM solutions on (locally) fine meshes.

Admittedly, on curves satisfactory resolution can already be achieved with moderate numbers of degrees of freedom, which allows the assembly of the dense Galerkin matrices and the use of direct solvers. This is no longer the case for the three-dimensional counterpart of (1.1), where \mathcal{C} has to be replaced with an oriented two-dimensional Lipschitz manifold. Then we encounter a genuine *screen problem*, for which we may have to resort to fine triangulations of \mathcal{C} , which, in turns, entails the use of matrix compression and iterative solvers. Then preconditioning becomes a key issue. Thus, this thesis with its focus on curves and numerical analysis, should be viewed as a first “proof of concept” for a preconditioning strategy that, we believe, can be extended to three dimensions.

A powerful preconditioning technique for BEM on closed surfaces is the so-called policy of *Calderón preconditioning*, which exploits Calderón identities, that is, the fact that certain products of boundary integral operators evaluate to the identity map plus a compact perturbation (Sauter & Schwab, 2010, Sect. 3.6). It fits the more general strategy of *operator preconditioning* for Galerkin discretizations, introduced in (Hiptmair, 2006), see also (Mardal & Winther, 2011). For low-order Galerkin BEM on closed surfaces, it takes pairs of primal and dual meshes to realize this approach to preconditioning, as has been discovered by Steinbach and Wendland in (Steinbach & Wendland, 1998). A very general perspective was developed by Buffa and Christiansen in (Buffa & Christiansen, 2007) and it paved the way for the application of Calderón preconditioning to electromagnetic boundary integral equations. The new technique has quickly been adopted in computational engineering (Bagci, Andriulli, Cools, Olyslager, & Michielssen, 2009; Andriulli et al., 2008; Cools, Andriulli, & Olyslager, 2009), which highlights its huge potential for practical simulations.

For open curves, analogues of Calderón identities had been elusive until recently, which hampered the adaption of Calderón preconditioning. One can still pursue a weaker version, the idea of preconditioning with operators of opposite order. This was done by McLean and Steinbach (McLean & Steinbach, 1999), where the single layer operator provided a preconditioner for the discrete hypersingular BIE on an arc. Yet, this method is not asymptotically optimal in a strict sense, because the condition number of the preconditioned linear system still grows like $O(|\log h|)$. The reason is that on open curves the boundary integral operators have to be considered on Sobolev spaces that take into account special conditions at the endpoints. These spaces fail to provide the duality relationships that form the foundations of operator preconditioning.

Several approaches have been proposed in the literature to overcome this difficulty by extending the classical Calderón relations to the case of open surfaces. Recently, Bruno and Lintner in (Lintner & Bruno, 2012; Bruno & Lintner, 2012) have developed a generalized Calderón formula for open surfaces. When combined with their high-order numerical methods, they observe excellent performance of their Calderón preconditioner for a wide range of geometries and wave propagation problems. However, no mathematical analysis of this method is available, let alone results about asymptotic optimality of the preconditioner.

In this thesis we propose the first provably asymptotically optimal Calderón preconditioning approach for low-order Galerkin BEM for the BIE arising from (1.1). This has been made possible by a breakthrough result achieved by Nédélec and one of the authors in (Jerez-Hanckes & Nédélec, 2011; Jerez-Hanckes & Nédélec, 2012). They have found explicit inverses for weakly singular and hypersingular integral operators on a line segment. These new relations are a perfect substitute for the conventional Calderón identities in the context of operator preconditioning, and we are going to elaborate this rigorously.

Throughout we take pains to cover rather general *locally refined meshes* in our analysis. This is important, because we can expect pronounced singularities of the solutions of the BIE related to the weakly singular operator at the endpoints. More precisely, they behave as $1/\sqrt{d}$ where d is the distance to the endpoints (Costabel, Dauge, & Duduchava, 2003;

Meixner, 1972; Kelley, 1999). For piecewise polynomial approximation spaces this entails using algebraically or geometrically graded meshes, for which cells adjacent to the endpoints are much smaller than those in the middle of \mathcal{C} .

Operator preconditioning

Awareness of the gist of operator preconditioning as presented in (Hiptmair, 2006) is crucial for appreciating the considerations in the remainder of the thesis. Thus, we briefly recall the main result of (Hiptmair, 2006).

Theorem 1.1 (Theorem 2.1 (Hiptmair, 2006)). *Let X, Y be reflexive Banach spaces, $X_h := \text{span}\{\varphi_i\}_{i=0}^N \subset X$, $Y_h := \text{span}\{\phi_j\}_{j=0}^M \subset Y$ finite-dimensional subspaces with bases $\{\varphi_i\}_{i=0}^N$ and $\{\phi_j\}_{j=0}^M$. Further, let $\mathbf{a} \in L(X \times X, \mathbb{C})$ and $\mathbf{b} \in L(Y \times Y, \mathbb{C})$ be continuous sesquilinear forms (with norms $\|\mathbf{a}\|$ and $\|\mathbf{b}\|$, resp.), each satisfying discrete inf-sup conditions with constants $c_A, c_B > 0$ on X_h and Y_h , respectively. If there is a continuous sesquilinear form $\mathbf{t} \in L(X \times Y, \mathbb{C})$ that also satisfies a discrete inf-sup condition on $X_h \times Y_h$ with constant $c_T > 0$, then the associated Galerkin matrices:*

$$\mathbf{A}_h := (\mathbf{a}(\varphi_i, \varphi_j))_{i,j=1}^N, \quad \mathbf{B}_h := (\mathbf{b}(\phi_i, \phi_j))_{i,j=1}^M, \quad \mathbf{T}_h := (\mathbf{t}(\varphi_i, \phi_j))_{i,j=1}^{N,M},$$

satisfy

$$\kappa(\mathbf{T}_h^{-1} \mathbf{B}_h \mathbf{T}_h^{-H} \mathbf{A}_h) \leq \frac{\|\mathbf{a}\| \|\mathbf{b}\| \|\mathbf{t}\|^2}{c_A c_B c_T^2}, \quad (1.3)$$

where κ designates the spectral condition number.

As this theorem targets variational problems and Galerkin discretization, we will always focus on the weak form of boundary integral equations. Moreover, as explained in (Hiptmair, 2006, Sect. 4), Calderón preconditioning boils down to an application of Theorem 1.1 where the spaces X and Y are dual to each other, with duality induced by the pairing sesquilinear form \mathbf{t} . For the concrete trace spaces, on which the weak BIEs are posed, \mathbf{t} will be an extension of the inner product in $L^2(\mathcal{C})$.

In light of Theorem 1.1, when confronted with a variational BIE $\mathbf{a}(u, v) = \ell(v)$, $v \in X$, $\ell \in X'$, on a trace space X , the key questions are,

- (Q1): whether we can find another boundary integral operator that induces a bounded sesqui-linear form on $Y := X'$,
- (Q2): what sub-spaces $X_h \subset X$ and $Y_h \subset Y$ furnish stable Galerkin discretizations,
- (Q3): if the pairs X_h and Y_h allow an X/Y -stable L^2 -pairing (\cdot, \cdot) , for which a necessary condition is $\dim X_h = \dim Y_h$).

Given positive answers to these questions and assuming that all inf-sup constants can be chosen independently of the (local) mesh width, Theorem 1.1 will permit us to conclude that the product $\mathbf{T}_h^{-1} \mathbf{B}_h \mathbf{T}_h^{-H}$ of Galerkin matrices represents an asymptotically optimal preconditioner for \mathbf{A}_h .

REMARK 1.1. *We stress that the assertion of Theorem 1.1 is valid for any choice of bases for X_h and Y_h and the associated Galerkin matrices. Thus, the focus can exclusively be on the construction of appropriate spaces X_h and Y_h .*

Outline

Next, Chapter 2 is dedicated to present the theoretical background and main results of this thesis. In Section 2.1 we give a precise description of the relevant Sobolev spaces, and afterwards, we introduce the boundary integral operators, along with *elliptic* boundary integral equations in variational form. This will be done on a straight line segment, but Section 2.1.4 will argue, why the case of a smooth open curved is fully covered. Theorems 2.1 and 2.4 will answer Questions (Q1) and (Q2). Piecewise polynomial boundary element spaces on primal and dual meshes are defined in Section 2.2. In Section 2.3 uniform inf-sup conditions for discrete L^2 -duality pairings are established, thus verifying the last missing assumption of Theorem 1.1, see Theorem 2.5. The proofs take the cue from the general technique developed by O. Steinbach in (Steinbach, 2003).

We dedicate Chapter 3 to explain the implementation of our method. With this purpose in mind, we first introduce the main tools to be used in our code. In Section 3.3 we give a description of the computational realization of our BIOs in their variational form, while we present their strong formulation in 3.4. The remaining of the Chapter gives details of other

operators related to our preconditioning technique and finishes introducing the implementation of the Helmholtz equation BIOs also on a straight line segment.

Finally, in Chapter 4, a number of numerical experiments confirm the power of Jerez-Nédélec's Calderón-type identities and asymptotic optimality of the new preconditioners arising from them. We conclude this thesis with the discussion of these results.

2. THEORY AND NOTATION

2.1. Boundary Integral Operators (BIO)

2.1.1. Sobolev spaces

We employ the usual notations for Sobolev spaces from (McLean, 2000, Ch. 3); let $\mathcal{O} \subseteq \mathbb{R}^d$, with $d = 1, 2$, be open. For $s \in \mathbb{R}$, $H^s(\mathcal{O})$ denotes standard Sobolev spaces (McLean, 2000; Steinbach, 2008). If $s > 0$ and $\mathcal{O} \subset \mathbb{R}^d$ is a Lipschitz domain, $\tilde{H}^s(\mathcal{O})$ stands for the space of distributions in $H^s(\mathcal{O})$ whose extension by zero to \mathbb{R}^d belongs to $H^s(\mathbb{R}^d)$. We introduce

$$\tilde{H}^{-1/2}(\mathcal{O}) \equiv (H^{1/2}(\mathcal{O}))' \quad \text{and} \quad H^{-1/2}(\mathcal{O}) \equiv (\tilde{H}^{1/2}(\mathcal{O}))'. \quad (2.1)$$

Here and below primes designate dual spaces and duality pairings will be indicated by angular brackets $\langle \cdot, \cdot \rangle$. Using $L^2(\mathcal{O})$ as pivot space, this yields the Gelfand triples

$$H^{1/2}(\mathcal{O}) \subset L^2(\mathcal{O}) \subset \tilde{H}^{-1/2}(\mathcal{O}) \quad , \quad \tilde{H}^{1/2}(\mathcal{O}) \subset L^2(\mathcal{O}) \subset H^{-1/2}(\mathcal{O}) \quad ,$$

with continuous and dense embeddings.

Below we are going to examine integral equations on a special curve, namely the straight line segment $(-1, 1) \times \{0\} \subset \mathbb{R}^2$. Thus, we abbreviate $\Gamma := (-1, 1)$. Based on the weight function

$$\omega(x) := \sqrt{1 - x^2}, \quad x \in \Gamma \quad ,$$

let us introduce the subspaces

$$\tilde{H}_{(0)}^{-1/2}(\Gamma) := \left\{ \varphi \in \tilde{H}^{-1/2}(\Gamma) : \langle 1, \varphi \rangle_{L^2(\Gamma)} = 0 \right\}, \quad (2.2)$$

$$H_*^{1/2}(\Gamma) := \left\{ g \in H^{1/2}(\Gamma) : \langle g, \omega^{-1} \rangle_{L^2(\Gamma)} = 0 \right\}. \quad (2.3)$$

We point out that in the above definitions $1 \in H^{1/2}(\Gamma)$ and $\omega^{-1} \in \tilde{H}_{(0)}^{-1/2}$.

2.1.2. Boundary integral operators on a segment

Following the notation in (Hsiao & Wendland, 2008), we introduce the standard weakly singular boundary integral operator (BIO) associated with the Laplacian $-\Delta$ as V , and recall that it is defined by

$$V\varphi(x) := \int_{\Gamma} \log \frac{1}{|x-y|} \varphi(y) dy, \quad x \in \Gamma, \quad \varphi \in C_0^\infty(\Gamma). \quad (2.4)$$

Additionally, taking the cue from (Jerez-Hanckes & Nédélec, 2012, Sec. 3), we define a modified version of the weakly singular BIO as

$$\bar{V}\varphi(x) := \int_{\Gamma} \log \frac{M(x,y)}{|x-y|} \varphi(y) dy, \quad x \in \Gamma, \quad \varphi \in C^\infty(\Gamma), \quad (2.5)$$

where

$$M(x,y) := \frac{1}{2} \left((y-x)^2 + (\omega(x) + \omega(y))^2 \right), \quad (x,y) \in \Gamma \times \Gamma.$$

Analogously, we define the Laplace standard hypersingular operator W and its modified version \bar{W} as

$$W := -\left(\frac{d}{dx}\right)^* \circ V \circ \frac{d}{dx}, \quad \bar{W} := -\frac{d}{dx} \circ \bar{V} \circ \left(\frac{d}{dx}\right)^*. \quad (2.6)$$

Here, $\frac{d}{dx}$ is a derivation operator defined distributionally, which gives rise to a mapping $\frac{d}{dx} : \tilde{H}^{1/2}(\Gamma) \rightarrow \tilde{H}_{(0)}^{-1/2}(\Gamma)$ with continuous adjoint $\left(\frac{d}{dx}\right)^* : H_*^{1/2}(\Gamma) \rightarrow H^{-1/2}(\Gamma)$. The following fundamental result establishes key continuity properties of the integral operators.

Theorem 2.1 ((Jerez-Hanckes & Nédélec, 2012, Prop. 3.1 and 3.3)). *The boundary integral operators introduced above can be extended to bounded operators*

$$\begin{aligned} V : \tilde{H}_{(0)}^{-1/2}(\Gamma) &\rightarrow H_*^{1/2}(\Gamma), & W : \tilde{H}^{1/2}(\Gamma) &\rightarrow H^{-1/2}(\Gamma), \\ \bar{V} : H^{-1/2}(\Gamma) &\rightarrow \tilde{H}^{1/2}(\Gamma), & \bar{W} : H_*^{1/2}(\Gamma) &\rightarrow \tilde{H}_{(0)}^{-1/2}(\Gamma). \end{aligned} \quad \text{and}$$

The significance of this theorem for operator preconditioning is evident: we see that \bar{W} and \bar{V} induce continuous bilinear forms on the image spaces of V and W , respectively. In a sense, Theorem 2.1 answers Question (Q1) for the operators V and W .

We would like to point out that the pairs $V \leftrightarrow \bar{W}$ and $W \leftrightarrow \bar{V}$ of operators are even connected by a particularly simple ‘‘Calderón identity’’, expressed in the next theorem.

Theorem 2.2 ((Jerez-Hanckes & Nédélec, 2012, Prop. 3.6)). *The following identities hold:*

$$\bar{V} \circ W = \text{Id}_{\tilde{H}^{1/2}(\Gamma)}, \quad V \circ \bar{W} = \text{Id}_{H_*^{1/2}(\Gamma)}, \quad (2.7a)$$

$$\bar{W} \circ V = \text{Id}_{\tilde{H}_{(0)}^{-1/2}(\Gamma)}, \quad W \circ \bar{V} = \text{Id}_{H^{-1/2}(\Gamma)}. \quad (2.7b)$$

However, we emphasize that it is Theorem 2.1 that paves the way for operator preconditioning. The result of Theorem 2.2 merely bolsters confidence that excellent condition numbers can be achieved.

REMARK 2.1. *We would like to alert the reader to the striking differences between the cases of closed (boundaries) and open curves. In the former the single layer and hypersingular operators map continuously back and forth between $H^{1/2}(\partial\Omega)$ and $H^{-1/2}(\partial\Omega)$. These spaces are in natural duality, so that operator preconditioning can rely on these operators alone. Conversely, on open curves the ‘‘ \sim -spaces’’ come into play and we need to modify the integral operators in order to ensure continuity on the L^2 -duals of these \sim -spaces.*

2.1.3. (Augmented) boundary integral equations

In line with the perspective of operator preconditioning, we introduce the weak form of the boundary integral equations. First, consider the variational problem for the weakly singular operator V : given $g \in H_*^{1/2}(\Gamma)$ find $\varphi \in \tilde{H}_{(0)}^{-1/2}(\Gamma)$ such that

$$a_V(\varphi, \psi) = \langle V \varphi, \psi \rangle_{\tilde{H}^{-1/2}(\Gamma)} = \langle g, \psi \rangle_{\tilde{H}^{-1/2}(\Gamma)}, \quad \forall \psi \in \tilde{H}_{(0)}^{-1/2}(\Gamma). \quad (2.8)$$

This variational problem is connected with the Dirichlet problem of (1.1), when \mathcal{C} is the line segment $\{0\} \times \Gamma$, see (E. P. Stephan & Wendland, 1984).

The variational problem for the hypersingular operator W (**Case B**) can be stated as: find $u \in \tilde{H}^{1/2}(\Gamma)$ such that for $f \in H^{-1/2}(\Gamma)$

$$a_W(u, w) = \langle W u, w \rangle_{\tilde{H}^{1/2}(\Gamma)} = \langle f, w \rangle_{\tilde{H}^{1/2}(\Gamma)}, \quad \forall w \in \tilde{H}^{1/2}(\Gamma). \quad (2.9)$$

As demonstrated in (Wendland & Stephan, 1990), this variational problem is satisfied by the jump of the Dirichlet trace of the solution of the Neumann problem (1.1) in the exterior of the line segment.

The next two variational problems are not directly related to the boundary value problems (1.1). Nevertheless, we are going to discuss operator preconditioning also for them. For the modified weakly singular operator \bar{V} the associated variational problem reads as follows (**Case C**): for $g \in \tilde{H}^{1/2}(\Gamma)$ find $\phi \in H^{-1/2}(\Gamma)$ such that

$$\mathbf{a}_{\bar{V}}(\phi, \psi) = \langle \bar{V}\phi, \psi \rangle_{H^{-1/2}(\Gamma)} = \langle g, \psi \rangle_{H^{-1/2}(\Gamma)} \quad \forall \psi \in H^{-1/2}(\Gamma). \quad (2.10)$$

Finally the variational problem for the modified hypersingular operator \bar{W} is: find $v \in H_*^{1/2}(\Gamma)$ such that for a given $f \in \tilde{H}_{(0)}^{-1/2}(\Gamma)$, it holds

$$\mathbf{a}_{\bar{W}}(v, w) := \langle \bar{W}v, w \rangle_{H^{1/2}(\Gamma)} = \langle f, w \rangle_{H^{1/2}(\Gamma)} \quad \forall w \in H_*^{1/2}(\Gamma). \quad (2.11)$$

Direct Galerkin discretization of $\mathbf{a}_{\bar{V}}(\varphi, \psi)$ and $\mathbf{a}_{\bar{W}}(w, v)$ would require trial and test spaces to comply with the constraints in (2.2) and (2.3). In order to avoid this, we suppress the orthogonality restrictions and define two *augmented* bilinear forms. First introduce for $\alpha \in \mathbb{R}$

$$\tilde{\mathbf{a}}_{\bar{V}}[\alpha](\varphi, \psi) := \langle \bar{V}\varphi, \psi \rangle + \alpha \langle 1, \varphi \rangle \langle 1, \psi \rangle, \quad \varphi, \psi \in \tilde{H}^{-1/2}(\Gamma), \quad (2.12)$$

with duality pairings $\langle \cdot, \cdot \rangle$ on $\tilde{H}^{-1/2}(\Gamma)$. Obviously, $\tilde{\mathbf{a}}_{\bar{V}}[\alpha] : \tilde{H}^{-1/2}(\Gamma) \times \tilde{H}^{-1/2}(\Gamma) \rightarrow \mathbb{C}$ is continuous for any $\alpha \in \mathbb{R}$. Similarly, define for $\beta \in \mathbb{R}$

$$\tilde{\mathbf{a}}_{\bar{W}}[\beta](v, w) := \langle \bar{W}v, w \rangle + \beta \langle v, \omega^{-1} \rangle \langle w, \omega^{-1} \rangle, \quad v, w \in H^{1/2}(\Gamma), \quad (2.13)$$

where $\tilde{\mathbf{a}}_{\bar{W}}[\beta] : H^{1/2}(\Gamma) \times H^{1/2}(\Gamma) \rightarrow \mathbb{C}$ is bounded for any $\beta \in \mathbb{R}$. Now we consider $\alpha > 0$ and $\beta > 0$ fixed and usually drop $[\alpha]$ and $[\beta]$ from the notation for the bilinear forms. To begin with we note that augmentation does not change the solutions of the variational problems. The proof is given in Appendix B.

Theorem 2.3. *The variational problem (2.8) is equivalent to the augmented variational problem (Case A): find $\varphi \in \tilde{H}^{-1/2}(\Gamma)$ such that*

$$\tilde{a}_V(\varphi, \psi) = \langle g, \psi \rangle, \quad \forall \psi \in \tilde{H}^{-1/2}(\Gamma), \quad (2.14)$$

and the variational problem (2.11) is equivalent to the augmented variational problem (Case D): find $v \in H^{1/2}(\Gamma)$ such that

$$\tilde{a}_W(v, w) = \langle f, w \rangle_{H^{1/2}(\Gamma)}, \quad \forall w \in H^{1/2}(\Gamma). \quad (2.15)$$

The next result essentially confirms the unique solvability of all (augmented) variational problems. Its proof relies on the $\tilde{H}_{(0)}^{-1/2}(\Gamma)$ -ellipticity of V and the $H_*^{1/2}(\Gamma)$ -ellipticity of \bar{W} , both established in (Jerez-Hanckes & Nédélec, 2012, Prop. 3.1).

Theorem 2.4. *For any $\alpha, \beta \in \mathbb{R}_+$ the (augmented) bilinear forms \tilde{a}_V , a_W , $a_{\bar{V}}$, and $\tilde{a}_{\bar{V}}$ are bounded and elliptic on $\tilde{H}^{-1/2}(\Gamma)$, $\tilde{H}^{1/2}(\Gamma)$, $H^{-1/2}(\Gamma)$, and $H^{1/2}(\Gamma)$, respectively.*

Thanks to the Lax-Milgram lemma, Theorem 2.4 gives a positive answer to Question (Q2) for any conforming choice of trial/test spaces for the Galerkin discretization of the variational problems (2.9), (2.10), (2.14), and (2.15): throughout the ellipticity constants will supply possible constants in the inf-sup conditions and those will obviously be independent of the finite dimensional spaces.

2.1.4. Generalizations

We argue that the setting of the line segment $\{0\} \times \Gamma$ is sufficiently general for the discussion of operator preconditioning, because the variational problems (2.8)–(2.11) can be lifted to an open curve \mathcal{C} defined by a C^2 -parametrization $\mathbf{s} : \Gamma \rightarrow \mathcal{C}$ with $\|\dot{\mathbf{s}}(\tau)\| = 1$ for all $\tau \in \Gamma$. For instance, the bilinear form associated with the weakly singular integral operator on \mathcal{C} reads

$$a_{V,\mathcal{C}}(\phi, \psi) := \int_{-1}^1 \int_{-1}^1 \log \frac{1}{\|\mathbf{s}(x) - \mathbf{s}(y)\|} \phi(\mathbf{s}(x)) \psi(\mathbf{s}(y)) dy dx, \quad \phi, \psi \in \tilde{H}^{-1/2}(\mathcal{C}).$$

It can be pulled back to Γ , which yields

$$\mathbf{a}_{\mathbb{V},\mathcal{C}}(\phi, \psi) := \int_{-1}^1 \int_{-1}^1 \log \frac{1}{\|\mathbf{s}(x) - \mathbf{s}(y)\|} \phi(x) \psi(y) dy dx, \quad \phi, \psi \in \tilde{H}^{-1/2}(\Gamma).$$

Slightly abusing notation, we have kept the same symbol $\mathbf{a}_{\mathbb{V},\mathcal{C}}$. Analogous considerations apply to the other bilinear forms $\mathbf{a}_{\mathbb{W},\mathcal{C}}$, $\mathbf{a}_{\mathbb{V},\mathcal{C}}$, and $\mathbf{a}_{\mathbb{W},\mathcal{C}}$ defined for functions on \mathcal{C} . We point out that it is exactly the bilinear forms $\mathbf{a}_{\mathbb{V},\mathcal{C}}$ and $\mathbf{a}_{\mathbb{W},\mathcal{C}}$ that occur in the variational boundary integral equations associated with (1.1).

PROPOSITION 2.1. *The following bilinear forms are compact*

$$\begin{aligned} \mathbf{a}_{\mathbb{V}} - \mathbf{a}_{\mathbb{V},\mathcal{C}} : \tilde{H}^{-1/2}(\Gamma) \times \tilde{H}^{-1/2}(\Gamma) &\rightarrow \mathbb{R}, & \mathbf{a}_{\mathbb{W}} - \mathbf{a}_{\mathbb{W},\mathcal{C}} : \tilde{H}^{1/2}(\Gamma) \times \tilde{H}^{1/2}(\Gamma) &\rightarrow \mathbb{R}, \\ \mathbf{a}_{\mathbb{V}} - \mathbf{a}_{\mathbb{V},\mathcal{C}} : H^{-1/2}(\Gamma) \times H^{-1/2}(\Gamma) &\rightarrow \mathbb{R}, & \mathbf{a}_{\mathbb{W}} - \mathbf{a}_{\mathbb{W},\mathcal{C}} : H^{1/2}(\Gamma) \times H^{1/2}(\Gamma) &\rightarrow \mathbb{R}. \end{aligned}$$

PROOF. We focus on the modified weakly singular integral operator $\bar{\mathbb{V}}$ and note that

$$(\mathbf{a}_{\bar{\mathbb{V}}} - \mathbf{a}_{\bar{\mathbb{V}},\mathcal{C}})(\phi, \psi) = \int_{-1}^1 \int_{-1}^1 \left(\log \frac{\|\mathbf{s}(x) - \mathbf{s}(y)\|}{|x - y|} + \log \frac{M_{\mathcal{C}}(\mathbf{s}(x), \mathbf{s}(y))}{M(x, y)} \right) \phi(x) \psi(y) dy dx,$$

where $M_{\mathcal{C}}(\mathbf{x}, \mathbf{y}) := \frac{1}{2} (\|\mathbf{x} - \mathbf{y}\|^2 + (\text{dist}(\mathbf{x}, \partial\mathcal{C}) + \text{dist}(\mathbf{y}, \partial\mathcal{C}))^2)$. By Taylor expansion about $x = y$ and using $\|\dot{\mathbf{s}}\| = 1$, we find for $x \approx y$

$$\begin{aligned} \log \frac{\|\mathbf{s}(x) - \mathbf{s}(y)\|}{|x - y|} &= \log(1 + \dot{\mathbf{s}}(x) \cdot \ddot{\mathbf{s}}(x)(x - y) + O(|x - y|^2)) = O(|x - y|), \\ \log \frac{M_{\mathcal{C}}(\mathbf{s}(x), \mathbf{s}(y))}{M(x, y)} &= \log \frac{\|\mathbf{s}(x) - \mathbf{s}(y)\|^2 + (\omega(x) + \omega(y))^2}{|x - y|^2 + (\omega(x) + \omega(y))^2} \leq O(|x - y|). \end{aligned}$$

Hence, the difference $\mathbf{a}_{\bar{\mathbb{V}}} - \mathbf{a}_{\bar{\mathbb{V}},\mathcal{C}}$ of the bilinear forms is induced by an integral operator $\delta\mathbb{V}$ with a piecewise smooth and globally Lipschitz continuous kernel $\delta k = \delta k(x, y)$, see Figure 2.1 for plots of two specimens.

In particular, the kernel δk belongs to $W^{1,1}(\Gamma \times \Gamma)$, the Sobolev space of functions in $L^1(\Gamma \times \Gamma)$ such that its first order weak derivatives are also $L^1(\Gamma \times \Gamma)$. Recalling that integral operators with L^1 -kernels induce compact mappings $L^2(\Gamma) \rightarrow L^2(\Gamma)$, we conclude that a kernel in $W^{1,1}(\Gamma \times \Gamma)$ generates a compact operator $L^2(\Gamma) \rightarrow H^1(\Gamma)$. Hence, after

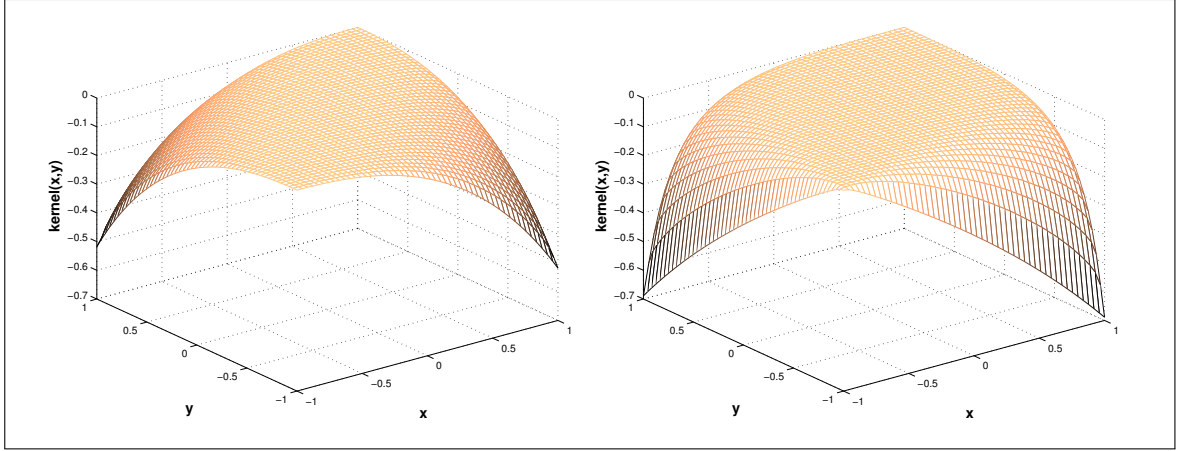


FIGURE 2.1. Plot of kernel δk associated with $a_{\bar{V}} - a_{\bar{V},C}$ for $\mathbf{s}(t) = \begin{pmatrix} \sin(t) \\ \cos(t) \end{pmatrix}$ (arc curve, left) and $\mathbf{s}(t) = \frac{t+0.01}{\sqrt{2}} \begin{pmatrix} \cos(\log(\frac{t+0.01}{\sqrt{2}})) \\ \sin(\log(\frac{t+0.01}{\sqrt{2}})) \end{pmatrix}$ (spiral, right). The kernels are piecewise smooth and continuous.

subtracting a linear function, which is a simple compact modification, we end up with a compact mapping $L^2(\Gamma) \rightarrow H_0^1(\Gamma)$. Thanks to the symmetry of the kernel, it agrees with its adjoint (modulo a compact perturbation), which will be a compact mapping $H^{-1}(\Gamma) \rightarrow L^2(\Gamma)$. By interpolation between $L^2(\Gamma)/H^{-1}(\Gamma)$ and $H^1(\Gamma)/L^2(\Gamma)$ we finally infer that δV is an integral operator mapping compactly $H^{-1/2}(\Gamma) \rightarrow H^{1/2}(\Gamma)$.

Similar arguments apply to the other differences of bilinear forms. As regards $a_V - a_{V,C}$ and $a_W - a_{W,C}$ we can simply appeal to the continuous embeddings $\tilde{H}^{-1/2}(\Gamma) \subset H^{-1/2}(\Gamma)$ and $\tilde{H}^{1/2}(\Gamma) \subset H^{1/2}(\Gamma)$. \square

A first conclusion we can draw from this theorem is that the stability of Galerkin discretizations of the bilinear forms on \mathcal{C} can be inferred from Theorem 2.4, provided that the resolution of the trial and test spaces is large enough, cf. (Sauter & Schwab, 2010, Sect. 4.2.3).

Further, as compact perturbations of a bilinear form do not affect the asymptotic performance of operator preconditioning, this result confirms that $a_{\tilde{W}}$ is suitable for preconditioning $a_{V,C}$, $a_{\tilde{V}}$ spawns a preconditioner for $a_{W,C}$, and so on. Of course, the constants will depend on the shape of \mathcal{C} .

The building blocks of operator preconditioning as they have been assembled so far, are listed in Table 2.1. The missing pieces, namely the families of boundary element spaces X_h and Y_h , will be specified in the next section.

	a	b	X	Y
Case A:	$\tilde{a}_{V,C}$, cf. (2.14)	$a_{\tilde{W},C}$	$\tilde{H}^{-1/2}(\mathcal{C})$	$H^{1/2}(\mathcal{C})$
Case B:	$a_{W,C}$, cf. (2.9)	$a_{\tilde{V},C}$	$\tilde{H}^{1/2}(\mathcal{C})$	$H^{-1/2}(\mathcal{C})$
Case C:	$a_{\tilde{V},C}$, cf. (2.10)	$a_{W,C}$	$H^{-1/2}(\mathcal{C})$	$\tilde{H}^{1/2}(\mathcal{C})$
Case D:	$\tilde{a}_{\tilde{W},C}$, cf. (2.15)	$a_{V,C}$	$H^{1/2}(\mathcal{C})$	$\tilde{H}^{-1/2}(\mathcal{C})$

TABLE 2.1. (Partial) summary of operator preconditioning strategy for variational boundary integral equations on an open curve \mathcal{C} . For notations see Theorem 1.1.

REMARK 2.2. As another generalization of the variational problems studied in Section 2.1.3 we may consider the boundary integral operators associated with boundary value problems for the Helmholtz equation $-\Delta u - k^2 u = 0$ with wave number $k > 0$. For the line segment the corresponding weakly singular and hypersingular operators, V^k and W^k , read

$$\begin{aligned}
 V^k \varphi(x) &:= \frac{i}{4} \int_{\Gamma} H_0^{(1)}(k|x-y|) \varphi(y) dy, \quad x \in \Gamma, \quad \varphi \in C_0^\infty(\Gamma), \\
 W^k &:= -\left(\frac{d}{dx}\right)^* \circ V^k \circ \frac{d}{dx} + k^2 V^k,
 \end{aligned} \tag{2.16}$$

where $H_0^{(1)}(\xi)$ stands for the Hankel function of the first kind (Sauter & Schwab, 2010, Eq. (3.3)). Since the following representation holds (Shestopalov et al., 2000, Sect. 2.3.1)

$$H_0^{(1)}(k|x-y|) = \frac{1}{\pi} \log \frac{1}{|x-y|} + K(k|x-y|), \tag{2.17}$$

one can write the operators as

$$V^k = \frac{i}{4\pi} V + H^k, \quad \text{and} \quad W^k = \frac{i}{4\pi} (W + k^2 V) + L^k, \tag{2.18}$$

with compact operators $H^k : \tilde{H}_{(0)}^{-1/2}(\Gamma) \rightarrow H_*^{1/2}(\Gamma)$ and $L^k : \tilde{H}^{1/2}(\Gamma) \rightarrow H^{-1/2}(\Gamma)$, as the convolution kernel $K(\cdot)$ is piecewise smooth and continuous, and integration is over a bounded domain (Moiseiwitsch, 1977). As a consequence, the bilinear forms for the Helmholtz counterparts of the variational problems (2.8) and (2.9) will be compact perturbations of a_V and a_W , respectively, cf. (Sauter & Schwab, 2010, Lemma 3.9.8).

2.2. Boundary Element Spaces

We employ low-order mapped piecewise polynomial conforming boundary element spaces $X_h \subset X$ and $Y_h \subset Y$ for the Galerkin discretization of the various bilinear forms a and b as listed in Table 2.1 and defined in Section 2.1.4. These spaces are built upon partitions of Γ and, by virtue of the mapping approach outlined in Section 2.1.4, all considerations can be confined to Γ .

2.2.1. Primal and dual meshes

First we construct primal and dual meshes of Γ as explained in (Steinbach, 2003, Sect. 2.2), (Hiptmair, 2006, Section 4), and (Buffa & Christiansen, 2007). We introduce a *primal mesh* Γ_h of the interval Γ and denote its N nodes by $-1 =: x_1 < x_2 < \dots < x_{N-1} < x_N := 1$, $N \in \mathbb{N}$.

Based on Γ_h we build a *dual mesh* $\hat{\Gamma}_h$ of Γ , whose nodes are the midpoints of intervals of Γ_h plus the points -1 and $+1$. More explicitly, the $N + 1$ nodes η_i , $i = 0, \dots, N$, of the dual mesh $\hat{\Gamma}_h$ are given by

$$\eta_0 := -1, \quad \eta_i := \frac{1}{2}(x_i + x_{i+1}), \quad i = 1, \dots, N-1, \quad \eta_N := 1. \quad (2.19)$$

2.2.2. Dual pairs of spaces

A positive answer to Question (Q3) entails a judicious construction of dual pairs of spaces $X_h \subset X$, $Y_h \subset Y$ in each of the four cases. They will be based on pairs of primal and dual meshes. Throughout, we write \mathbb{P}_m for the space of uni-variate polynomials of degree $\leq m$.

Case A: Discrete spaces for $X := \tilde{H}^{-1/2}$, $Y := H^{1/2}$ (Row 1 of Table 2.1)

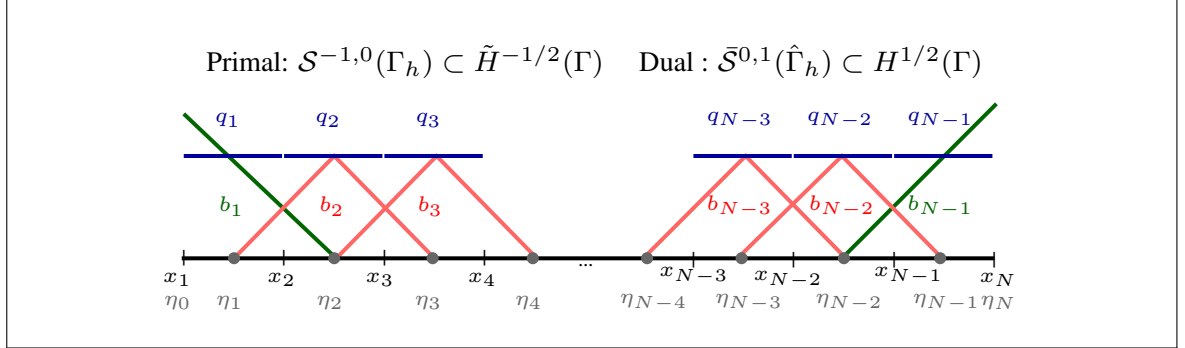


FIGURE 2.2. **Case A:** $X := \tilde{H}^{-1/2}$, $Y := H^{1/2}$, piecewise constant basis functions q_j for $X_h := \mathcal{S}^{-1,0}(\Gamma_h)$ in blue, piecewise linear basis functions (“tent functions”) b_j for $Y_h := \bar{\mathcal{S}}^{0,1}(\hat{\Gamma}_h)$ in red/green. Note the extended “ramp functions” (in green) supported in the two leftmost and rightmost intervals of the dual mesh.

This case addresses the variational equation (2.14) with $\mathbf{a} = \tilde{\mathbf{a}}_v$ using $\mathbf{b} = \tilde{\mathbf{a}}_w$ as preconditioning bilinear form, cf. Theorem 1.1. The primal and dual boundary element spaces are given by

$$X_h := \mathcal{S}^{-1,0}(\Gamma_h) = \{\varphi_h \in L^2(\Gamma) : \varphi_h|_{[x_j, x_{j+1}]} \in \mathbb{P}_0, j = 1, \dots, N-1\} \subset X,$$

$$Y_h := \bar{\mathcal{S}}^{0,1}(\hat{\Gamma}_h) := \left\{ v_h \in C^0(\bar{\Gamma}) : \begin{array}{l} v_h|_{[\eta_{j-1}, \eta_j]} \in \mathbb{P}_1, j = 3, \dots, N-2 \\ v_h|_{[\eta_0, \eta_2]}, v_h|_{[\eta_{N-2}, \eta_N]} \in \mathbb{P}_1 \end{array} \right\} \subset Y.$$

By means of their canonical basis functions the spaces are visualized in Figure 2.2. Obviously, they have the *same dimension*, which is N .

Case B: Discrete spaces for $X := \tilde{H}^{1/2}$, $Y := H^{-1/2}$ (Row 2 of Table 2.1)

This setting arises from the variational equation (2.9) where $\mathbf{a} = \mathbf{a}_w$. Thus, we precondition \mathbf{a} by the bilinear form $\mathbf{b} = \mathbf{a}_v$, cf. Theorem 1.1. The primal and dual boundary element spaces are defined as follows

$$X_h := \mathcal{S}_0^{0,1}(\Gamma_h) := \{v_h \in C^0(\bar{\Gamma}), v_h|_{[x_{j-1}, x_j]} \in \mathbb{P}_1, j = 2, \dots, N-1\} \subset X,$$

$$Y_h := \bar{\mathcal{S}}^{-1,0}(\hat{\Gamma}_h) := \left\{ \varphi_h \in L^2(\Gamma) : \begin{array}{l} \varphi_h|_{[\eta_j, \eta_{j+1}]} \in \mathbb{P}_0, j = 2, \dots, N-3 \\ \varphi_h|_{[\eta_0, \eta_2]}, \varphi_h|_{[\eta_{N-2}, \eta_N]} \in \mathbb{P}_0 \end{array} \right\} \subset Y.$$

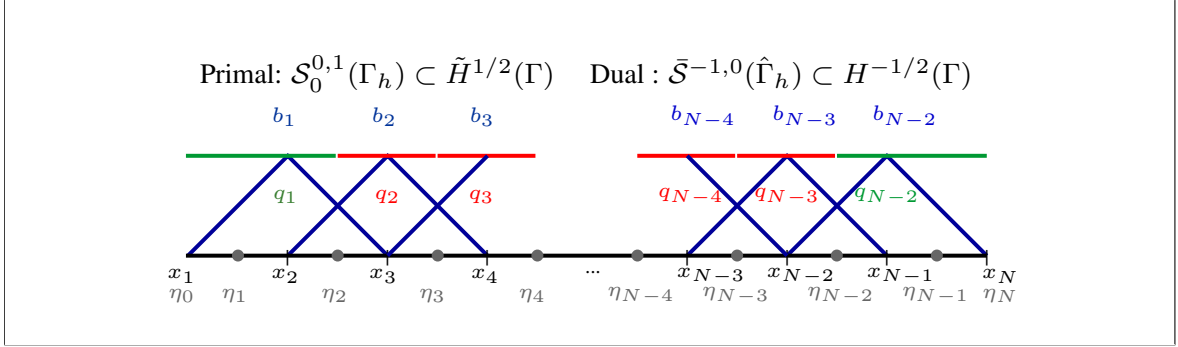


FIGURE 2.3. **Case B:** $X := \tilde{H}^{1/2}$, $Y := H^{-1/2}$, piecewise linear basis functions (“tent functions”) b_j for $X_h := \mathcal{S}_0^{0,1}(\Gamma_h)$ in blue, piecewise constant basis functions q_j for $Y_h := \bar{\mathcal{S}}^{-1,0}(\hat{\Gamma}_h)$ in red/green. Note the extended “characteristic functions” (in green) for the two leftmost and rightmost intervals of the dual mesh.

Figure 2.3 shows these spaces’ representation in terms of their canonical basis functions. Note that both spaces have dimension $N - 2$.

Case C: Discrete spaces for $X := H^{-1/2}$, $Y := \tilde{H}^{1/2}$ (Row 3 of Table 2.1)

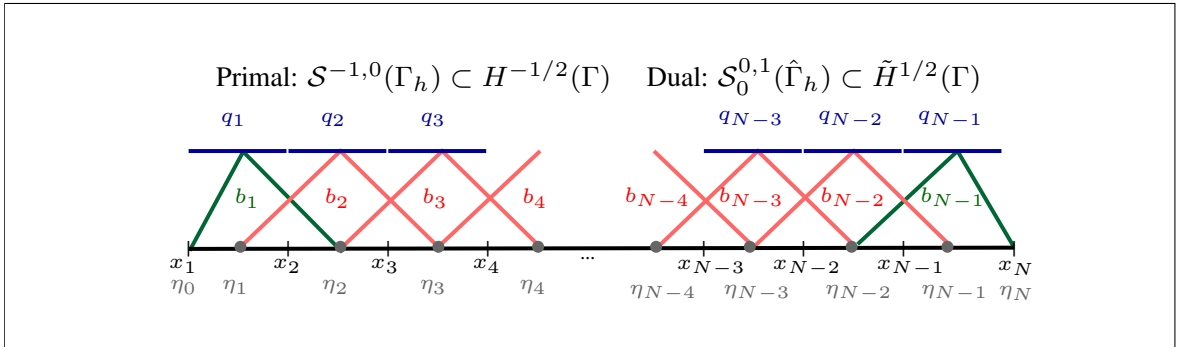


FIGURE 2.4. **Case C:** $X := H^{-1/2}$, $Y := \tilde{H}^{1/2}$, piecewise constant basis functions q_j for $X_h := \mathcal{S}^{-1,0}(\Gamma_h)$ in blue, piecewise linear basis functions (“tent functions”) b_j for $Y_h := \mathcal{S}_0^{0,1}(\hat{\Gamma}_h)$ in red/green. Note that no basis functions are assigned to η_0 and η_N .

In order to perform operator preconditioning for the variational equation (2.10), we employ $\mathbf{b} = \mathbf{a}_W$ as preconditioning bilinear form. The primal and dual boundary element spaces

are given by

$$X_h := \mathcal{S}^{-1,0}(\Gamma_h) = \{\varphi_h \in L^2(\Gamma) : \varphi_h|_{[x_j, x_{j+1}]} \in \mathbb{P}_0, j = 1, \dots, N-1\} \subset X,$$

$$Y_h := \mathcal{S}_0^{0,1}(\hat{\Gamma}_h) := \left\{ v_h \in C^0(\bar{\Gamma}) : \begin{array}{l} v_h|_{[\eta_{j-1}, \eta_j]} \in \mathbb{P}_1, j = 1, \dots, N, \\ v_h(\eta_0) = v_h(\eta_N) = 0 \end{array} \right\} \subset Y.$$

This yields dimension $N-1$ in both cases, as the reader may see from Figure 2.4, where the boundary element spaces are illustrated using their canonical basis functions.

Case D: Discrete spaces for $X := H^{1/2}$, $Y := \tilde{H}^{-1/2}$ (Row 4 of Table 2.1)

This last case corresponds to the variational equation (2.11) where $a = \tilde{a}_W$. Hence, we use bilinear form $b = \tilde{a}_V$ to build the preconditioner. One can define the primal and dual boundary element spaces as follows

$$X_h := \mathcal{S}^{0,1}(\Gamma_h) = \{v_h \in C^0(\bar{\Gamma}), v_h|_{[x_{j-1}, x_j]} \in \mathbb{P}_1, j = 2, \dots, N\} \subset X,$$

$$Y_h := \mathcal{S}^{-1,0}(\hat{\Gamma}_h) := \{\varphi_h \in L^2(\Gamma) : \varphi_h|_{[\eta_{j-1}, \eta_j]} \in \mathbb{P}_0, j = 1, \dots, N\} \subset Y.$$

As in the previous cases, we provide their canonical representation in Figure 2.5. Observe both spaces have dimension N .

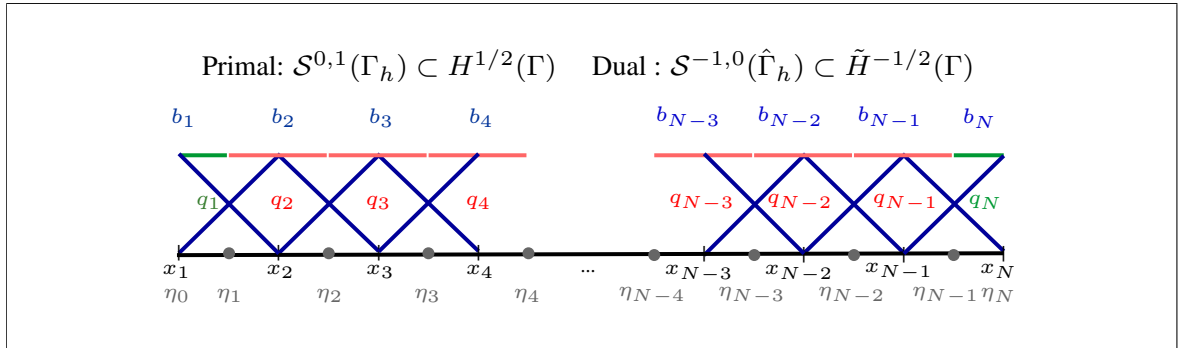


FIGURE 2.5. **Case D:** $X := H^{1/2}$, $Y := \tilde{H}^{-1/2}$, piecewise linear basis functions (“tent functions”) b_j for $X_h := \mathcal{S}^{0,1}(\Gamma_h)$ in blue, basis functions q_j for $Y_h := \mathcal{S}^{-1,0}(\hat{\Gamma}_h)$, the characteristic functions of the dual mesh intervals, in red/green.

The choices for the discrete spaces X_h and Y_h are summarized in Table 2.2, whose rows correspond to those of Table 2.1.

TABLE 2.2. Summary of operator preconditioning strategy for variational boundary integral equations on the interval Γ . For notations see Theorem 1.1.

	Continuous				Discrete	
	a	b	X	Y	X_h	Y_h
Case A	\tilde{a}_V	\tilde{a}_W	$\tilde{H}^{-1/2}(\Gamma)$	$H^{1/2}(\Gamma)$	$\mathcal{S}^{-1,0}(\Gamma_h)$	$\bar{\mathcal{S}}^{0,1}(\hat{\Gamma}_h)$
Case B	a_W	a_V	$\tilde{H}^{1/2}(\Gamma)$	$H^{-1/2}(\Gamma)$	$\mathcal{S}_0^{0,1}(\Gamma_h)$	$\bar{\mathcal{S}}^{-1,0}(\hat{\Gamma}_h)$
Case C	a_V	a_W	$H^{-1/2}(\Gamma)$	$\tilde{H}^{1/2}(\Gamma)$	$\mathcal{S}^{-1,0}(\Gamma_h)$	$\mathcal{S}_0^{0,1}(\hat{\Gamma}_h)$
Case D	\tilde{a}_W	\tilde{a}_V	$H^{1/2}(\Gamma)$	$\tilde{H}^{-1/2}(\Gamma)$	$\mathcal{S}^{0,1}(\Gamma_h)$	$\mathcal{S}^{-1,0}(\hat{\Gamma}_h)$

2.3. Stability of Discrete Duality Pairings

Now we tackle Question (Q3) for the pairs (X_h, Y_h) of discrete spaces defined for Cases A–D in Section 2.2.2. We closely follow the policy developed by O. Steinbach in (Steinbach, 2001, 2002, 2003) for the case when $X = H^{1/2}(\Gamma)$ (Case D), and we are going to extend his results to the other remaining cases.

Since we aim for mesh-uniform stability results, we consider an infinite family of meshes $\{\Gamma_h\}_{h \in \mathbb{H}}$ of Γ , whose members are labelled by h from the index set \mathbb{H} and serve as primal meshes. Concrete specimens of such families will be presented in Section 2.3.3. All of the constants introduced below can be chosen independently of h . Suppressing the dependence on h we continue using the notations x_i and η_j to designate the nodes of the primal mesh Γ_h and its associated dual mesh $\hat{\Gamma}_h$, see Section 2.2.1. We also keep N for the total number of nodes of Γ_h .

2.3.1. Assumptions on mesh geometry

The stability results will hinge on certain assumptions on local properties of the meshes $\Gamma_h, h \in \mathbb{H}$. From the elaborations of Section 2.3.2 it will become clear that cases A, D, and B,C are connected by duality. Therefore, only two sets of assumptions on the geometry of the meshes will suffice, corresponding to the cases A/D and B/C.

Below, we are going to use the same notations for entities that will be different for different cases. The concrete meaning should always be clear from the context of the current case being discussed. Moreover, in what follows, many notations are borrowed from (Steinbach,

2003). In particular, we designate by $\tau_l := (x_l, x_{l+1})$ a mesh interval of the primal mesh Γ_h with length $h_l := x_{l+1} - x_l$, $l = 1, \dots, N - 1$.

Case D (Case A)

In this case we set $\hat{h}_1 := \frac{1}{3}h_1$, $\hat{h}_k := \frac{1}{3}(h_{k-1} + h_k)$, $k = 2, \dots, N - 1$, $\hat{h}_N := h_{N-1}$.

Then we define the following 2×2 matrices associated with the intervals of the primal mesh

$$\tilde{G}_l = \frac{h_l}{8} \begin{pmatrix} 3 & 1 \\ 1 & 3 \end{pmatrix}, \quad G_l = \frac{h_l}{6} \begin{pmatrix} 2 & 1 \\ 1 & 2 \end{pmatrix}, \quad H_l = \begin{pmatrix} \hat{h}_l^{1/2} & 0 \\ 0 & \hat{h}_{l+1}^{1/2} \end{pmatrix}, \quad (2.20)$$

for $l = 1, \dots, N - 1$.

Case B (Case C)

In this case we define $\hat{h}_k := \frac{1}{3}(h_k + h_{k+1})$, $k = 1, \dots, N - 2$.

Further, for $l = 2, \dots, N - 2$, the 2×2 -matrices \tilde{G}_l , G_l , and H_l are defined exactly as in (2.20). Besides, for mesh intervals adjacent to the endpoints -1 and 1 these matrices reduce to the following 1×1 -matrices (numbers)

$$\tilde{G}_l = \frac{h_l}{2}, \quad D_l = \frac{h_l}{3}, \quad H_l = \hat{h}_l, \quad \text{for } l = 1, N - 1. \quad (2.21)$$

Using the notations just introduced, we now state geometric assumptions on the meshes Γ_h valid for all cases. Throughout, l runs through the maximum possible index interval, and $M_l \in \{1, 2\}$ designates the size of the matrices \tilde{G}_l , G_l , and H_l , from (2.20) and (2.21), respectively.

ASSUMPTION 2.1 (Assumption 1.1 in (Steinbach, 2003)). *There are constants $c_1^G, c_2^G > 0$ independent of h and l such that*

$$c_1^G(D_l \mathbf{x}_l, \mathbf{x}_l) \leq (G_l \mathbf{x}_l, \mathbf{x}_l) \leq c_2^G(D_l \mathbf{x}_l, \mathbf{x}_l), \quad \forall \mathbf{x}_l \in \mathbb{R}^{M_l}, \quad (2.22)$$

where $D_l := \text{diag}(D_l)$.

ASSUMPTION 2.2 (Assumption 2 in (Steinbach, 2003)). *We can find a constant $c_0 > 0$ such that*

$$(H_l \tilde{G}_l^T H_l^{-1} \mathbf{x}_l, \mathbf{x}_l) \geq c_0 \cdot (D_l \mathbf{x}_l, \mathbf{x}_l), \quad \forall \mathbf{x}_l \in \mathbb{R}^{M_l} \quad (2.23)$$

for all l and h .

2.3.2. Stability Results

Now we establish the crucial stability results for the four cases A-D. Their proof will be elaborated in several steps throughout this section.

Theorem 2.5. *Let Assumptions 2.1 and 2.2 be satisfied. Then, for the following combinations of discrete spaces*

$$\begin{aligned} \text{Case A: } & X_h = \mathcal{S}^{-1,0}(\Gamma_h) \subset X = \tilde{H}^{-1/2}(\Gamma), \quad Y_h = \bar{\mathcal{S}}^{0,1}(\hat{\Gamma}_h) \subset Y = H^{1/2}(\Gamma), \\ \text{Case B: } & X_h = \mathcal{S}_0^{0,1}(\Gamma_h) \subset X = \tilde{H}^{1/2}(\Gamma), \quad Y_h = \bar{\mathcal{S}}^{-1,0}(\hat{\Gamma}_h) \subset Y = H^{-1/2}(\Gamma), \\ \text{Case C: } & X_h = \mathcal{S}^{-1,0}(\Gamma_h) \subset X = H^{-1/2}(\Gamma), \quad Y_h = \mathcal{S}_0^{0,1}(\hat{\Gamma}_h) \subset Y = \tilde{H}^{1/2}(\Gamma), \\ \text{Case D: } & X_h = \mathcal{S}_0^{0,1}(\Gamma_h) \subset X = H^{1/2}(\Gamma), \quad Y_h = \mathcal{S}^{-1,0}(\hat{\Gamma}_h) \subset Y = \tilde{H}^{-1/2}(\Gamma), \end{aligned}$$

the discrete inf-sup condition:

$$\sup_{v_h \in Y_h} \frac{|\langle w_h, v_h \rangle|}{\|v_h\|_Y} \geq \frac{1}{c_s} \|w_h\|_X, \quad \forall w_h \in X_h. \quad (2.24)$$

holds with a positive constant c_s independent of h .

Given the assertion of this theorem, all the abstract assumptions of Theorem 1.1 have now been verified. Theorem 2.1 provides the continuity of the bilinear forms, Theorem 2.4 uniform stability of the (discrete) variational problems, and, finally, Theorem 2.5 the stability of the discrete duality pairing. Hence, for all the concrete choices listed in Table 2.2 operator preconditioning will yield preconditioners that achieve bounded condition numbers *independently of the resolution of the mesh*: they are asymptotically optimal.

We split the proof of Theorem 2.5 into the individual cases. Moreover, inherent dependencies suggest to treat them in the order to D-B-C-A.

Proof of Theorem 2.5 for Case D

As stated before, this case follows as a Corollary of (Steinbach, 2003, Theorem 2.1 and 2.2).

Proof of Theorem 2.5 for Case B

In order to prove this case, we extend the stability results developed for Case D (Steinbach, 2003, Theorem 2.2), using an analogous policy. We start with an assertion of L^2 -stability of the discrete pairing, see Appendix C for a proof using elementary local estimates.

Lemma 2.1. *The L^2 -stability holds*

$$\sup_{\psi_h \in \mathcal{S}^{-1,0}(\hat{\Gamma}_h)} \frac{|\langle \psi_h, w_h \rangle|}{\|\psi_h\|_{L^2(\Gamma)}} \geq c_{st} \|w_h\|_{L^2(\Gamma)}, \quad \forall w_h \in \mathcal{S}_0^{0,1}(\Gamma_h), \quad \forall h \in \mathbb{H}, \quad (2.25)$$

where $c_{st} = \frac{1}{2}$.

Next, consider the standard Galerkin L^2 -Projection $Q_h : L^2(\Gamma) \rightarrow \mathcal{S}_0^{0,1}(\Gamma_h)$, and the generalized Galerkin L^2 -Projection $\tilde{Q}_h : L^2(\Gamma) \rightarrow \mathcal{S}_0^{0,1}(\Gamma_h)$, for a given $u \in L^2(\Gamma)$ defined according to

$$\langle Q_h u, v_h \rangle_{L^2(\Gamma)} = \langle u, v_h \rangle_{L^2(\Gamma)}, \quad \forall v_h \in \mathcal{S}_0^{0,1}(\Gamma_h), \quad (2.26)$$

$$\langle \tilde{Q}_h u, \phi_h \rangle_{L^2(\Gamma)} = \langle u, \phi_h \rangle_{L^2(\Gamma)}, \quad \forall \phi_h \in \mathcal{S}^{-1,0}(\hat{\Gamma}_h). \quad (2.27)$$

Lemma 2.1 ensures that \tilde{Q}_h is well-defined, because it guarantees unique solvability of (2.27). It also furnishes the stability estimate

$$\left\| \tilde{Q}_h u \right\|_{L^2(\Gamma)} \leq \frac{1}{c_{st}} \|u\|_{L^2(\Gamma)}, \quad \text{for all } u \in L^2(\Gamma). \quad (2.28)$$

Additionally, we want to prove the H^1 -stability of \tilde{Q}_h and, following (Steinbach, 2003, Section 1.5), resort to a quasi-interpolation operator. For the sake of clarity, the proof of the following will also be provided in Appendix C.

PROPOSITION 2.2. *Let Assumptions 2.1 and 2.2 be satisfied. Then the L^2 -projection $\tilde{Q}_h : H_0^1(\Gamma) \rightarrow X_h = \mathcal{S}_0^{0,1}(\Gamma_h)$ defined in (2.27) satisfies*

$$\left\| \tilde{Q}_h u \right\|_{H^1(\Gamma)} \leq \tilde{c}_{st} \|u\|_{H^1(\Gamma)}, \quad \forall u \in H_0^1(\Gamma), \quad (2.29)$$

with \tilde{c}_{st} a positive constant independent of h .

Now we are in a position to prove the key stability results for Case B.

Proof of Theorem 2.5 for Case B. $\tilde{H}^{1/2}(\Gamma)$ can be obtained by interpolating between $L^2(\Gamma)$ and $H_0^1(\Gamma)$, see (Lions & Magenes, 1972, Thm. 11.7). Thus, by interpolation of bounded linear operators we obtain from (2.28) and Proposition 2.2 that

$$\left\| \tilde{Q}_h u \right\|_{\tilde{H}^{1/2}(\Gamma)} \leq c_B \|u\|_{\tilde{H}^{1/2}(\Gamma)}, \quad \forall u \in \tilde{H}^{1/2}(\Gamma), h \in \mathbb{H}. \quad (2.30)$$

Introduce the projection operators $\Pi_h : \tilde{H}^{1/2}(\Gamma) \rightarrow \mathcal{S}^{-1,0}(\hat{\Gamma}_h) \subseteq H^{-1/2}(\Gamma)$, satisfying

$$\langle \Pi_h u, w_h \rangle_{L^2(\Gamma)} = \langle u, w_h \rangle_{\tilde{H}^{1/2}(\Gamma)}, \quad \forall w_h \in \mathcal{S}_0^{0,1}(\Gamma_h), h \in \mathbb{H}, \quad (2.31)$$

where $\langle u, w_h \rangle_{\tilde{H}^{1/2}(\Gamma)}$ denotes the $\tilde{H}^{1/2}(\Gamma)$ -inner product. By the dual norm definition and continuity of \tilde{Q}_h , we have

$$\begin{aligned} \|\Pi_h u\|_{H^{-1/2}(\Gamma)} &= \sup_{0 \neq w \in \tilde{H}^{1/2}(\Gamma)} \frac{|\langle \Pi_h u, w \rangle_{L^2(\Gamma)}|}{\|w\|_{\tilde{H}^{1/2}(\Gamma)}} \\ &= \sup_{0 \neq w \in \tilde{H}^{1/2}(\Gamma)} \frac{|\langle \Pi_h u, \tilde{Q}_h w \rangle_{L^2(\Gamma)}|}{\|w\|_{\tilde{H}^{1/2}(\Gamma)}} \\ &= \sup_{0 \neq w \in \tilde{H}^{1/2}(\Gamma)} \frac{|\langle u, \tilde{Q}_h w \rangle_{\tilde{H}^{1/2}(\Gamma)}|}{\|w\|_{\tilde{H}^{1/2}(\Gamma)}} \\ &\leq c_B \sup_{0 \neq w \in \tilde{H}^{1/2}(\Gamma)} \frac{|\langle u, \tilde{Q}_h w \rangle_{\tilde{H}^{1/2}(\Gamma)}|}{\|\tilde{Q}_h w\|_{\tilde{H}^{1/2}(\Gamma)}} \\ \|\Pi_h u\|_{H^{-1/2}(\Gamma)} &\leq c_B \|u\|_{\tilde{H}^{1/2}(\Gamma)}. \end{aligned}$$

So now, for any $w_h \in \mathcal{S}_0^{0,1}(\Gamma_h)$ we can define $v_h := \Pi_h w_h$, and by the above inequality we obtain the assertion

$$\begin{aligned} \|w_h\|_{\tilde{H}^{1/2}(\Gamma)} &= \frac{|\langle w_h, w_h \rangle_{\tilde{H}^{1/2}(\Gamma)}|}{\|w_h\|_{\tilde{H}^{1/2}(\Gamma)}} = \frac{|\langle w_h, \Pi_h w_h \rangle_{L^2(\Gamma)}|}{\|w_h\|_{\tilde{H}^{1/2}(\Gamma)}} \\ &\leq c_B \frac{|\langle w_h, \Pi_h w_h \rangle_{L^2(\Gamma)}|}{\|\Pi_h w_h\|_{H^{-1/2}(\Gamma)}} \leq c_B \sup_{0 \neq v_h \in \mathcal{S}^{-1,0}(\hat{\Gamma}_h)} \frac{|\langle w_h, v_h \rangle_{L^2(\Gamma)}|}{\|v_h\|_{H^{-1/2}(\Gamma)}}. \end{aligned}$$

Proof of Theorem 2.5 for Case C

We appeal to an analogue of Lemma 2.1 to define $\tilde{Q}_h^2 : L^2(\Gamma) \rightarrow \mathcal{S}_0^{0,1}(\hat{\Gamma}_h)$ for a given $u \in L^2(\Gamma)$ as solution of the variational problem

$$\left\langle \tilde{Q}_h^2 u, \phi_h \right\rangle_{L^2(\Gamma)} = \langle u, \phi_h \rangle_{L^2(\Gamma)}, \quad \forall \phi_h \in \mathcal{S}^{-1,0}(\Gamma_h). \quad (2.32)$$

Along the same lines as above one can prove that

$$\left\| \tilde{Q}_h^2 u \right\|_{\tilde{H}^{1/2}(\Gamma)} \leq c_C \|u\|_{\tilde{H}^{1/2}(\Gamma)}, \quad \forall u \in \tilde{H}^{1/2}(\Gamma), h \in \mathbb{H}. \quad (2.33)$$

The arguments are very similar to those employed in the proof of Proposition 2.2 and (2.28) for \tilde{Q}_h . Next, using the dual norm definition and (2.33), we have for all $v_h \in \mathcal{S}^{-1,0}(\Gamma_h)$ that

$$\begin{aligned} \|v_h\|_{H^{-1/2}(\Gamma)} &= \sup_{0 \neq w \in \tilde{H}^{1/2}(\Gamma)} \frac{|\langle v_h, w \rangle_{L^2(\Gamma)}|}{\|w\|_{\tilde{H}^{1/2}(\Gamma)}} = \sup_{0 \neq w \in \tilde{H}^{1/2}(\Gamma)} \frac{|\langle v_h, \tilde{Q}_h^2 w \rangle_{L^2(\Gamma)}|}{\|w\|_{\tilde{H}^{1/2}(\Gamma)}} \\ &\leq c_C \sup_{0 \neq w \in \tilde{H}^{1/2}(\Gamma)} \frac{|\langle v_h, \tilde{Q}_h^2 w \rangle_{L^2(\Gamma)}|}{\left\| \tilde{Q}_h^2 w \right\|_{\tilde{H}^{1/2}(\Gamma)}} \leq c_C \sup_{0 \neq w_h \in \tilde{\mathcal{S}}_0^{0,1}(\hat{\Gamma}_h)} \frac{|\langle v_h, w_h \rangle_{L^2(\Gamma)}|}{\|w_h\|_{\tilde{H}^{1/2}(\Gamma)}}, \end{aligned}$$

which amounts to the assertion in Case C.

Proof of Theorem 2.5 for Case A

The assertion for Case A follows in a similar way from Case D as Case C from Case B.

2.3.3. Local mesh conditions

For important families of meshes that feature local refinement towards the endpoints of Γ , we demonstrate that the constraints imposed by Assumption 2.2 are not severe. As explained above, we need consider only the cases D and B.

In the interest of reducing this mesh condition to an eigenvalue problem, we use the symmetric form of Assumption 2.2 as in (Steinbach, 2003, Assumption 2.1): with

$$G_l^S := \frac{1}{2} \left[H_l \tilde{G}_l^T H_l^{-1} + H_l^{-1} \tilde{G}_l H_l \right], \quad (2.34)$$

(2.23) becomes equivalent to

$$(G_l^S \mathbf{x}_l, \mathbf{x}_l) \geq c_0 \cdot (D_l \mathbf{x}_l, \mathbf{x}_l), \quad \text{for all } \mathbf{x}_l \in \mathbb{R}^{M_l}. \quad (2.35)$$

We will study the following non-uniform meshes, all of which are symmetric to $x = 0$:

- For odd N and $q > 1$ geometric meshes whose nodes are

$$x_k := \begin{cases} -1 & , \text{ for } k = 1, \\ -1 + q^{-\frac{N-1}{2} + k - 1} & , \text{ for } k = 2, \dots, \frac{N-1}{2} + 1, \\ 1 - q^{\frac{N-1}{2} - k + 1} & , \text{ for } k = \frac{N-1}{2} + 2, \dots, N - 1, \\ 1 & , \text{ for } k = N. \end{cases} \quad (2.36)$$

- For even N and grading factor $\alpha > 0$ algebraically graded meshes defined by

$$x_k := \begin{cases} -1 + \left(2 \frac{k-1}{N-1}\right)^\alpha, & \text{for } k = 1, \dots, \frac{N}{2}, \\ 1 - \left(2 - 2 \frac{k-1}{N-1}\right)^\alpha, & \text{for } k = \frac{N}{2} + 1, \dots, N. \end{cases} \quad (2.37)$$

- Chebychev meshes with nodes

$$x_k := -\cos\left(\pi \frac{k-1}{N-1}\right), \quad k = 1, \dots, N. \quad (2.38)$$

Case D

As can easily be deduced from the definition of the matrices from (2.20), Assumption 2.2 boils down to

$$\begin{aligned} \lambda_{\min} \left(\begin{array}{cc} 6 & \sqrt{\frac{\hat{h}_l}{\hat{h}_{l+1}}} + \sqrt{\frac{\hat{h}_{l+1}}{\hat{h}_l}} \\ \sqrt{\frac{\hat{h}_l}{\hat{h}_{l+1}}} + \sqrt{\frac{\hat{h}_{l+1}}{\hat{h}_l}} & 6 \end{array} \right) \\ = 6 - \left(\sqrt{\frac{\hat{h}_l}{\hat{h}_{l+1}}} + \sqrt{\frac{\hat{h}_{l+1}}{\hat{h}_l}} \right) \geq \frac{16}{3} c_0 \quad \text{for } l = 1, \dots, N-1. \end{aligned}$$

Hence, if this minimal eigenvalue is positive, we can set

$$c_0 = \min_{l=1, \dots, N-1} \frac{3}{16} \left(6 - \left(\sqrt{\frac{\hat{h}_l}{\hat{h}_{l+1}}} + \sqrt{\frac{\hat{h}_{l+1}}{\hat{h}_l}} \right) \right). \quad (2.39)$$

Note that the minimum will be attained for extremal values of the ratios $\hat{h}_l : \hat{h}_{l+1}$.

Case B

As mentioned in Section 2.3.1, we get the same matrices (2.20) for $l = 2, \dots, N-2$. Hence, for the internal mesh intervals, we obtain the same formulas as in Case D. For the terminal intervals we merely have to compare the numbers from (2.21) and find that this just means $c_0 \leq \frac{3}{2}$.

Hence, for all cases we have to check the existence of $c_0 > 0$ given by (2.39).

We introduce the abbreviation $r_l := \frac{\hat{h}_l}{\hat{h}_{l+1}}$ and note that thanks to symmetry, only the mesh intervals in $[-1, 0]$ have to be examined.

For the geometrically graded mesh (2.36) we find $h_l = q^{-\frac{N-1}{2}+l-1}(q-1)$, $k = 1, \dots, \frac{N-1}{2}$, and end up with

$$r_l = \begin{cases} 1 + q & \text{for } l = 1, \\ q & \text{for } l = 2, \dots, \frac{N-1}{2} + 1. \end{cases}$$

From this we conclude

$$c_0 = \frac{3}{16} \left(6 - \sqrt{1+q} - \sqrt{1+q^{-1}} \right) > 0, \quad \text{if } q < 16 + 12\sqrt{2} \approx 32.9 .$$

For the algebraically graded mesh (2.37) we obtain

$$r_l = \begin{cases} 2^\alpha & \text{for } l = 1, \\ \frac{(l+1)^\alpha - (l-1)^\alpha}{(l)^\alpha - (l-2)^\alpha} & \text{for } l = 2, \dots, \frac{N}{2}. \end{cases}$$

Here, r_l attains its extremal value for $l = 1$ and we find

$$c_0 = \frac{3}{16} \left(6 - 2^{\alpha/2} - \frac{1}{2^{\alpha/2}} \right) > 0, \quad \text{if } \alpha < 2 \frac{\log(3 + \sqrt{2})}{\log 2} \approx 4.28 .$$

For the Chebychev meshes, we find

$$r_l = \begin{cases} \frac{\sin^2(\frac{\pi}{2(N-1)})}{\sin^2(\frac{\pi}{N-1})} & \text{for } l = 1, N-1, \\ \frac{\sin(\frac{\pi l}{N-1})}{\sin(\frac{\pi(l-1)}{N-1})} & \text{for } l = 2, \dots, N-2, \end{cases}$$

which attains its extremal values for $l = 1, N-1$. Furthermore, $\lambda_{\min} \searrow \frac{7}{2}$ as $N \rightarrow \infty$ and we can chose $c_0 = \frac{21}{32}$.

3. IMPLEMENTATION

3.1. Quadrature

For numerical integration we use Gauss-Legendre quadrature. In order to explain how it was implemented, let us consider Legendre polynomials defined as follows

$$P_0 = 1, \quad P_1 = x \quad \text{and} \quad P_{n+1} = \frac{(2n+1)xP_n(x) - nP_{n-1}(x)}{n+1}.$$

Also introduce

$$L_k = \frac{1}{P'_{n+1}(x)} \frac{P_{n+1}}{(x - z_k)},$$

where z_k is k -th root of the Legendre's polynomial. Then, Gauss-Legendre quadrature with Nq quadrature points is defined as

$$I(h) \sim \int_{-1}^1 h_n(t) dt = \sum_{k=0}^{Nq} h(z_k) w_k dt$$

where $w_k := \int_{-1}^1 L_k(s) ds = \frac{2}{(1-z_k^2)(P'_{Nq+1}(z_k))^2}$.

Suppose we are interested in integrating the following

$$\int_a^b f(x) dx.$$

Since Gauss-Legendre quadrature is designed to integrate over $[-1, 1]$, we need to introduce the following change of variable

$$f(x) = f\left(\frac{(b-a)t + (a+b)}{2}\right),$$
$$dx = \frac{(b-a)}{2} dt.$$

Finally, by introducing the following auxiliary variables

$$x_k = \frac{(b-a)z_k + b + a}{2}, \quad k = 0, \dots, Nq,$$

the quadrature is calculated by

$$\int_a^b f(x)dx \sim \sum_{k=0}^{Nq} f(x_k) \frac{b-a}{2} w_k.$$

This quadrature is implemented for simple integration following the above. For the two-dimensional case, we use a product tensor of one-dimensional quadratures. However, to avoid the singularity of the integrands at $x = y$, we consider Nq points for one axis and $Nq + 1$ points for the other one.

3.2. Trial and Test Spaces

Recall from Section 2.2 (Figures 2.2, 2.5, 2.4, and 2.3), the following finite dimensional basis defined over the primal mesh

$$\begin{aligned} \mathcal{S}^{-1,0}(\Gamma_h) &:= \text{span}\{q_k\}_{k=1}^{N-1} \subseteq H^{-1/2}(\Gamma), \\ \mathcal{S}_0^{0,1}(\Gamma_h) &:= \text{span}\{b_k\}_{k=1}^{N-2} \subseteq \tilde{H}^{1/2}(\Gamma), \\ \mathcal{S}^{0,1}(\Gamma_h) &:= \text{span}\{b_k\}_{k=1}^N \subseteq H^{1/2}(\Gamma), \end{aligned}$$

where q_i and b_j are p.w. constant and p.w. linear functions, respectively. The reader should notice we use the same basis for $H^{-1/2}(\Gamma)$ and $\tilde{H}^{-1/2}(\Gamma)$, hence there is no ambiguity in the above definition for q_k . However, even though b_k will always refer to ‘‘hat functions’’, it admits two different connotations. For this reason, whenever we use this notation, we will explicit its meaning.

3.3. Boundary Integral Operator’s implementation

3.3.1. Weakly singular operator

We recall from (2.8) the variational form of the weakly singular for $\varphi \in \tilde{H}_{(0)}^{-1/2}(\Gamma)$

$$\mathbf{a}_V(\varphi, \psi) = \langle \mathbf{V} \varphi, \psi \rangle_{\tilde{H}^{-1/2}(\Gamma)} \quad \forall \psi \in \tilde{H}_{(0)}^{-1/2}(\Gamma).$$

The $(N - 1) \times (N - 1)$ Galerkin Matrix corresponding to this variational form can be expressed as follows

$$\begin{aligned} \mathbf{V}_h [i, j] &= \langle \mathbf{V} q_i, q_j \rangle \\ &= \int_{-1}^1 \int_{-1}^1 -\log |x - y| 1_{\text{supp}\{q_i\}}(x) 1_{\text{supp}\{q_j\}}(y) dx dy \\ &= \int_{x_j}^{x_{j+1}} \int_{x_i}^{x_{i+1}} -\log |x - y| dx dy. \end{aligned}$$

One can calculate this integral analytically by using the following formula,

$$\begin{aligned} - \int_a^b \int_c^d \log |x - y| dx dy &= - \left\{ \frac{(d - a)^2}{4} (2 \log |d - a| - 1) - \frac{(d - b)^2}{4} (2 \log |d - b| - 1) \right. \\ &\quad - \frac{(c - a)^2}{4} (2 \log |c - a| - 1) + \frac{(c - b)^2}{4} (2 \log |c - b| - 1) \\ &\quad \left. - (b - a)(d - c) \right\}. \end{aligned}$$

Moreover, since $\lim_{z \rightarrow 0} z^2 \log |z| = 0$, this expression allows us to get rid of the singularity. However, since matlab does not calculate limits, the implementation takes into account the special cases of the diagonal and subdiagonals of \mathbf{V}_h and eliminates the corresponding terms.

This formula reduces the calculations associated to this matrix. Unfortunately, when $h \rightarrow 0$, it is no longer a stable way to compute this integral because cancellation comes into play. We tackle this difficulty by using a semi-analytical formula. This is to calculate the first integral analytically employing the next formula

$$f(y) := \int_c^d -\log |x - y| dx = -(d - y) \log |d - y| + (c - y) \log |c - y| + (d - c), \quad (3.1)$$

and then integrate $\int_a^b f(y) dy$ by using the aforementioned Gauss-Legendre Quadrature.

3.3.2. Hypersingular operator

The weak formulation of the hypersingular operator for $u \in \tilde{H}^{1/2}(\Gamma)$ is given by

$$a_W(u, w) = \langle W u, w \rangle_{\tilde{H}^{1/2}(\Gamma)} \quad \forall w \in \tilde{H}^{1/2}(\Gamma).$$

Moreover, by integrating by parts, it can be written as

$$a_W(u, w) = \langle V u', w' \rangle_{\tilde{H}^{1/2}(\Gamma)} \quad \forall w \in \tilde{H}^{1/2}(\Gamma).$$

Then, its Galerkin Matrix is

$$W_h [i, j] = \langle V b'_i, b'_j \rangle, \quad b_i, b_j \in \mathcal{S}_0^{0,1}(\Gamma_h)$$

where

$$\forall k = 1, \dots, N-2, \quad b'_k(x) := \begin{cases} b_k^a := \frac{1}{x_k - x_{k-1}} & x \in [x_{k-1}, x_k], \\ b_k^b := -\frac{1}{x_{k+1} - x_k} & x \in (x_k, x_{k+1}] \\ 0 & \text{else.} \end{cases}$$

From this, we can compute our $(N-2) \times (N-2)$ matrix as

$$\begin{aligned} W_h [i, j] &= \langle V b'_i, b'_j \rangle \\ &= b_i^a b_j^a V_h [i-1, j-1] + b_i^a b_j^b V_h [i-1, j] \\ &\quad + b_i^b b_j^a V_h [i, j-1] + b_i^b b_j^b V_h [i, j], \end{aligned}$$

Finally, because its entries rely on the implementation of V_h , it will depend on the mesh if this matrix is computed analytically or semi-analytically, as it was explained in the previous section.

3.3.3. Modified weakly singular operator

The associated variational form (see (2.10)) for $\varphi \in H^{-1/2}(\Gamma)$ is

$$a_{\bar{V}}(\phi, \psi) = \langle \bar{V} \phi, \psi \rangle_{H^{-1/2}(\Gamma)} \quad \forall \psi \in H^{-1/2}(\Gamma).$$

Its corresponding Galerkin Matrix is given by

$$\begin{aligned}
\bar{V}_h [i, j] &= \langle \bar{V}q_i, q_j \rangle \\
&= \int_{-1}^1 \int_{-1}^1 \log \frac{M(x, y)}{|x - y|} 1_{\text{supp}\{q_i\}}(x) 1_{\text{supp}\{q_j\}}(y) dx dy \\
&= \int_{x_j}^{x_{j+1}} \int_{x_i}^{x_{i+1}} \log \frac{M(x, y)}{|x - y|} dx dy,
\end{aligned}$$

Now, by defining

$$M_h [i, j] = \int_{x_j}^{x_{j+1}} \int_{x_i}^{x_{i+1}} \log M(x, y) dx dy.$$

and splitting the logarithm, we implemented $\bar{V}_h \in \mathbb{R}^{(N-1) \times (N-1)}$ by

$$\bar{V}_h = M_h + V_h,$$

where M_h is calculated by quadrature and V_h as explained in section 3.3.1.

3.3.4. Modified hypersingular operator

From (2.11) we know the weak formulation of the modified hypersingular operator for $u \in H^{1/2}(\Gamma)$ is

$$\mathbf{a}_{\bar{W}}(u, w) = \langle \bar{W}u, w \rangle_{H^{1/2}(\Gamma)} = \langle \bar{V}u', w' \rangle_{H^{1/2}(\Gamma)}$$

for all $w \in H^{1/2}(\Gamma)$, as it is shown in (Jerez-Hanckes & Nédélec, 2012, Prop. 3.1). Now, since $\mathcal{S}^{0,1}(\Gamma_h) = \text{span}\{b_k\}_1^N$, we have

$$\begin{aligned}
b'_1(x) &:= \begin{cases} -\frac{1}{x_2 - x_1}, & x \in [x_1, x_2] \\ 0, & \text{else} \end{cases}, & b'_N(x) &:= \begin{cases} \frac{1}{x_N - x_{N-1}} & x \in [x_{N-1}, x_N] \\ 0 & \text{else} \end{cases}, \\
b'_k &:= \begin{cases} b_k^a & x \in [x_{k-1}, x_k] \\ b_k^b & x \in (x_k, x_{k+1}] \\ 0 & \text{else} \end{cases}, & \forall k &= 2, \dots, N-1.
\end{aligned}$$

Consequently, the associated Galerkin Matrix has entries

$$\begin{aligned}\bar{W}_h [i, j] &= \langle \mathbf{V} b'_i, b'_j \rangle \\ &= b_i^a b_j^a \bar{V}_h [i - 1, j - 1] + b_i^a b_j^b \bar{V}_h [i - 1, j] \\ &\quad + b_i^b b_j^a \bar{V}_h [i, j - 1] + b_i^b b_j^b \bar{V}_h [i, j],\end{aligned}$$

where $\bar{W}_h \in \mathbb{R}^{N \times N}$. Lastly, we point out that we implemented this operator considering the above formula and the decomposition of \bar{V}_h explained in the previous section.

3.4. Calderón-type Identities and Strong Formulations

In the interest of numerically testing the Calderón-type identities proposed by Jerez-Hanckes and Nédélec ([Jerez-Hanckes & Nédélec, 2012](#)), we also need to implement strong formulations of our operators.

We deduce the discrete strong formulation for the weakly singular and modified weakly singular operators from their definition in (2.4) and (2.5). Then, by using our trial basis and $\varphi_h(y) = \sum_{k=1}^{N-1} \varphi_k q_k(y)$, we derive

$$\begin{aligned}[\mathbf{V}(\varphi_h)]_h &= \int_{-1}^1 -\log |x - y| 1_{\text{supp}\{q_i\}}(x) 1_{\text{supp}\{q_k\}}(y) \varphi_k dx, \\ [\bar{\mathbf{V}}(\varphi_h)]_h &= \int_{-1}^1 \log \frac{M(x, y)}{|x - y|} 1_{\text{supp}\{q_i\}}(x) 1_{\text{supp}\{q_j\}}(y) \varphi_j dx,\end{aligned}$$

which can be rewritten as

$$\begin{aligned}[\mathbf{V}(\varphi_h)]_h &= \mathbf{V}_h^S \underline{\varphi}_h \\ [\bar{\mathbf{V}}(\varphi_h)]_h &= \bar{\mathbf{V}}_h^S \underline{\varphi}_h,\end{aligned}$$

where $\mathbf{V}_h^S, \bar{\mathbf{V}}_h^S \in \mathbb{R}^{N \times (N-1)}$, and $\underline{\varphi}_h = (\varphi_1, \dots, \varphi_{N-1})^T$.

\mathbf{V}_h^S was implemented using the analytical formula (3.1), while $\bar{\mathbf{V}}_h^S$ was computed through Gauss-Legendre quadrature.

For the remaining operators, first recall $\frac{d}{dx} : \tilde{H}^{1/2}(\Gamma) \rightarrow \tilde{H}_{(0)}^{-1/2}(\Gamma)$ and $(\frac{d}{dx})^* : H_*^{1/2}(\Gamma) \rightarrow H^{-1/2}(\Gamma)$ as defined in Section 2.1.2. It is worth mentioning the first operator corresponds to the classical derivative while the second should be considered in a distributional sense.

Nevertheless, for implementation purposes, they behave the same. Since we have N mesh points and $N - 1$ mesh elements, we define the discrete operator $\mathcal{D} \in \mathbb{R}^{(N-1) \times N}$ through the following decomposition

$$\mathcal{D}_h = \Delta x^{-1} \mathbf{L}$$

where

$$\Delta x^{-1} = \text{diag}\left(\frac{1}{x_{i+1} - x_i}\right) \in \mathbb{R}^{(N-1) \times (N-1)},$$

and

$$\mathbf{L} = \begin{pmatrix} -1 & 1 & 0 & \cdots & 0 \\ 0 & -1 & 1 & \cdots & 0 \\ \vdots & & \ddots & & \vdots \\ 0 & \cdots & 0 & -1 & 1 \end{pmatrix}, \quad \in \mathbb{R}^{(N-1) \times (N)}.$$

Then, combining the above and the definitions in (2.6), we can write the strong formulations of the hypersingular and modified hypersingular operators in the discrete proxy as the following matrix products

$$\mathbf{W}_h^S := -\mathcal{D}_h \mathbf{V}_h^S \mathcal{D}_h, \quad \bar{\mathbf{W}}_h^S := -\mathcal{D}_h \bar{\mathbf{V}}_h^S \mathcal{D}_h.$$

3.5. Tensors for the Augmented Operators

Since $\ker \mathbf{V}_h \neq \emptyset$ and $\ker \bar{\mathbf{W}}_h \neq \emptyset$, the preconditioners arising from \mathbf{V} and $\bar{\mathbf{W}}$ are singular. Therefore, the augmented operators allow us not only to avoid the related space restrictions but also correct the matrices required for our preconditioning strategy. These corrections are done via adding tensor operators defined in (2.12) and (2.13). We will call them \mathbf{O}_V and $\mathbf{O}_{\bar{W}}$ respectively, honoring the operator they rectify. In the aim of implementing these tensors,

we introduce the following auxiliary vectors

$$\begin{aligned}\mathbf{f}_1[j] &:= \langle 1, q_j \rangle = \text{diff}(\mathbf{x}), & q_j &\in \mathcal{S}^{-1,0}(\Gamma_h), \\ \mathbf{g}_\omega^\perp[j] &:= \left\langle \frac{1}{\omega}, b_j \right\rangle, & b_j &\in \mathcal{S}^{0,1}(\Gamma_h).\end{aligned}$$

Then, we reduce our implementation to the following vector product

$$\mathbf{O}_V := \mathbf{f}_1 \mathbf{f}_1^T \in \mathbb{R}^{N-1}, \quad \mathbf{O}_W := \mathbf{g}_\omega^\perp \mathbf{g}_\omega^{\perp T} \in \mathbb{R}^N.$$

3.6. Dual Parity Operators

We point out that the dual parity operator \mathbf{t} from Theorem 1.1 agrees with the inner product in $L^2(\Gamma)$. The spaces X_h and Y_h in Cases A-D are chosen as defined in Section 2.2, see Table 2.2 for a summary.

The following subsections develop the explicit computation of \mathbf{T}_h for each setting. Since we use the locally supported basis functions illustrated in Figures 2.2– 2.5, the resulting “primal-dual mass matrices” \mathbf{T}_h are tridiagonals.

3.6.1. $X := \tilde{H}^{-1/2}(\Gamma), Y := H^{1/2}(\Gamma)$ (Case A)

Since $\mathbf{t} : \tilde{H}^{-1/2}(\Gamma) \rightarrow H^{1/2}(\Gamma)$, we have $\mathbf{t} := \langle \psi_h, w_h \rangle$, where $\psi_h \in \mathcal{S}^{-1,0}(\Gamma_h)$ and $w_h \in \bar{\mathcal{S}}^{0,1}(\hat{\Gamma}_h)$. Therefore, it’s discretized version is given by

$$\mathbf{T}_h[i, j] := \langle q_i, b_j \rangle,$$

which leads us to the following expression

$$\mathbf{T}_h = \frac{1}{4} \begin{pmatrix} h_1 & b_1 & \cdots & 0 & \cdots & 0 & 0 \\ \vdots & & \ddots & & \ddots & & \vdots \\ 0 & \cdots & a_i & d_i & b_i & \cdots & 0 \\ \vdots & & \ddots & & \ddots & & \vdots \\ 0 & 0 & \cdots & 0 & \cdots & a_{n-1} & h_{n-1} \end{pmatrix},$$

where $a_i = \frac{h_{i-1}^2}{h_{i-1}+h_i}$, $b_i = \frac{h_{i+1}^2}{h_i+h_{i+1}}$, and $d_i := \left(\frac{h_i^2+2h_{i-1}h_i}{h_{i-1}+h_i} + \frac{h_i^2+2h_ih_{i+1}}{h_i+h_{i+1}} \right)$.

3.6.2. $X := \tilde{H}^{1/2}(\Gamma)$, $Y := H^{-1/2}(\Gamma)$ (Case B)

In this case $\mathbf{t} : \tilde{H}^{1/2}(\Gamma) \rightarrow H^{-1/2}(\Gamma)$, consequently $w_h \in \mathcal{S}_0^{0,1}(\Gamma_h)$, $\psi_h \in \bar{\mathcal{S}}^{-1,0}(\hat{\Gamma}_h)$, and $\mathbf{t} := \langle w_h, \psi_h \rangle$.

Moreover, its associated $(N-2) \times (N-2)$ matrix has entries

$$\mathbf{T}_h = \frac{1}{8} \begin{pmatrix} h_1 + 3c_1 & h_2 & 0 & 0 & 0 & 0 & \cdots & 0 & 0 \\ \vdots & & \ddots & & \ddots & & & \vdots & 0 \\ 0 & 0 & \cdots & h_i & 3c_i & h_{i+1} & \cdots & 0 & 0 \\ 0 & \vdots & & \ddots & & & \ddots & & \vdots \\ 0 & 0 & \cdots & 0 & 0 & 0 & 0 & h_{N-2} & 3c_{N-2} + h_{N-1} \end{pmatrix}, \quad (3.2)$$

where $h_i = x_{i+1} - x_i > 0$ and $c_i := h_i + h_{i+1} > 0$.

3.6.3. $X := H^{-1/2}(\Gamma)$, $Y := \tilde{H}^{1/2}(\Gamma)$ (Case C)

Now, due to $\psi_h \in \mathcal{S}^{-1,0}(\Gamma_h)$ and $w_h \in \mathcal{S}_0^{0,1}(\hat{\Gamma}_h)$, the Galerkin Matrix corresponding to $\mathbf{t} : H^{-1/2}(\Gamma) \rightarrow \tilde{H}^{1/2}(\Gamma)$ is given by $\mathbf{t} := \langle \psi_h, w_h \rangle$.

We explicitly compute it as

$$\mathbf{T}_h = \frac{1}{4} \begin{pmatrix} h_1 + c_1 & b_1 & 0 & 0 & 0 & 0 & \cdots & 0 & 0 \\ a_2 & d_2 & b_2 & 0 & 0 & 0 & \cdots & 0 & 0 \\ 0 & \vdots & & \ddots & \ddots & & & \vdots & 0 \\ 0 & 0 & \cdots & a_i & d_i & b_i & \cdots & 0 & 0 \\ 0 & \vdots & & \ddots & \ddots & & & \vdots & 0 \\ 0 & 0 & \cdots & 0 & 0 & 0 & a_{n-2} & d_{n-2} & b_{n-2} \\ 0 & 0 & \cdots & 0 & 0 & 0 & 0 & a_{n-1} & h_{n-1} + c_{n-1} \end{pmatrix},$$

where $c_1 = \frac{h_1^2+2h_2h_1}{h_1+h_2}$, $c_{n-1} = \frac{h_{n-1}^2+2h_{n-1}h_{n-2}}{h_{n-1}+h_{n-2}}$, $d_i = \frac{h_i^2+2h_{i-1}h_i}{h_{i-1}+h_i} + \frac{h_i^2+2h_ih_{i+1}}{h_i+h_{i+1}}$, $a_i = \frac{h_{i-1}^2}{h_{i-1}+h_i}$, and $b_i = \frac{h_{i+1}^2}{h_i+h_{i+1}}$.

3.6.4. $X := H^{1/2}(\Gamma), Y := \tilde{H}^{-1/2}(\Gamma)$ (Case D)

In this last case, the dual parity operator $\mathbf{t} : H^{1/2}(\Gamma) \rightarrow \tilde{H}^{-1/2}(\Gamma)$ satisfies $\mathbf{t} := \langle w_h, \psi_h \rangle$, where $w_h \in \mathcal{S}^{0,1}(\Gamma_h)$, and $\psi_h \in \mathcal{S}^{-1,0}(\hat{\Gamma}_h)$. From this, the associated “primal-dual mass matrix” has entries

$$\mathbf{T}_h [i, j] := \langle b_i, q_j \rangle,$$

which can be expressed as follows

$$\mathbf{T}_h = \frac{1}{8} \begin{pmatrix} 3h_1 & h_1 & 0 & 0 & 0 & 0 & \cdots & 0 & 0 \\ h_1 & 3d_2 & h_2 & 0 & 0 & 0 & \cdots & 0 & 0 \\ 0 & \vdots & & \ddots & & \ddots & & \vdots & 0 \\ 0 & 0 & \cdots & h_{i-1} & 3s_I & h_i & \cdots & 0 & 0 \\ 0 & \vdots & & \ddots & & \ddots & & \vdots & 0 \\ 0 & 0 & \cdots & 0 & 0 & 0 & h_{n-2} & 3d_{n-1} & h_{n-1} \\ 0 & 0 & \cdots & 0 & 0 & 0 & 0 & h_{n-1} & 3h_{n-1} \end{pmatrix},$$

where $d_i = h_{i-1} + h_i = h_i = x_{i+1} - x_i > 0$.

3.7. Helmholtz Equation Integral Operators Implementation

The boundary integral operators corresponding to the Helmholtz equation were already introduced in Remark 2.2. We recall from (2.18) that they admit the next splitting

$$\mathbf{V}^k = \frac{i}{4\pi} \mathbf{V} + \mathbf{H}^k, \quad \mathbf{W}^k = \frac{i}{4\pi} (\mathbf{W} + k^2 \mathbf{V}) + \mathbf{L}^k.$$

Therefore, as \mathbf{V}_h and \mathbf{W}_h were addressed in Sections 3.3.1 and 3.3.2, the remaining step to complete the implementation of our Helmholtz BIOs is to compute the following matrices:

$$\begin{aligned} \mathbf{H}_h^k [i, j] &= \langle \mathbf{H}^k q_i, q_j \rangle, \\ \mathbf{L}_h^k [i, j] &= \langle \mathbf{L}^k b_i, b_j \rangle, \quad b_i, b_j \in \mathcal{S}_0^{0,1}(\Gamma_h). \end{aligned}$$

Since H^k and L^k are compact, we use Gauss-Legendre quadrature to calculate their corresponding matrices. For the sake of completeness, we dedicate the remaining of this Section to show how we derived the decomposition for W^k .

Consider the usual definition of this operator

$$W^k \alpha(x) := \frac{i}{4} \frac{\partial}{\partial n_x} \int_{\Gamma} u(x) \frac{\partial}{\partial n_{x'}} H_0^{(1)}(k|x-x'|) dx', \quad \forall x \in \Gamma,$$

By defining $r = \sqrt{(x-x')^2 + (y-y')^2}$, we can rewrite the following

$$\frac{\partial H_0^{(1)}(k|x-x'|)}{\partial n_{x'}} = \left[\frac{\partial H_0^{(1)}(kr)}{\partial y'} \right]_{|y'=0+}, \quad \forall x \in \Gamma,$$

Then

$$\left[\frac{\partial H_0^{(1)}(kr)}{\partial y'} \right]_{|y'=0+} = \frac{i}{4} \frac{H_1^{(1)}(kr)}{r} ky,$$

where $r = \sqrt{(x-x')^2 + (y)^2}$. Analogously, since the integral and the differential operator are interchangeable for this case, we derive

$$\begin{aligned} \frac{\partial}{\partial n_x} \frac{\partial H_0^{(1)}(kr)}{\partial n_{x'}} &= \left[\frac{\partial}{\partial y} \frac{i}{4} \frac{H_1^{(1)}(kr)}{r} ky \right]_{|y=0+} \\ &= \frac{ik}{4} \frac{H_1^{(1)}(k|x-x'|)}{|x-x'|}. \end{aligned}$$

Then, by Hankel function's properties we have the following identity

$$\frac{ik}{4} \frac{H_1^{(1)}(k|x-x'|)}{|x-x'|} = \frac{i}{4} \left[k^2 H_0^{(1)}(k|x-x'|) - \frac{d}{dx} \frac{d}{dx'} H_0^{(1)}(k|x-x'|) \right],$$

from where

$$\begin{aligned} \langle W^k u, v \rangle &:= \frac{i}{4} \int_{\Gamma} \frac{\partial}{\partial n_x} \int_{\Gamma} u(x) \frac{\partial}{\partial n_{x'}} H_0^{(1)}(k|x-x'|) dx' dx \\ &= \frac{ik^2}{4} \int_{\Gamma} \int_{\Gamma} H_0^{(1)}(k|x-x'|) u(x) v(x') dx' dx \\ &\quad - \frac{i}{4} \int_{\Gamma} \int_{\Gamma} \frac{d}{dx} \frac{d}{dx'} H_0^{(1)}(k|x-x'|) u(x) v(x') dx' dx. \end{aligned}$$

Finally, using integration by parts in the second term, we obtain

$$\begin{aligned}\langle \mathbf{W}^k u, v \rangle &= \frac{i}{4} k^2 \int_{\Gamma} \int_{\Gamma} H_0^{(1)}(k|x-x'|) u(x) v(x') dx' dx \\ &\quad + \frac{i}{4} \int_{\Gamma} \int_{\Gamma} H_0^{(1)}(k|x-x'|) u'(x) v'(x') dx' dx,\end{aligned}$$

which is

$$\langle \mathbf{W}^k u, v \rangle = \frac{i}{4} k^2 \langle \mathbf{V}^k u, v \rangle + \frac{i}{4} \langle \mathbf{V}^k u', v' \rangle.$$

Then, the proposed decomposition for \mathbf{W}^k follows from this result combined with the decomposition for \mathbf{V}^k .

3.8. Norms

Numerical errors are calculated by using the discrete energy norms inherited by the continuity and coercivity of our BIOs as shown in (Jerez-Hanckes & Nédélec, 2012; Jerez-Hanckes & Nédélec, 2011). We explicitly implemented them as follows

$$\|\varphi_h\|_{\tilde{H}_{(0)}^{-1/2}(\Gamma)}^2 = \underline{\varphi}_h^T \mathbf{V}_h \underline{\varphi}_h, \quad \forall \varphi_h = \sum_{k=1}^{N-1} \varphi_k q_k \in \mathcal{S}^{-1,0}(\Gamma_h), \quad (3.3)$$

$$\|\phi_h\|_{H^{-1/2}(\Gamma)}^2 = \underline{\phi}_h^T \bar{\mathbf{V}}_h \underline{\phi}_h, \quad \forall \phi_h = \sum_{k=1}^{N-1} \phi_k q_k \in \mathcal{S}^{-1,0}(\Gamma_h), \quad (3.4)$$

$$\|u_h\|_{\tilde{H}^{1/2}(\Gamma)}^2 = \underline{u}_h^T \mathbf{W}_h \underline{u}_h, \quad \forall u_h = \sum_{k=1}^{N-2} u_k b_k \in \mathcal{S}_0^{0,1}(\Gamma_h), \quad (3.5)$$

$$\|v_h\|_{H_*^{1/2}(\Gamma)}^2 = \underline{v}_h^T \bar{\mathbf{W}}_h \underline{v}_h, \quad \forall v_h = \sum_{k=1}^N v_k b_k \in \mathcal{S}^{0,1}(\Gamma_h), \quad (3.6)$$

where the underlined symbols represent the vector containing the coefficients of their corresponding functions. For instance, $\underline{\varphi}_h = (\varphi_1, \dots, \varphi_{N-1})^T$ denotes the coefficients for φ_h .

4. NUMERICAL EXPERIMENTS

We now provide numerical tests using three families of meshes: (i) uniform meshes with equidistant nodes, (ii) Chebychev meshes according to (2.38), which gives a smooth local refinement around the singularities, and (iii) algebraically graded meshes with grading factor $\alpha = 3$ as specified in (2.37). This last mesh also allows us to achieve a local refinement around the two end points (McLean & Steinbach, 1999).

We recall from Section 2.3.1 that these three meshes satisfy the mesh conditions required for our stability results.¹

4.1. Calderón-type Identities

On the one hand, we need to validate the implementation of our BIOs by numerically testing them. In order to achieve this purpose, we will derive systems of equations for each BIO by using the series expansion of their kernels and the Chebychev polynomial's properties summarized in Appendix A. Then we will compare the results obtained by MATLAB's command “\ ” with our analytical solution.

On the other hand, we are interested in numerically solving the integral equations for the Laplace kernel using the Calderón-type identities defined in Proposition 2.2 as inverses. Recall these inverses arise from the strong formulation of our BIOs. We will compare solutions obtained via the *direct* application of the inverses over the right hand side and their standard discrete variational forms and mandatory matrix inversion. They will be identified by subscripts \cdot_d and \cdot_v , respectively.

For each method, we will provide the obtained errors and their corresponding slopes. These slopes are calculated using

$$\tau(k) = \frac{\log(\text{Error}_{k+1}) - \log(\text{Error}_k)}{\log(N_{k+1}) - \log(N_k)}. \quad (4.1)$$

¹The numerical experiments presented in this section were performed with MATLAB R2013a, 64-bit.

4.1.1. Weakly singular operator

We consider the next formula

$$\mathbf{V} \varphi = \pi x, \quad (4.2)$$

where the exact solution is $\varphi(x) = \frac{x}{\sqrt{1-x^2}}$. We calculate the error using the energy norm combined with Chebyshev polynomial's properties as follows

$$\begin{aligned} \|\varphi - \varphi_h\|_{\mathbf{V}} &= \langle \mathbf{V}(\varphi - \varphi_h), (\varphi - \varphi_h) \rangle \\ &= \langle \mathbf{V} \varphi, \varphi \rangle - \langle \mathbf{V} \varphi_h, \varphi_h \rangle \\ (4.2) &= \left\langle \pi x, \frac{x}{\sqrt{1-x^2}} \right\rangle - \langle \mathbf{V} \varphi_h, \varphi_h \rangle \\ &= \frac{\pi^2}{2} - \underline{\varphi}_h^t \mathbf{V}_h \underline{\varphi}_h. \end{aligned} \quad (4.3)$$

The results documented in Table 4.1 and Figure 4.1 validate both methods and the implementation of \mathbf{V}_h . You may observe the direct approach performs in a poorer way, which can be explained by the fact that it uses a strong formulation of the BIOs.

TABLE 4.1. Errors obtained for \mathbf{V}_h . The first part shows the error obtained by indirect solving ($\varphi_v = \mathbf{V}_h \underline{g}_h$), while the second part exhibits our results when applying the inverse deduced from Proposition 2.2 to right hand side ($\varphi_d = \bar{\mathbf{W}}_h^S \pi x$).

N	Uniform mesh		Chebychev mesh		Algebraic mesh	
	$\ \varphi - \varphi_v\ _{\tilde{H}_{(0)}^{-1/2}}$	τ	$\ \varphi - \varphi_v\ _{\tilde{H}_{(0)}^{-1/2}}$	τ	$\ \varphi - \varphi_v\ _{\tilde{H}_{(0)}^{-1/2}}$	τ
128	1.3395e-01	-0.5041	1.9303e-02	-1.006	4.0350e-03	-1.445
256	9.4451e-02	-0.5020	9.6138e-03	-1.003	1.4819e-03	-1.452
512	6.6694e-02	-0.5010	4.7975e-03	-1.001	5.4165e-04	-1.465
1024	4.7127e-02	-0.5005	2.3964e-03	-1.002	1.9626e-04	-1.487
2048	3.3312e-02	-0.5002	1.1970e-03	-0.9969	7.0019e-05	-1.531
4096	2.3551e-02		5.9976e-04		2.4230e-05	
	$\ \varphi - \varphi_d\ _{\tilde{H}_{(0)}^{-1/2}}$	τ	$\ \varphi - \varphi_d\ _{\tilde{H}_{(0)}^{-1/2}}$	τ	$\ \varphi - \varphi_d\ _{\tilde{H}_{(0)}^{-1/2}}$	τ
128	6.7883e-02	-0.2351	9.3583e-02	-0.5290	9.3186e-02	-0.5699
256	5.7674e-02	-0.3579	6.4854e-02	-0.5148	6.2772e-02	-0.5377
512	4.5004e-02	-0.4138	4.5389e-02	-0.5075	4.3243e-02	-0.5196
1024	3.3783e-02	-0.4445	3.1929e-02	-0.5038	3.0166e-02	-0.5099
2048	2.4825e-02	-0.4631	2.2518e-02	-0.5019	2.1183e-02	-0.5051
4096	1.8010e-02		1.5902e-02		1.4926e-02	

In addition, it is worth recalling from Section 3.3 that due to cancellation phenomena, the operators used for the algebraic mesh differ from the other meshes. Hence, the fact that

its convergence rate for φ_v is slightly above the theoretical bound might be caused by the numerical errors introduced by the quadrature. Although it is not a proof of our hypothesis, Table 4.2 shows how this slope is regularized by increasing the number of quadrature nodes.

TABLE 4.2. Errors slopes τ obtained for V_h when using algebraic mesh and different numbers of quadrature nodes Nq .

Nq	N				
	128	256	512	1024	2048
2	-1.485	-1.529	-1.641	-2.075	-1.114
3	-1.453	-1.467	-1.495	-1.552	-1.699
4	-1.445	-1.452	-1.465	-1.487	-1.531

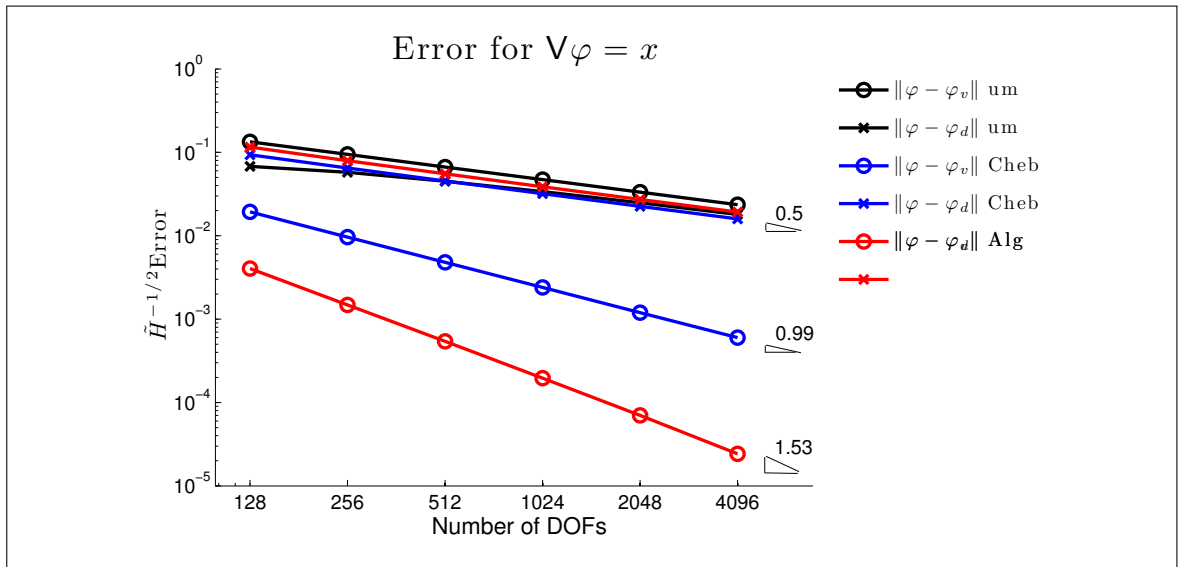


FIGURE 4.1. Plot of errors obtained by both methods for V_h . We use black to show the results when using a uniform mesh, blue for the Chebyshev mesh, and red for the algebraically graded mesh.

4.1.2. Hypersingular operator

Now we propose the following equation

$$W\psi = \pi, \tag{4.4}$$

which has $\psi(x) = \sqrt{1 - x^2}$ as its exact solution. This time, the errors shown in Table 4.3 and Figure 4.2, are calculated using the next error measurement

$$\|\varphi - \varphi_h\|_W = \frac{\pi^2}{2} - \underline{\varphi}_h^t W_h \underline{\varphi}_h,$$

which has been derived by using the same ideas as in (4.3).

TABLE 4.3. Errors obtained for W_h . The first part shows the error obtained by indirect solving ($\varphi_v = W_h \setminus \underline{g}_h$), while the second part exhibits our results when applying the inverse deduced from Proposition 2.2 to right hand side ($\varphi_d = \bar{V}_h^S \pi$).

N	Uniform mesh		Chebychev mesh		Algebraic mesh	
	$\ \varphi - \varphi_v\ _{\tilde{H}^{1/2}(\Gamma)}$	τ	$\ \varphi - \varphi_v\ _{\tilde{H}^{1/2}(\Gamma)}$	τ	$\ \varphi - \varphi_v\ _{\tilde{H}^{1/2}(\Gamma)}$	τ
128	1.3395e-01	-0.5041	1.9303e-02	-1.006	4.1464e-03	-1.359
256	9.4451e-02	-0.5020	9.6138e-03	-1.003	1.6168e-03	-1.205
512	6.6694e-02	-0.5010	4.7975e-03	-1.001	7.0152e-04	-0.9466
1024	4.7127e-02	-0.5005	2.3964e-03	-1.001	3.6399e-04	-0.7394
2048	3.3312e-02	-0.5003	1.1970e-03	-0.9970	2.1803e-04	-0.6109
4096	2.3551e-02		5.9976e-04		1.4276e-04	
	$\ \varphi - \varphi_d\ _{\tilde{H}^{1/2}(\Gamma)}$	τ	$\ \varphi - \varphi_d\ _{\tilde{H}^{1/2}(\Gamma)}$	τ	$\ \varphi - \varphi_d\ _{\tilde{H}^{1/2}(\Gamma)}$	τ
128	8.4742e-02	-0.3185	7.4689e-02	-0.5510	9.3182e-02	-0.5700
256	6.7956e-02	-0.3944	5.0978e-02	-0.5250	6.2769e-02	-0.5377
512	5.1702e-02	-0.4334	3.5428e-02	-0.5124	4.3241e-02	-0.5196
1024	3.8285e-02	-0.4562	2.4838e-02	-0.5061	3.0164e-02	-0.5099
2048	2.7906e-02	-0.4705	1.7488e-02	-0.5031	2.1182e-02	-0.5051
4096	2.0141e-02		1.2340e-02		1.4925e-02	

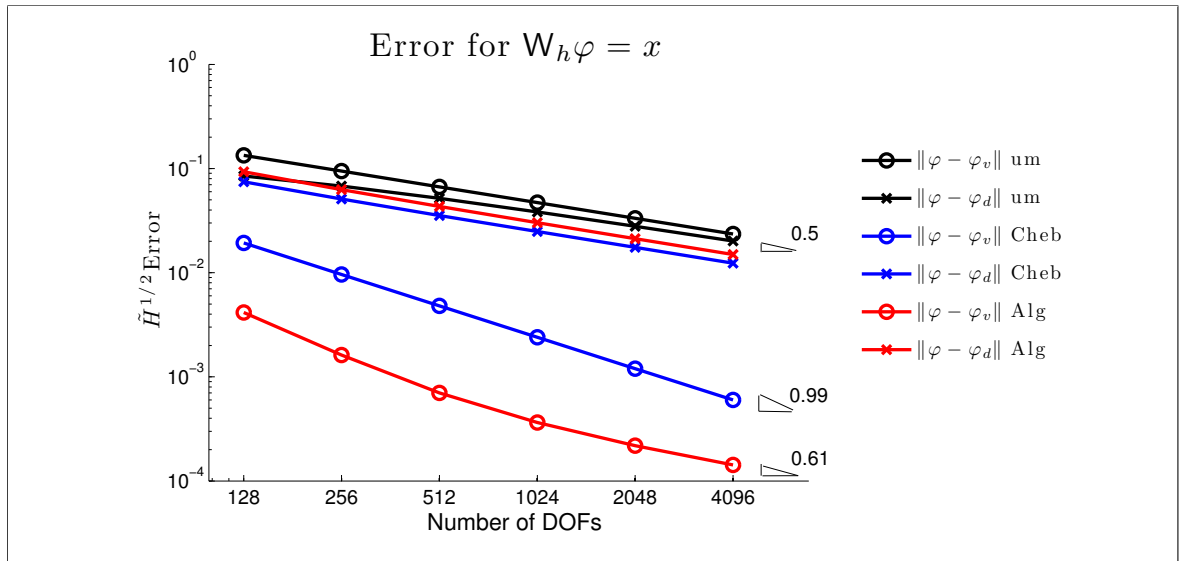


FIGURE 4.2. Plot of errors obtained by both methods for W_h . We use black to show the results when using a uniform mesh, blue for the Chebyshev mesh, and red for the algebraically graded mesh.

One would expect the convergence rates obtained for the algebraically graded mesh to be better than the ones corresponding to the Chebychev mesh. However, since W_h ponderates the entries of V_h by b'_i as shown in Section 3.3.2, the cancellation phenomena observed for the algebraic mesh might explain this behaviour.

4.1.3. Modified weakly singular operator

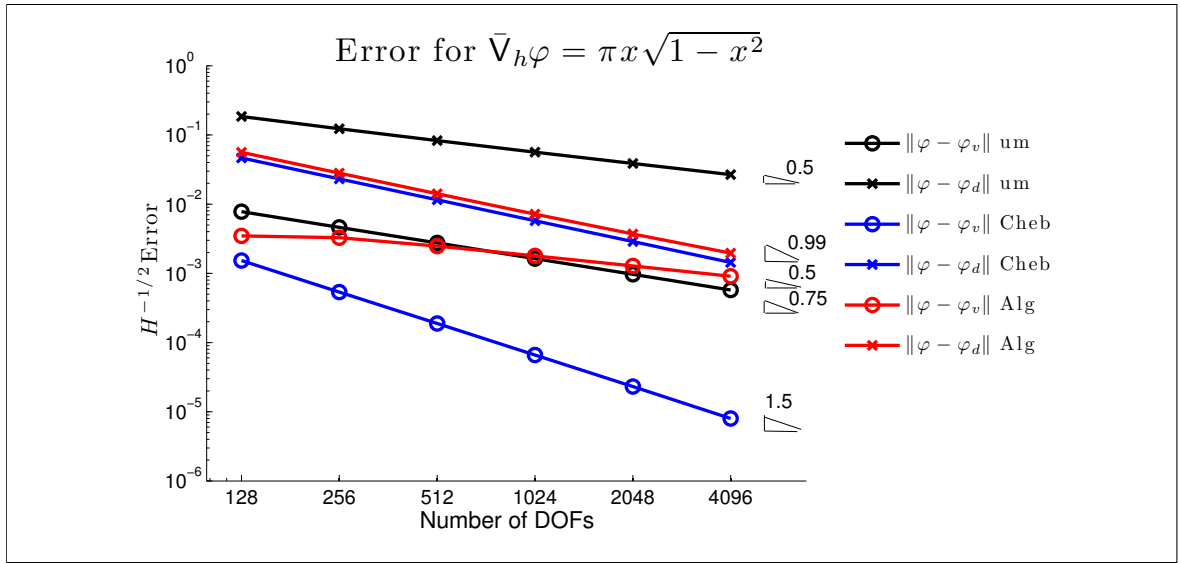


FIGURE 4.3. Plot of errors obtained by both methods for \bar{V}_h . We use black to show the results when using a uniform mesh, blue for the Chebyshev mesh, and red for the algebraically graded mesh.

We test this operator using the next formula

$$\bar{V}\phi = \pi x \sqrt{1-x^2}, \quad (4.5)$$

since its exact solution is $\phi = 2x$. We develop the following error measurement

$$\begin{aligned} \|\varphi - \varphi_h\|_{\bar{V}} &= \langle \bar{V}(\varphi - \varphi_h), (\varphi - \varphi_h) \rangle \\ (4.5) &= \langle \pi x \sqrt{1-x^2}, 2x \rangle - \langle \bar{V}\varphi_h, \varphi_h \rangle \\ &= \frac{\pi^2}{4} - \underline{\varphi}_h^t \bar{V}_h \underline{\varphi}_h, \end{aligned}$$

by using the energy norm, (4.5) and Chebyshev polynomial's orthogonality.

The results in Table 4.4, which are also summarized in Figure 4.3, support the implementation of our operator and the effectiveness of the proposed Calderón type identity.

TABLE 4.4. Errors obtained for \bar{V}_h . The first part shows the error obtained by indirect solving ($\varphi_v = \bar{V}_h \setminus g_h$), while the second part exhibits our results when applying the inverse deduced from Proposition 2.2 to right hand side ($\varphi_d = W_h^S \pi x \sqrt{1-x^2}$).

N	Uniform mesh		Chebychev mesh		Algebraic mesh	
	$\ \varphi - \varphi_v\ _{H^{-1/2}(\Gamma)}$	τ	$\ \varphi - \varphi_v\ _{H^{-1/2}(\Gamma)}$	τ	$\ \varphi - \varphi_v\ _{H^{-1/2}(\Gamma)}$	τ
128	7.8061e-03	-0.7537	1.5284e-03	-1.510	3.4716e-03	-0.0858
256	4.6296e-03	-0.7510	5.3649e-04	-1.508	3.2711e-03	-0.4019
512	2.7508e-03	-0.7515	1.8859e-04	-1.510	2.4757e-03	-0.4663
1024	1.6339e-03	-0.7533	6.6203e-05	-1.518	1.7919e-03	-0.4864
2048	9.6930e-04	-0.7559	2.3120e-05	-1.535	1.2791e-03	-0.4940
4096	5.7398e-04		7.9765e-06		9.0822e-04	
	$\ \varphi - \varphi_d\ _{H^{-1/2}(\Gamma)}$	τ	$\ \varphi - \varphi_d\ _{H^{-1/2}(\Gamma)}$	τ	$\ \varphi - \varphi_d\ _{H^{-1/2}(\Gamma)}$	τ
128	1.8481e-01	-0.5877	4.6544e-02	-1.009	5.6165e-02	-0.9986
256	1.2297e-01	-0.5706	2.3132e-02	-1.004	2.8110e-02	-0.9899
512	8.2801e-02	-0.5553	1.1531e-02	-1.002	1.4153e-02	-0.9773
1024	5.6347e-02	-0.5423	5.7567e-03	-1.001	7.1887e-03	-0.9553
2048	3.8692e-02	-0.5318	2.8762e-03	-1.001	3.7073e-03	-0.9178
4096	2.6763e-02		1.4375e-03		1.9624e-03	

4.1.4. Modified hypersingular operator

Finally, consider the following equation

$$\bar{W}\psi = \frac{x}{\sqrt{1-x^2}} \quad (4.6)$$

which has $\psi = \pi x$ as its exact solution.

We exhibit the obtained errors for the variational and direct approach in Table 4.5 and Figure 4.4. Once again, both methods show the expected convergence rates, due to the solution's regularity. However, even though they support the effectiveness of the proposed Calderón type identity, we still observe a smaller convergence by this method.

TABLE 4.5. Errors obtained for \bar{W}_h . The first part shows the error obtained by indirect solving ($\varphi_v = \bar{W}_h \setminus g_h$), while the second part exhibits our results when applying the inverse deduced from Proposition 2.2 to right hand side ($\varphi_d = V_h^S x / \sqrt{1 - x^2}$).

N	Uniform mesh		Chebychev mesh		Algebraic mesh	
	$\ \varphi - \varphi_v\ _{H^{1/2}(\Gamma)}$	τ	$\ \varphi - \varphi_v\ _{H^{1/2}(\Gamma)}$	τ	$\ \varphi - \varphi_v\ _{H^{1/2}(\Gamma)}$	τ
128	1.2908e-02	-0.7772	1.3678e-02	-0.9984	5.0877e-03	-1.499
256	7.5316e-03	-0.7289	6.8462e-03	-0.9994	1.7994e-03	-1.492
512	4.5444e-03	-0.6840	3.4246e-03	-0.9997	6.3954e-04	-1.480
1024	2.8287e-03	-0.6441	1.7126e-03	-0.9999	2.2922e-04	-1.457
2048	1.8101e-03	-0.6102	8.5638e-04	-0.9999	8.3492e-05	-1.414
4096	1.1858e-03		4.2821e-04		3.1335e-05	
	$\ \varphi - \varphi_d\ _{H^{1/2}(\Gamma)}$	τ	$\ \varphi - \varphi_d\ _{H^{1/2}(\Gamma)}$	τ	$\ \varphi - \varphi_d\ _{H^{1/2}(\Gamma)}$	τ
128	4.4294e-01	-0.4203	6.3383e-02	-0.9328	8.8522e-03	-1.321
256	3.3100e-01	-0.4280	3.3203e-02	-0.9369	3.5443e-03	-1.342
512	2.4602e-01	-0.4345	1.7344e-02	-0.9411	1.3985e-03	-1.361
1024	1.8205e-01	-0.4399	9.0335e-03	-0.9451	5.4442e-04	-1.378
2048	1.3421e-01	-0.4444	4.6920e-03	-0.9487	2.0946e-04	-1.392
4096	9.8625e-02		2.4309e-03		7.9798e-05	

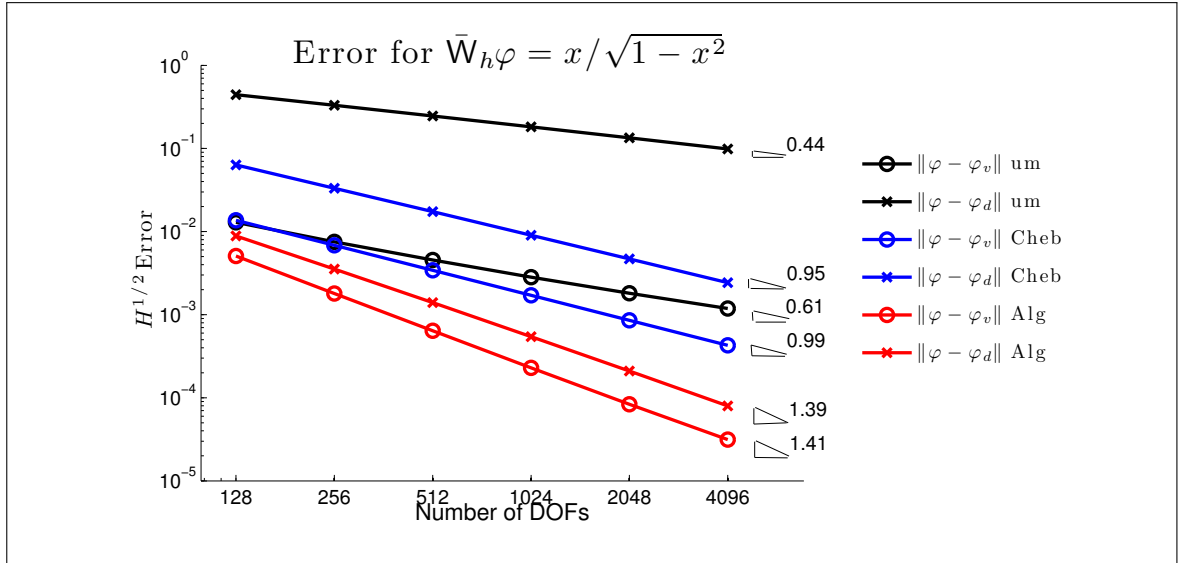


FIGURE 4.4. Plot of errors obtained by both methods for \bar{W}_h . We use black to show the results when using a uniform mesh, blue for the Chebyshev mesh, and red for the algebraically graded mesh.

4.2. Preconditioning

Theory merely gives estimates with undetermined constants. In order to get clues of their sizes, we report the practical performance of operator preconditioning for the line segment,

for all cases listed in Table 2.2, and our three different families of meshes. As elaborated in Section 2.3.3, all these meshes meet the geometric constraints of Assumptions 2.1, 2.2. The parameters α and β in the augmented bilinear forms from (2.12) and (2.13) were simply set to 1 throughout.

As stipulated by Theorem 1.1 the matrix $\mathbf{M}_h := \mathbf{T}_h^{-1} \mathbf{B}_h \mathbf{T}_h^{-H}$ was used as a preconditioner for the Galerkin matrix \mathbf{A}_h ; please refer to Theorem 1.1 for the definition of the matrices. The spaces X_h and Y_h in Cases A-D are chosen as defined in Section 2.2, see Table 2.2 for a summary.

In the numerical experiments we monitor the spectral condition numbers $\kappa(\mathbf{D}_h^{-1} \mathbf{A}_h)$ and $\kappa(\mathbf{M}_h \mathbf{A}_h)$ for sequences of meshes with increasing number of nodes. Here \mathbf{D}_h stands for the diagonal part of \mathbf{A}_h . We also plot the spectrum of $\mathbf{M}_h \mathbf{A}_h$. In addition, we recorded the number of iterations it took the preconditioned conjugate gradient method² to achieve a reduction of the residual norm by a factor 10^{10} . Initial guess was zero and the right hand side vectors had entries $+1$ in its upper half, -1 for the remaining components.

4.2.1. Weakly singular operator (Case A, row 1 of Table 2.2)

In this case \mathbf{A}_h is related to the weakly singular operator \mathbf{V} , whereas \mathbf{B}_h arises from the modified hypersingular operator $\bar{\mathbf{W}}$. The results are shown in Table 4.6 and reveal that the new operator preconditioning strategy achieves condition numbers that are essentially independent of the resolution of the meshes. Moreover, in Figure 4.5 we observe pronounced and mesh-independent clustering of the eigenvalues of the preconditioned matrices.

For comparison we include results obtained for operator preconditioning with “operators of opposite order” in the spirit of (McLean & Steinbach, 1999). There \mathbf{B}_h is replaced with Galerkin matrices associated with the *unmodified* hypersingular operator \mathbf{W} . For its discretization we used two different boundary element spaces:

²We used the implementation of the preconditioned conjugate gradient method provided by MATLAB’s `pcg` function. For the Helmholtz equation we used MATLAB’s `gmres` function instead.

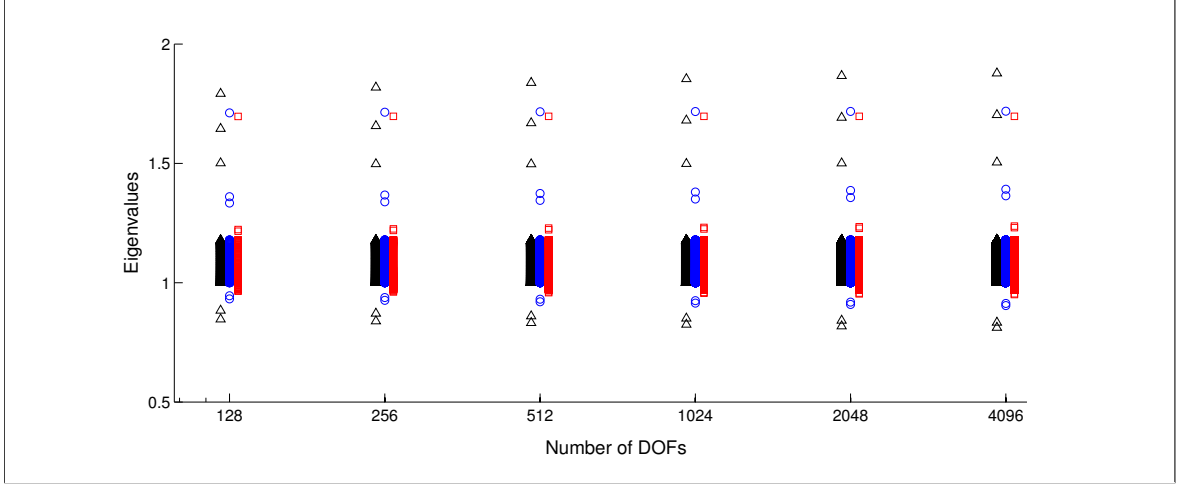


FIGURE 4.5. Plot of spectrum for V_h preconditioned by M_h (Case A, row 1 of Table 2.2) for our three meshes. We use black triangles to show the eigenvalues when using a uniform mesh, blue circles for the Chebychev mesh, and red squares for the algebraically graded mesh.

- (i) We may choose the trial and test space $S_0^{0,1}(\hat{\Gamma}_h)$ on the dual mesh (from Case C, see Figure 2.4) and obtain the Galerkin matrix \hat{B}_h^C . This spawns the preconditioning matrix $\hat{M}_h^C := \mathbf{T}_h^{-1} \hat{B}_h^C \mathbf{T}_h^{-T}$.
- (ii) We may also refrain from enforcing zero boundary conditions and use the space $\bar{S}^{0,1}(\hat{\Gamma}_h)$ on the dual mesh (from Case A, see Figure 2.2). However, by doing this, we will end up with a singular Galerkin matrix \hat{B}_h^A . Consequently, we have to regularize it by adding a rank-1 correction that removes the kernel. To state it, we use the same notation as in Section 3.5 and we write \mathbf{g}_1 and $\mathbf{g}_{\frac{1}{\omega}}$ for the column vectors that arise from the Galerkin discretization of the linear forms $v \mapsto \langle 1, v \rangle$ and $v \mapsto \langle \omega^{-1}, v \rangle$, respectively, on $\bar{S}^{0,1}(\hat{\Gamma}_h)$. Then the correction can be implemented by adding the matrices $\mathbf{g}_1 \mathbf{g}_1^T$ or $\mathbf{g}_{\frac{1}{\omega}} \mathbf{g}_{\frac{1}{\omega}}^T$. This yields the following matrix representations of the preconditioners:

$$\hat{M}_{1h}^A := \mathbf{T}_h^{-1} \left(\hat{B}_h^A + \mathbf{g}_1 \mathbf{g}_1^T \right) \mathbf{T}_h^{-T}, \quad \hat{M}_{\omega h}^A := \mathbf{T}_h^{-1} \left(\hat{B}_h^A + \mathbf{g}_{\frac{1}{\omega}} \mathbf{g}_{\frac{1}{\omega}}^T \right) \mathbf{T}_h^{-T},$$

For all these preconditioners we still expect a logarithmic growth of $\kappa(\hat{M}_{*h}^* \mathbf{A}_h)$. The measured condition numbers are listed in Table 4.7 and display the expected moderate growth as the meshes are refined. Obviously, judged by the condition numbers, our new preconditioner

\mathbf{M}_h is superior to any $\widehat{\mathbf{M}}_{*h}^*$. The gain in terms of speed of convergence of the CG iteration is not as impressive.

TABLE 4.6. Performance of preconditioners for V_h (Case A, row 1 of Table 2.2).

N	Uniform mesh			Chebychev mesh			Algebraic mesh		
	$\mathbf{D}_h^{-1}\mathbf{A}_h$	$\widehat{\mathbf{M}}_h^C\mathbf{A}_h$	$\mathbf{M}_h\mathbf{A}_h$	$\mathbf{D}_h^{-1}\mathbf{A}_h$	$\widehat{\mathbf{M}}_h^C\mathbf{A}_h$	$\mathbf{M}_h\mathbf{A}_h$	$\mathbf{D}_h^{-1}\mathbf{A}_h$	$\widehat{\mathbf{M}}_h^C\mathbf{A}_h$	$\mathbf{M}_h\mathbf{A}_h$
Spectral Condition numbers κ									
128	272.8	26.56	2.117	314.2	57	1.836	392.7	94.62	1.760
256	547.7	30.51	2.167	660.8	64.53	1.852	845.6	108.2	1.765
512	1098	33.95	2.210	1375	72.03	1.865	1794	122.1	1.771
1024	2198	37.11	2.248	2841	79.62	1.878	3765	136.2	1.776
2048	4397	40.13	2.282	5837	87.34	1.890	7843	150.7	1.781
4096	8797	43.08	2.313	11950	95.17	1.901	16240	165.4	1.785
Numbers of PCG iterations									
128	56	11	10	67	13	10	63	15	8
256	77	12	10	98	14	10	90	15	8
512	106	12	10	140	14	11	127	15	8
1024	145	12	10	205	14	11	177	16	8
2048	201	12	10	290	15	11	249	16	8
4096	273	12	10	417	15	11	347	16	8

TABLE 4.7. Results for operator preconditioning of V_h (Case A) with different (regularized) discrete versions of the unmodified hypersingular operator W

N	Uniform mesh			Chebychev mesh			Algebraic mesh		
	$\widehat{\mathbf{M}}_{1h}^A\mathbf{A}_h$	$\widehat{\mathbf{M}}_{\omega h}^A\mathbf{A}_h$	$\widehat{\mathbf{M}}_h^C\mathbf{A}_h$	$\widehat{\mathbf{M}}_{1h}^A\mathbf{A}_h$	$\widehat{\mathbf{M}}_{\omega h}^A\mathbf{A}_h$	$\widehat{\mathbf{M}}_h^C\mathbf{A}_h$	$\widehat{\mathbf{M}}_{1h}^A\mathbf{A}_h$	$\widehat{\mathbf{M}}_{\omega h}^A\mathbf{A}_h$	$\widehat{\mathbf{M}}_h^C\mathbf{A}_h$
Spectral Condition numbers κ									
128	7.113	7.035	26.56	9.661	9.638	57	16.18	16.17	94.62
256	7.714	7.648	30.51	11.61	11.59	64.53	20.38	20.38	108.2
512	8.370	8.311	33.95	13.75	13.75	72.03	25.08	25.08	122.1
1024	9.082	9.028	37.11	16.12	16.12	79.62	30.29	30.29	136.2
2048	9.845	9.796	40.13	18.68	18.67	87.34	36.01	36.01	150.7
4096	10.66	10.61	43.08	21.43	21.42	95.17	42.25	42.25	165.4
Numbers of PCG iterations									
128	11	11	11	13	12	13	15	14	15
256	11	11	12	14	13	14	16	15	15
512	12	11	12	14	14	14	16	16	15
1024	12	11	12	15	14	14	17	16	16
2048	12	12	12	16	15	15	18	17	16
4096	12	12	12	16	15	15	18	17	16

4.2.2. Hypersingular operator (Case B, row 2 of Table 2.2)

Now, \mathbf{A}_h is the Galerking matrix corresponding to the hypersingular operator W , and the modified weakly singular operator \bar{V} gives rise to \mathbf{B}_h . As before, we also compare

with the sub-optimal “opposite order” preconditioner \widehat{M}_h obtained by replacing \bar{V} with the unmodified operator V .

TABLE 4.8. Performance of preconditioners for for W_h (Case B, row 2 of Table 2.2).

N	Uniform mesh			Chebychev mesh			Algebraic mesh		
	$D_h^{-1}A_h$	$\widehat{M}_h A_h$	$M_h A_h$	$D_h^{-1}A_h$	$\widehat{M}_h A_h$	$M_h A_h$	$D_h^{-1}A_h$	$\widehat{M}_h A_h$	$M_h A_h$
128	62.1	6.16	1.335	46.46	13.27	4.729	42.07	54.72	12.89
256	124.8	7.003	1.335	93.28	16.36	4.731	84.51	69.87	12.89
512	250.2	7.902	1.335	186.9	19.79	4.732	169.7	86.95	12.89
1024	500.9	8.861	1.335	374.2	23.58	4.732	341.3	105.8	12.90
2048	1002	9.879	1.335	748.8	27.71	4.732	682.8	126.7	12.90
4096	2006	10.96	1.335	1499	32.2	4.732	1366	149.6	12.90
Numbers of PCG iterations									
128	28	9	9	26	13	9	27	16	10
256	40	9	8	37	14	9	39	17	10
512	58	10	8	52	15	9	57	17	10
1024	84	10	8	74	16	9	110	18	10
2048	119	12	8	101	16	9	156	18	10
4096	169	11	8	136	16	9	222	20	10

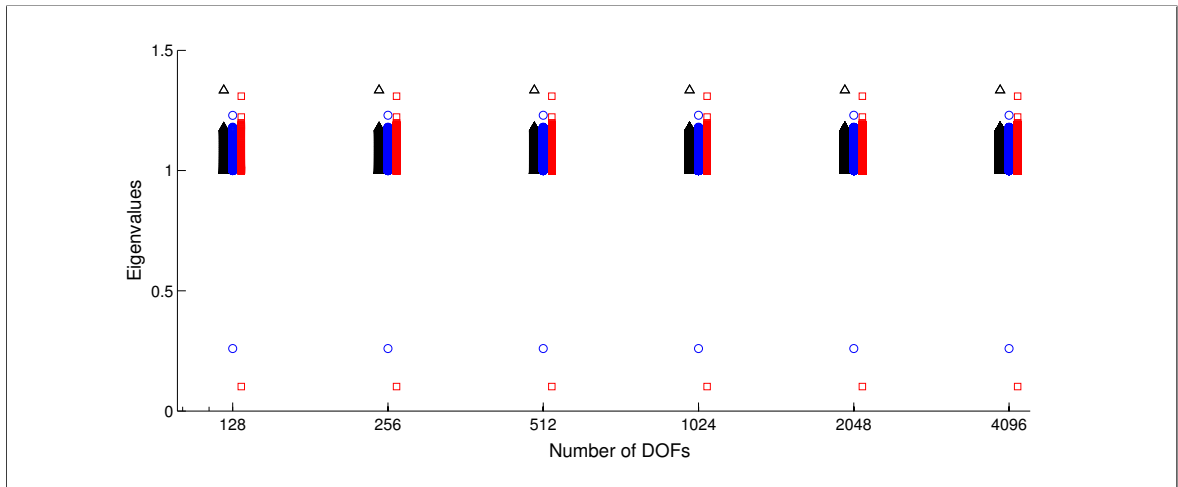


FIGURE 4.6. Plot of spectrum for W_h preconditioned by M_h (Case B, row 2 of Table 2.2) for our three meshes. We use black triangles to show the eigenvalues when using a uniform mesh, blue circles for the Chebychev mesh, and red squares for the algebraically graded mesh.

Mesh-independent performance of the new preconditioner and its superiority to other approaches is confirmed by the data of Table 4.8. These results are consistent with the plot of the spectrum for $M_h A_h$, which is shown in Figure 4.6.

4.2.3. Modified weakly singular operator (Case C, row 3 of Table 2.2)

Although one would not try to solve an equation associated to \bar{V} , it is interesting to also study the preconditioning strategy related to the case when \mathbf{A}_h and \mathbf{B}_h arise from \bar{V} and W , respectively. For this reason do not show PCG results for this operator. Spectral condition numbers are documented in Table 4.9, while the obtained spectrum is shown in Figure 4.7. We observe the growth of the condition number is once again minimal.

TABLE 4.9. Spectral condition numbers obtained for \bar{V}_h (Case C, row 3 of Table 2.2).

N	Uniform mesh		Chebychev mesh		Algebraic mesh	
	$\kappa(\mathbf{D}_h^{-1}\mathbf{A}_h)$	$\kappa(\mathbf{M}_h\mathbf{A}_h)$	$\kappa(\mathbf{D}_h^{-1}\mathbf{A}_h)$	$\kappa(\mathbf{M}_h\mathbf{A}_h)$	$\kappa(\mathbf{D}_h^{-1}\mathbf{A}_h)$	$\kappa(\mathbf{M}_h\mathbf{A}_h)$
128	210	8.726	154	11.78	111.5	13.01
256	420.4	9.195	308.5	11.82	223.8	13.01
512	840	9.442	616.7	11.83	448.1	13.01
1024	1677	9.569	1232	11.83	895.9	13.01
2048	3348	9.634	2459	11.83	1812	13.01
4096	6684	9.666	4911	11.84	3675	13.01

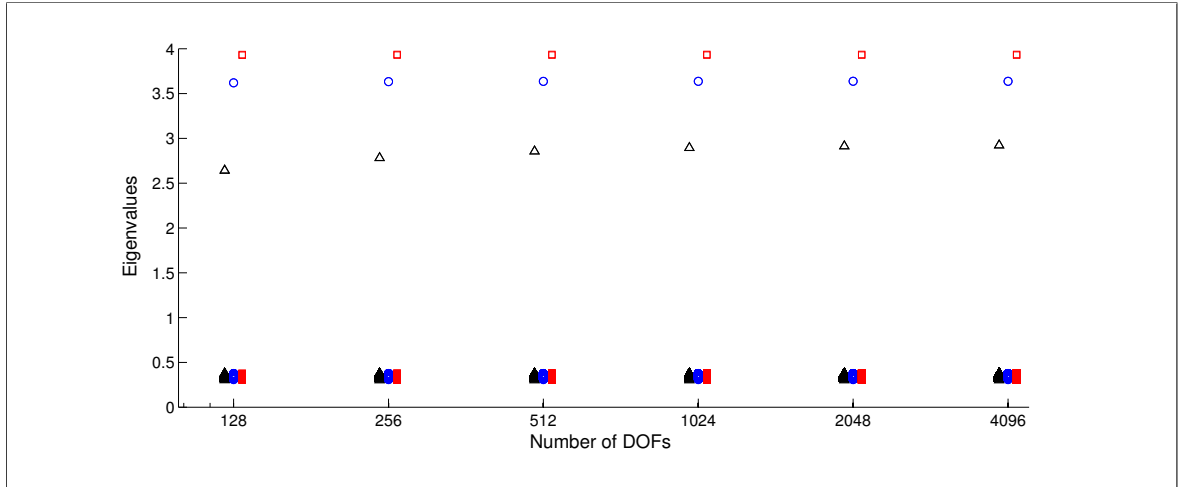


FIGURE 4.7. Plot of spectrum for \bar{V}_h preconditioned by \mathbf{M}_h (Case C, row 3 of Table 2.2) for our three meshes. We use black triangles to show the eigenvalues when using a uniform mesh, blue circles for the Chebychev mesh, and red squares for the algebraicly graded mesh.

4.2.4. Modified hypersingular operator (Case D, row 4 of Table 2.2)

For this final case, \mathbf{A}_h is related to \bar{W} and \mathbf{B}_h comes from V . Once again, since the operator is not related to a BVP, we are just interested in studying the obtained condition

numbers and eigenvalues. The results in Table 4.10 and Figure 4.8 support that our preconditioner is effective. Notice that for the Algebraicly graded mesh, the behaviour of the eigenvalues differs from the other two meshes. This might be explained for the special code considerations included in that case to avoid cancellation.

TABLE 4.10. Spectral condition numbers obtained for \bar{W}_h (Case D, row 4 of Table 2.2).

N	Uniform mesh		Chebychev mesh		Algebraic mesh	
	$\kappa(\mathbf{D}_h^{-1}\mathbf{A}_h)$	$\kappa(\mathbf{M}_h\mathbf{A}_h)$	$\kappa(\mathbf{D}_h^{-1}\mathbf{A}_h)$	$\kappa(\mathbf{M}_h\mathbf{A}_h)$	$\kappa(\mathbf{D}_h^{-1}\mathbf{A}_h)$	$\kappa(\mathbf{M}_h\mathbf{A}_h)$
128	54.17	1.695	51.53	1.693	72.14	1.741
256	108.9	1.694	103.3	1.693	144.2	1.744
512	218.4	1.694	206.8	1.693	288.2	1.744
1024	437.3	1.693	413.9	1.693	576.4	1.745
2048	875.2	1.693	828.1	1.693	1153	1.745
4096	1751	1.693	1657	1.693	2305	1.745

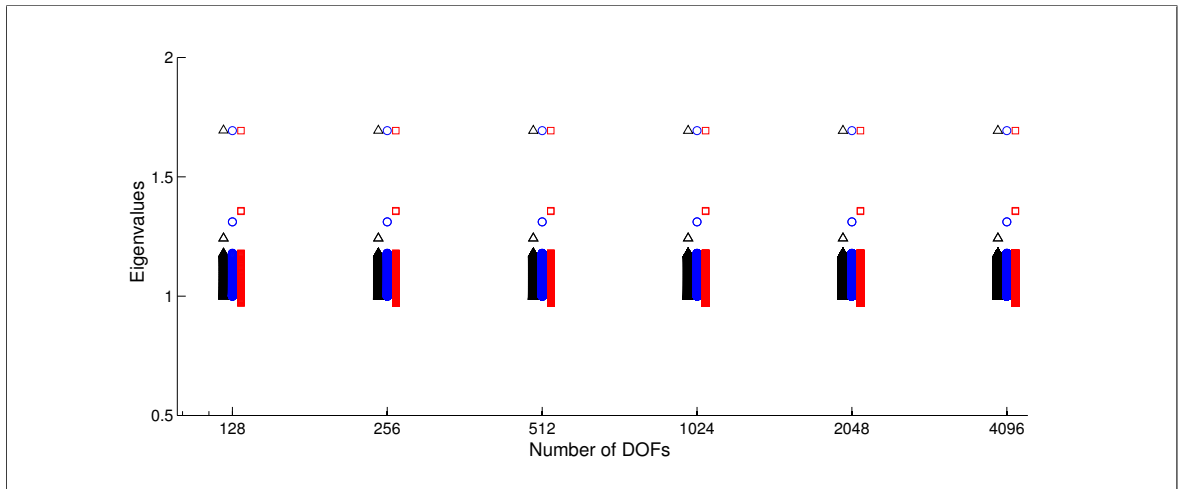


FIGURE 4.8. Plot of spectrum for \bar{W}_h preconditioned by \mathbf{M}_h (Case D, row 4 of Table 2.2) for our three meshes. We use black triangles to show the eigenvalues when using a uniform mesh, blue circles for the Chebychev mesh, and red squares for the algebraicly graded mesh.

4.2.5. Boundary integral operators for Helmholtz equation

In order to precondition the Galerkin matrices spawned by \mathbf{V}_h^k and \mathbf{W}_h^k from (2.16), we use the splittings (2.18) and pursue the same strategy that we used for \mathbf{V}_h (case A) and \mathbf{W}_h (case B), respectively. For the sake of clarity, we will denote by \mathbf{M}_h the preconditioner

arising from \bar{W}_h , and \widetilde{M}_h the one related to \bar{V}_h . Table 4.11 gives measurements of numbers of GMRES iterations for the diagonally scaled and operator preconditioned Helmholtz operators using *uniform* mesh and for different wave numbers k . Observe that for fixed k , the number of iterations for each operator becomes almost independent of N , when our new operator preconditioning approach is applied. This is also documented in Figures 4.9, 4.10, and 4.11, which reveals relative error convergence results for the GMRES implementations already described.

TABLE 4.11. GMRES iteration counts for Helmholtz operators using $k = 1, 4, 8$ as wave numbers.

N	Case A						Case B					
	V_h^1	$M_h V_h^1$	V_h^4	$M_h V_h^4$	V_h^8	$M_h V_h^8$	W_h^1	$\widetilde{M}_h W_h^1$	W_h^4	$\widetilde{M}_h W_h^4$	W_h^8	$\widetilde{M}_h W_h^8$
128	43	10	44	14	44	19	26	9	24	12	21	16
256	55	10	55	14	56	19	38	8	36	12	31	16
512	69	10	70	14	70	19	56	8	51	12	44	16
1024	87	11	87	14	87	19	79	8	73	12	63	15
2048	109	11	109	14	109	19	112	7	104	12	89	15
4096	136	11	136	14	136	19	158	7	147	11	126	15

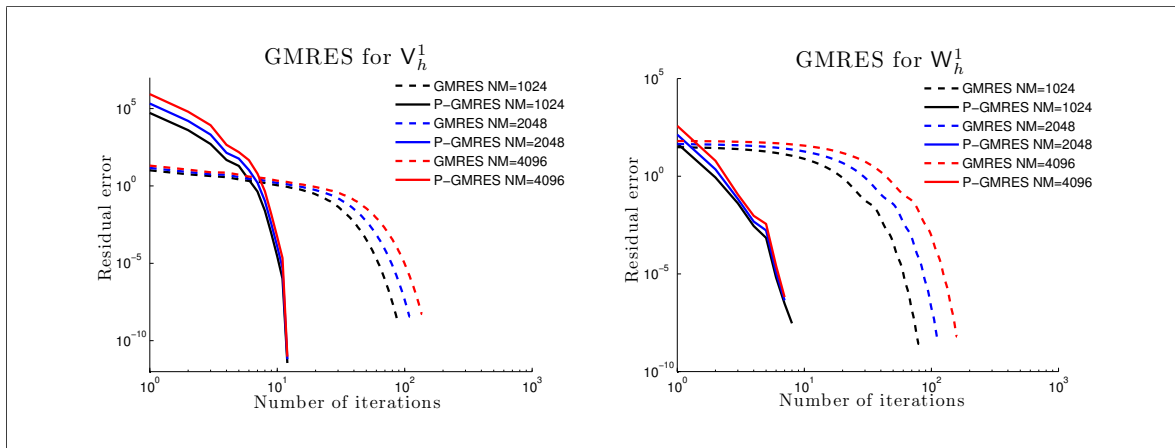


FIGURE 4.9. Helmholtz GMRES results when using an uniform mesh and wave number $k = 1$.

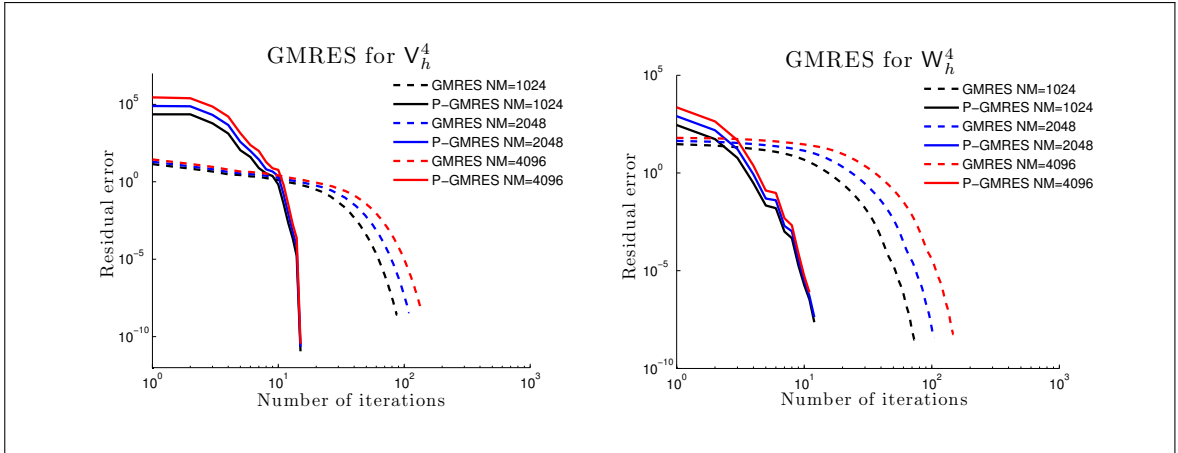


FIGURE 4.10. Helmholtz GMRES results when using a uniform mesh and wave number $k = 4$.

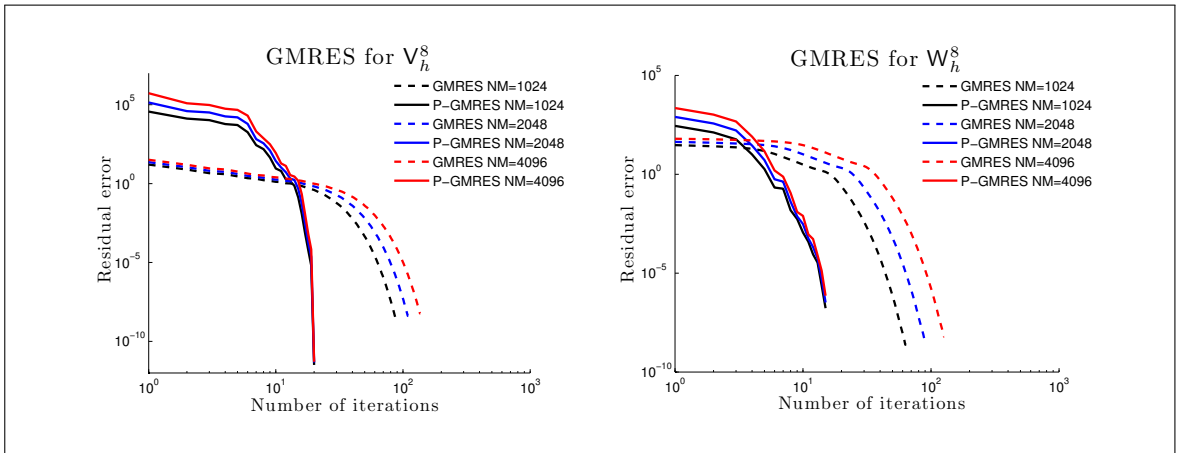


FIGURE 4.11. Helmholtz GMRES results when using a uniform mesh and wave number $k = 8$.

5. CONCLUSIONS AND FUTURE RESEARCH

We have proven the amenability of the Jerez-Hanckes and Nédélec Calderón-type identities to act as optimal preconditioners on a straight line and its extension to any smooth curve. Moreover, we observed the desired behavior in the numerical tests in Section 4.2 and its applicability to compact perturbations, as we showed for the Helmholtz Equation BIOs in section 4.2.5.

We have also extended the existing stability results in order to apply the preconditioning theory to globally non-uniform meshes satisfying some local assumptions. Furthermore, we have shown in Section 2.3.3 that the required local mesh conditions are satisfied by a large family of meshes. This is important, as mentioned in the Introduction, since the singularities of the solutions of the weakly singular operator behave as $1/\sqrt{d}$ where d is the distance to the endpoints. Therefore, allowing the use of adaptive meshes means allowing the achievement of more accuracy. In addition, these stability results are relevant for applications besides preconditioning.

However, we believe the convergence rates achieved in Section 4.1 by applying the inverses arising from the Calderón-type identities might be suboptimal. Even though, we did not carry out the analysis of the error sources related to the strong formulations of our operators, further investigation can be done by studying the effect of the underlying interpolation and projection operators, and by improving the existing code to reduce these numerical errors.

Further work relates to the implementation of the Calderón-type identities and the development of an analogous framework in a spectral discretization scheme in order to tackle high frequency problems.

On the other hand, motivated by our developments, Professor Nédélec's group is currently working on carrying out the extension of the Calderón-type identities to screens in three-dimensions using the same concepts. Moreover, we have begun working in applying their preliminaries results for preconditioning. However, as promising as it might be, this is still ongoing and future work.

APPENDIX A. CHEBYSHEV POLYNOMIALS AND PROPERTIES.

Here we list some useful identities described in (Jerez-Hanckes & Nédélec, 2012, Section 4.1.2) involving the Chebyshev polynomials of the first and second kind, i.e. $T_n(x)$ and $U_n(x)$, respectively. These are polynomials of degree n , defined for $x = \cos \theta \in (-1, 1)$ as

$$T_n(x) = \cos n\theta \quad \text{and} \quad U_n(x) = \frac{\sin(n+1)\theta}{\sin \theta}, \quad (\text{A.1})$$

Futhermore, they satisfy the following recurrence relations

$$P_n(x) = 2xP_{n-1}(x) - P_{n-2}(x), \quad n = 2, 3, \dots, \quad (\text{A.2})$$

with initial conditions $T_0(x) = 1$, $T_1(x) = x$, $U_0(x) = 1$ and $U_1(x) = 2x$.

Introduce the weight function ω as

$$\omega(x) := \sqrt{1 - x^2} \quad \text{for } x \in (-1, 1). \quad (\text{A.3})$$

The first kind Chebychev polynomials T_n are orthogonal with respect to ω^{-1} :

$$\int_{-1}^1 T_n(x) T_m(x) \omega^{-1}(x) dx = \begin{cases} 0 & n \neq m, \\ \pi/2 & n = m \neq 0, \\ \pi & n = m = 0, \end{cases} \quad (\text{A.4})$$

while the second kind Chebychev polynomials U_n verify

$$\int_{-1}^1 U_n(x) U_m(x) \omega(x) dx = \begin{cases} 0 & n \neq m, \\ \pi/2 & n = m \neq 0. \end{cases} \quad (\text{A.5})$$

Moreover, these identities allow us to define the next weighted function spaces and norms

$$L_{1/\omega}^2 := \left\{ u \text{ measurable} : \|f\|_{1/\omega}^2 := \int_{-1}^1 |f(x)|^2 \omega^{-1}(x) dx < \infty \right\},$$

$$L_{\omega}^2 := \left\{ u \text{ measurable} : \|f\|_{\omega}^2 := \int_{-1}^1 |f(x)|^2 \omega(x) dx < \infty \right\}.$$

Now, after introducing all of their notation, we are in a position to recall one of their main results:

Theorem A.1. *For a given $x \in I$, the following expansions on Chebychev polynomials as a function in $L^2_{1/\omega}$ hold:*

$$\log \frac{1}{|x-y|} = \log 2 + \sum_{n=1}^{\infty} \frac{2}{n} T_n(x) T_n(y), \quad \forall y \in I,$$

$$\log \frac{M(x,y)}{|x-y|} = \sum_{n=1}^{\infty} \frac{2w(x)w(y)}{n} U_{n-1}(x) U_{n-1}(y), \quad \forall y \in I, x \neq y.$$

Moreover, for all $(x,y) \in I \times I$, with $x \neq y$, their derivatives have the following expressions

$$\frac{1}{|x-y|^2} = \sum_{n=1}^{\infty} 2n U_{n-1}(x) U_{n-1}(y),$$

$$\frac{d^2}{dx dy} \log \frac{M(x,y)}{|x-y|} = \sum_{n=1}^{\infty} 2n \frac{T_n(x) T_n(y)}{w(x)w(y)}.$$

In addition, we summarize the relation between the Chebyshev series and the Sobolev spaces related to our BIOs.

- We express $\varphi \in \tilde{H}^{-1/2}(\Gamma)$ by:

$$\varphi(x) = \sum_{n=1}^{\infty} \varphi_n T_n(x) \omega^{-1}(x), \quad (\text{A.7})$$

$$\text{where } \varphi_n(x) = \begin{cases} \frac{1}{\pi} (\omega\varphi, T_1)_{1/\omega} & \text{if } n = 1, \\ \frac{2}{\pi} (\omega\varphi, T_n)_{1/\omega} & \text{if } n \geq 1. \end{cases}$$

And we calculate its norm as

$$\|\phi\|_{\tilde{H}^{-1/2}(\Omega)} = \sqrt{\varphi_1^2 + \sum_{n=2}^{\infty} \frac{1}{n-1} \varphi_n^2}. \quad (\text{A.8})$$

- Expand $g \in H^{1/2}(\Gamma)$ as

$$g(x) = \sum_{n=1}^{\infty} g_n T_n(x), \quad (\text{A.9})$$

$$\text{where } g_n(x) = \begin{cases} \frac{1}{\pi} (g, T_1)_{1/\omega} & \text{if } n = 1, \\ \frac{2}{\pi} (g, T_n)_{1/\omega} & \text{if } n \geq 1. \end{cases}$$

Its norm can be calculated by

$$\|g\|_{H^{1/2}(\Omega)} = \sqrt{g_1^2 + \sum_{n=2}^{\infty} (n-1)g_n^2}. \quad (\text{A.10})$$

- Consider $\phi \in H^{-1/2}(\Gamma)$, one can expand this function by

$$\phi(x) = \sum_{n=1}^{\infty} \phi_n U_n(x),$$

$$\text{where } \phi_n(x) = \begin{cases} \frac{1}{\pi} (\phi, U_1)_{\omega} & \text{if } n = 1, \\ \frac{2}{\pi} (\phi, U_n)_{\omega} & \text{if } n \geq 1. \end{cases},$$

and its norm is given by the following formula

$$\|\phi\|_{H^{-1/2}(\Omega)} = \sqrt{\sum_{n=1}^{\infty} \frac{1}{n} \phi_n^2}.$$

- Since $f \in \tilde{H}^{1/2}(\Gamma)$ we can write

$$f(x) = \sum_{n=1}^{\infty} f_n U_n(x) \omega(x),$$

$$\text{where } f_n(x) = \begin{cases} \frac{1}{\pi} (f, U_1)_\omega & \text{if } n = 1, \\ \frac{2}{\pi} (f, U_n)_\omega & \text{if } n \geq 2. \end{cases},$$

where the norm can be calculated by

$$\|f\|_{\tilde{H}^{1/2}(\Omega)} = \sqrt{\sum_{n=1}^{\infty} n f_n^2}.$$

REMARK A.1. *The following equalities hold*

$$\|\omega^{-1}\|_{\tilde{H}^{-1/2}(\Gamma)} = \|1\|_{H^{1/2}(\Gamma)} = 1, \tag{A.11}$$

due to (A.7) – (A.10),

$$\omega^{-1}(x) = 1 \frac{T_0(x)}{\omega(x)} \in \tilde{H}^{-1/2}(\Gamma),$$

and

$$1(x) = 1T_0(x) \in H^{1/2}(\Gamma).$$

APPENDIX B. PROOF OF THEOREM 2.3

Recall we first want to prove that the augmented operators pencil $\tilde{V}[\alpha]$ and $\tilde{W}[\beta]$ are bounded and elliptic in $\tilde{H}^{-1/2}(\Gamma)$ and $H^{1/2}(\Gamma)$, respectively, for $\alpha, \beta \in \mathbb{R}_+$ bounded.

Notice that $\tilde{a}_V[\alpha]$ is well defined by continuity and linearity of both V and the duality product, thus showing the boundedness of $\tilde{V}[\alpha]$. One can derive

$$\begin{aligned} \langle 1, \varphi \rangle &\leq \|1\|_{H^{1/2}(\Gamma)} \|\varphi\|_{\tilde{H}^{-1/2}(\Gamma)}, \\ (\text{Remark A.1}) \quad &\leq \|\varphi\|_{\tilde{H}^{-1/2}(\Gamma)}. \end{aligned}$$

From this we obtain the following bound

$$\begin{aligned} |\langle V \varphi, \phi \rangle + \alpha \langle 1, \varphi \rangle \langle 1, \phi \rangle| &\leq c_2^V \|\varphi\|_{\tilde{H}^{-1/2}(\Gamma)} \|\phi\|_{\tilde{H}^{-1/2}(\Gamma)} \\ &\quad + \alpha \|\varphi\|_{\tilde{H}^{-1/2}(\Gamma)} \|\phi\|_{\tilde{H}^{-1/2}(\Gamma)} \\ &= (c_2^V + \alpha) \|\varphi\|_{\tilde{H}^{-1/2}(\Gamma)} \|\phi\|_{\tilde{H}^{-1/2}(\Gamma)}, \end{aligned}$$

and we define the continuity constant

$$c_2^{\tilde{V}}(\alpha) := c_2^V + \alpha. \quad (\text{B.1})$$

Now, consider the unique decomposition for $\varphi \in \tilde{H}^{-1/2}(\Gamma)$:

$$\varphi = \tilde{\varphi} + \zeta \omega^{-1}, \quad \text{where } \tilde{\varphi} \in \tilde{H}_{(0)}^{-1/2}(\Gamma) \quad \text{and} \quad \zeta = \langle 1, \varphi \rangle. \quad (\text{B.2})$$

Given $\tilde{\varphi} \in \tilde{H}_{(0)}^{-1/2}(\Gamma)$, one can prove that $\tilde{V}[\alpha]\tilde{\varphi} = V\tilde{\varphi} \in H_*^{1/2}(\Gamma)$ in the weak sense, whence $\langle \tilde{V}[\alpha]\tilde{\varphi}, \omega^{-1} \rangle$ is equal to zero. From this we deduce

$$\begin{aligned}
\langle \tilde{V}[\alpha]\varphi, \varphi \rangle &= \langle \tilde{V}[\alpha](\tilde{\varphi} + \zeta\omega^{-1}), \tilde{\varphi} + \zeta\omega^{-1} \rangle \\
&= \langle \tilde{V}[\alpha]\tilde{\varphi}, \tilde{\varphi} \rangle + 2\zeta \langle \tilde{V}[\alpha]\tilde{\varphi}, \omega^{-1} \rangle + \zeta^2 \langle \tilde{V}[\alpha]\omega^{-1}, \omega^{-1} \rangle \\
&= \langle V\tilde{\varphi}, \tilde{\varphi} \rangle + \zeta^2 \langle \tilde{V}[\alpha]\omega^{-1}, \omega^{-1} \rangle \\
&\geq c_1^V \|\tilde{\varphi}\|_{\tilde{H}^{-1/2}(\Gamma)}^2 + \zeta^2 \langle \tilde{V}[\alpha]\omega^{-1}, \omega^{-1} \rangle \\
&\geq \min \left\{ c_1^V, \langle \tilde{V}[\alpha]\omega^{-1}, \omega^{-1} \rangle \right\} \left(\|\tilde{\varphi}\|_{\tilde{H}^{-1/2}(\Gamma)}^2 + \zeta^2 \right),
\end{aligned} \tag{B.3}$$

where c_1^V is the ellipticity constant of V (Jerez-Hanckes & Nédélec, 2012). Since $V\omega^{-1} = \pi \log 2 = C_\omega$, C_ω being a positive constant, the duality product on the second term on the right-hand side in (B.3) is equal to

$$\begin{aligned}
\langle \tilde{V}[\alpha]\omega^{-1}, \omega^{-1} \rangle &= \langle V\omega^{-1}, \omega^{-1} \rangle + \alpha \langle 1, \omega^{-1} \rangle^2 \\
&= \pi^2(\log 2 + \alpha) > 0,
\end{aligned} \tag{B.4}$$

by Chebychev's polynomial's properties on I . Furthermore, the decomposition (B.2) satisfies

$$\begin{aligned}
\|\varphi\|_{\tilde{H}^{-1/2}(\Gamma)}^2 &= \|\tilde{\varphi} + \zeta\omega^{-1}\|_{\tilde{H}^{-1/2}(\Gamma)}^2 \\
&\leq \left(\|\tilde{\varphi}\|_{\tilde{H}^{-1/2}(\Gamma)} + \zeta \|\omega^{-1}\|_{\tilde{H}^{-1/2}(\Gamma)} \right)^2 \\
&\leq 2 \left(\|\tilde{\varphi}\|_{\tilde{H}^{-1/2}(\Gamma)}^2 + \zeta^2 \|\omega^{-1}\|_{\tilde{H}^{-1/2}(\Gamma)}^2 \right) \\
&\text{(by Remark A.1)} \leq 2 \left(\|\tilde{\varphi}\|_{\tilde{H}^{-1/2}(\Gamma)}^2 + \zeta^2 \right).
\end{aligned} \tag{B.5}$$

Then, combining (B.4), (B.3), and (B.5), ellipticity follows with constant

$$c_1^{\tilde{V}}(\alpha) := \frac{\min \{ c_1^V, \pi^2(\log 2 + \alpha) \}}{2}, \quad \text{for all } \alpha > 0. \tag{B.6}$$

On the other hand, using similar steps to those employed in (B.1), the sesquilinear form $a_{\tilde{W}}[\beta](w, v)$ has a continuity constant equal to

$$c_2^{\tilde{W}}(\beta) := c_2^{\tilde{W}} + \beta, \tag{B.7}$$

for β fixed. Moreover, for $v \in H^{1/2}(\Gamma)$, the following decomposition holds

$$v = v_* + \eta \quad \text{where} \quad v_* \in H_*^{1/2}(\Gamma) \quad \text{and} \quad \eta = \langle v, \omega^{-1} \rangle. \quad (\text{B.8})$$

Since $\bar{W}\rho = 0$ for any constant ρ , we consider $\text{Ker}\bar{W} = \text{span}\{1\}$. In order to show ellipticity, we recall $g \in \tilde{H}_{(0)}^{-1/2}(\Gamma)$ and use $v_0 = 1$ as a test function. Consequently,

$$\begin{aligned} \langle \tilde{W}v_*, 1 \rangle &= \langle \bar{W}v_*, 1 \rangle + \beta \langle v_*, \omega^{-1} \rangle \langle 1, \omega^{-1} \rangle \\ &= \langle v_*, \bar{W}1 \rangle + \beta \langle v_*, \omega^{-1} \rangle \langle 1, \omega^{-1} \rangle = 0. \end{aligned}$$

Thus, as in (B.4), we observe

$$\begin{aligned} \langle \tilde{W}v, v \rangle &= \langle \tilde{W}(v_* + \eta), v_* + \eta \rangle \\ &\geq \min \left\{ c_1^{\bar{W}}, \langle \tilde{W}1, 1 \rangle \right\} \left(\|v_*\|_{H^{1/2}(\Gamma)}^2 + \eta^2 \right), \end{aligned}$$

by ellipticity of \bar{W} with constant $c_1^{\bar{W}}$, and derive

$$\langle \tilde{W}1, 1 \rangle = \langle \bar{W}1, 1 \rangle + \beta \langle 1, \omega^{-1} \rangle \langle 1, \omega^{-1} \rangle = \pi^2 \beta > 0.$$

Then, considering $\|1\|_{H^{1/2}(\Gamma)} = 1$, one can prove in an analogous way to (B.5) that

$$\begin{aligned} \|v\|_{H^{1/2}(\Gamma)}^2 &= \|v_* + \eta\|_{H^{1/2}(\Gamma)}^2 \\ &\leq 2 \left(\|v_*\|_{H^{1/2}(\Gamma)}^2 + \eta^2 \right), \end{aligned}$$

and so ellipticity of $\tilde{W}[\beta]$ follows with constant

$$c_1^{\tilde{W}}(\beta) := \frac{\min \left\{ c_1^{\bar{W}}, \pi^2 \beta \right\}}{2}, \quad \text{for all } \beta > 0. \quad (\text{B.9})$$

In what follows, we are interested in showing that the augmented variational problems are equivalent to their original problems. Our first departure problem is to find $\phi \in \tilde{H}_{(0)}^{-1/2}(\Gamma)$ such that (2.8) is satisfied for all $\psi \in \tilde{H}_{(0)}^{-1/2}(\Gamma)$. Instead of solving problem (2.8) with a constraint, consider the following saddle point problem: find $(\phi, \lambda) \in \tilde{H}^{-1/2}(\Gamma) \times \mathbb{R}$ such

that

$$\langle \mathbf{V} \phi, \psi \rangle + \lambda \langle 1, \psi \rangle = \langle f, \psi \rangle, \quad \forall \psi \in \tilde{H}^{-1/2}(\Gamma), \quad (\text{B.10a})$$

$$\langle 1, \phi \rangle = 0. \quad (\text{B.10b})$$

Again, since $\mathbf{V} \omega^{-1} = C_\omega$, $C_\omega > 0$, we have $\langle \mathbf{V} \omega^{-1}, \psi \rangle = 0$ for all $\psi \in \tilde{H}_{(0)}^{-1/2}(\Gamma)$. On the other hand, as it is shown in (Jerez-Hanckes & Nédélec, 2012, Proposition 3.1) $f \in \text{Im}_{\tilde{H}_{(0)}^{-1/2}(\Gamma)}(\mathbf{V}) \equiv H_*^{1/2}(\Gamma)$. Hence, we can use ω^{-1} as a test function in (B.10a) to derive

$$\langle \phi, \mathbf{V} \omega^{-1} \rangle + \lambda \langle 1, \omega^{-1} \rangle = 0,$$

where we have used the symmetry of \mathbf{V} . Finally, by (B.10b) we obtain

$$\lambda \langle 1, \omega^{-1} \rangle = 0,$$

and therefore $\lambda \equiv 0$. Consequently, the saddle point problem (B.10) is equivalent to finding $(\phi, \lambda) \in \tilde{H}^{-1/2}(\Gamma) \times \mathbb{R}$ such that

$$\begin{aligned} \langle \mathbf{V} \phi, \psi \rangle + \lambda \langle 1, \psi \rangle &= \langle f, \psi \rangle, \quad \forall \psi \in \tilde{H}^{-1/2}(\Gamma), \\ \langle 1, \phi \rangle - \lambda/\alpha &= 0, \end{aligned} \quad (\text{B.11})$$

with $\alpha \in \mathbb{R}_+$ a parameter to be chosen later. We obtain a new augmented variational problem by eliminating λ from (B.11): find $\phi \in \tilde{H}^{-1/2}(\Gamma)$ such that

$$\tilde{\mathbf{a}}_{\mathbf{V}}[\alpha](\phi, \psi) = \langle f, \psi \rangle, \quad \forall \psi \in \tilde{H}^{-1/2}(\Gamma), \quad \alpha > 0, \quad (\text{B.12})$$

where $\tilde{\mathbf{a}}_{\mathbf{V}}[\alpha] : \tilde{H}^{-1/2}(\Gamma) \times \tilde{H}^{-1/2}(\Gamma) \rightarrow \mathbb{C}$ is the sesquilinear form pencil associated to the augmented weakly singular operator $\tilde{\mathbf{V}}[\alpha]$ defined as

$$\langle \tilde{\mathbf{V}}[\alpha]\varphi, \psi \rangle := \langle \mathbf{V} \varphi, \psi \rangle + \alpha \langle 1, \varphi \rangle \langle 1, \psi \rangle, \quad \forall \varphi, \psi \in \tilde{H}^{-1/2}(\Gamma), \quad (\text{B.13})$$

with clear duality pairing.

Lastly, ellipticity allows the use of the Lax-Milgram lemma to guarantee uniqueness and existence of solutions for (B.12). Now, since $f \in H_*^{1/2}(\Gamma)$, when testing (B.12) with

$\psi = \omega^{-1}$ we obtain

$$C_\omega \langle 1, \varphi \rangle + \alpha \langle 1, \varphi \rangle \langle 1, \omega^{-1} \rangle = 0, \quad \text{with } \langle 1, \omega^{-1} \rangle > 0, \quad (\text{B.14})$$

and consequently, $\varphi \in \tilde{H}_{(0)}^{-1/2}(\Gamma)$, thereby proving the equivalence between the augmented problem (B.12) and the original one (2.8).

Now we focus on $\tilde{W}[\beta]$. Instead of solving problem (2.11) with a constraint, we consider the following saddle point problem: find $(w, \Lambda) \in H^{1/2}(\Gamma) \times \mathbb{R}$ such that

$$\langle \bar{W}w, v \rangle + \Lambda \langle \omega^{-1}, v \rangle = \langle g, v \rangle, \quad \forall v \in H^{1/2}(\Gamma), \quad (\text{B.15a})$$

$$\langle w, \omega^{-1} \rangle = 0. \quad (\text{B.15b})$$

The proof follows analogously to the previous case, only this time we use the fact that $\text{Ker}\bar{W} = \text{span}\{1\}$ and $v_0 = 1$ as a test function in (B.15a). Then, since $g \in \tilde{H}_{(0)}^{-1/2}(\Gamma)$ we get

$$\Lambda \langle \omega^{-1}, 1 \rangle = 0,$$

and therefore $\Lambda \equiv 0$. From this, and using similar arguments as before, we derive the augmented variational problem. The uniqueness and existence for any $g \in \tilde{H}_{(0)}^{-1/2}(\Gamma)$ follows from the ellipticity as well. In particular, when testing with $v = 1$, we deduce

$$\beta \langle w, \omega^{-1} \rangle \langle 1, \omega^{-1} \rangle = 0, \quad \langle 1, \omega^{-1} \rangle > 0, \quad (\text{B.16})$$

from where w must lie in $H_*^{1/2}(\Gamma)$, thus showing the equivalence between the augmented and original problem (2.11).

APPENDIX C. STABILITY RESULTS FOR CASE B.

As a tool we rely on the “tent functions” $b_k \in \mathcal{S}^{0,1}(\Gamma_h)$, $k = 1, \dots, N - 2$, defined by $b_k(x_i) = \delta_{(k+1)i}$ (Kronecker symbol), and we write $\omega_k := \text{supp}(b_k)$, which consists of two adjacent mesh intervals for $k = 1, \dots, N - 2$. Refer to Figure 2.3 for an illustration (drawn in blue). Moreover, we employ the piecewise constant functions $q_j \in \mathcal{S}^{-1,0}(\hat{\Gamma}_h)$, $j = 1, \dots, N - 2$ which are equal to 1 on (η_{j-1}, η_j) and vanish outside this interval of the dual mesh, see Figure 2.3 (red/green).

C.1. Proof of Lemma 2.1

We use our trial bases to write $w_h := \sum_{j=1}^{N-2} w_j b_j \in \mathcal{S}_0^{0,1}(\Gamma_h)$, and $\psi_h := \sum_{j=1}^{N-2} \psi_j q_j \in \mathcal{S}^{-1,0}(\hat{\Gamma}_h)$. Hence, we can write the dual product operator in its matricial form

$$|\langle \psi_h, w_h \rangle| := |\boldsymbol{\psi}^T \mathbb{T}_B \mathbf{w}|, \quad (\text{C.1})$$

where $\mathbb{T}_B[l, k] := \langle b_l, q_k \rangle$. Furthermore, $\mathbb{T}_B \in \mathbb{R}^{N-2, N-2}$ is a tridiagonal matrix given by the following expression

$$\mathbb{T}_B = \frac{1}{8} \begin{pmatrix} h_1 + 3c_1 & h_2 & 0 & 0 & 0 & 0 & \cdots & 0 & 0 \\ \vdots & \ddots & & \ddots & & \vdots & & 0 \\ 0 & 0 & \cdots & h_i & 3c_i & h_{i+1} & \cdots & 0 & 0 \\ 0 & \vdots & \ddots & & \ddots & & & \vdots \\ 0 & 0 & \cdots & 0 & 0 & 0 & 0 & h_{N-2} & 3c_{N-2} + h_{N-1} \end{pmatrix},$$

where $h_i = x_{i+1} - x_i > 0$ and $c_i := h_i + h_{i+1} > 0$. Observe \mathbb{T}_B is a strictly diagonal dominant matrix, furthermore it is symmetric. Then, by Gershgorin we know its eigenvalues $\lambda_1, \dots, \lambda_k, \dots, \lambda_{N-2} \in \mathbb{R}$ satisfy

$$\lambda_k \in (3c_1, 5h_1 + 3h_2) \cup \bigcup_{i=2}^{N-3} (2c_i, 4c_i) \cup (3c_{N-2}, 5h_{N-2} + 3h_{N-1}), \quad \forall k = 1, \dots, N - 2.$$

Consequently, $\lambda_{\min} > 0$ and \mathbb{T}_B is invertible. Recall $w_h := \sum_{i=1}^{N-2} w_i b_i$. Now let $\psi_h^* := \sum_{i=1}^{N-2} w_i q_i$. Then, by setting $w_0 = w_{N-1} = 0$, we have

$$\begin{aligned}
\langle \psi_h^*, w_h \rangle &= \mathbf{w}^T \mathbb{T}_B \mathbf{w} = \frac{1}{8} \left\{ w_1((4h_1 + 3h_2)w_1 + h_2w_2) \right. \\
&\quad + \sum_{i=2}^{N-3} w_i(h_i w_{i-1} + 3(h_i + h_{i+1})w_i + h_{i+1}w_{i+1}) \\
&\quad \left. + w_{N-2}(h_{N-2}w_{N-3} + (3h_{N-2} + 4h_{N-1})w_{N-2}) \right\} \\
&= \frac{1}{8} \left\{ \sum_{i=1}^{N-2} (h_i + h_{i+1})w_i^2 + h_1w_1^2 + h_{N-1}w_{N-2}^2 \right\} \\
&\quad + \frac{1}{8} \left\{ w_1(2(h_1 + h_2)w_1 + h_2w_2) \right. \\
&\quad \left. + \sum_{i=2}^{N-3} w_i(h_i w_{i-1} + 2(h_i + h_{i+1})w_i + h_{i+1}w_{i+1}) \right. \\
&\quad \left. + w_{N-2}(h_{N-2}w_{N-3} + 2(h_{N-2} + h_{N-1})w_{N-2}) \right\}, \quad (\text{C.2})
\end{aligned}$$

where the last expression on the right hand side can be seen as $\mathbf{w}^T \tilde{\mathbb{T}} \mathbf{w}$, with $\tilde{\mathbb{T}}$ denoting a strictly diagonal dominant matrix. Hence, that last term is positive and we can bound (C.2) by

$$\langle \psi_h^*, w_h \rangle \geq \frac{1}{8} \left\{ \sum_{i=1}^{N-2} (h_i + h_{i+1})w_i^2 + h_1w_1^2 + h_{N-1}w_{N-2}^2 \right\} \geq \frac{1}{3} (D_B \mathbf{w}, \mathbf{w}), \quad (\text{C.3})$$

where $D_B = \text{diag}(\mathbb{T}_B)$. On the other hand,

$$\|w_h\|_{L^2(\Gamma)}^2 = \langle w_h, w_h \rangle = \frac{1}{3} \mathbf{w}^T \text{diag}(h_i + h_{i+1}) \mathbf{w} \leq \frac{8}{9} \mathbf{w}^T \text{diag}(\mathbb{T}_B) \mathbf{w} = \frac{8}{9} (D_B \mathbf{w}, \mathbf{w}), \quad (\text{C.4})$$

and

$$\begin{aligned}
\|\psi_h^*\|_{L^2(\Gamma)}^2 &= \langle \psi_h^*, \psi_h^* \rangle \\
&= \frac{1}{2} \mathbf{w}^T \begin{pmatrix} (2h_1 + h_2) & 0 & 0 & \cdots & 0 \\ 0 & \vdots & \ddots & \vdots & 0 \\ \cdots & 0 & (h_i + h_{i+1}) & 0 & \cdots \\ 0 & \vdots & \ddots & \vdots & 0 \\ 0 & \cdots & 0 & 0 & (h_{N-2} + 2h_{N-1}) \end{pmatrix} \mathbf{w} \\
&\leq \frac{1}{2} \mathbf{w}^T \text{diag}(\mathbb{T}_B) \mathbf{w} = \frac{1}{2} (D_B \mathbf{w}, \mathbf{w}). \tag{C.5}
\end{aligned}$$

Finally, by combining (C.3), (C.5) and (C.4), we obtain

$$\begin{aligned}
\sup_{\psi_h \in \mathcal{S}^{-1,0}(\Gamma_h)} \frac{|\langle \psi_h, w_h \rangle|}{\|\psi_h\|_{L^2(\Gamma)}} &\geq \frac{\langle \psi_h^*, w_h \rangle}{\|\psi_h^*\|_{L^2(\Gamma)}} \\
&\geq \frac{\sqrt{2}}{3} (D_B \alpha, \alpha)^{1/2} \\
&\geq \sqrt{\frac{9}{8}} \frac{\sqrt{2}}{3} \|w_h\|_{L^2(\Gamma)} = \frac{1}{2} \|w_h\|_{L^2(\Gamma)}. \tag{C.6}
\end{aligned}$$

C.2. Proof of Proposition 2.2

We aim to prove the H^1 -stability for \tilde{Q}_h . With this purpose in mind, we will introduce a quasi interpolation operator as in (Steinbach, 2003, Section 1.5).

First recall $\omega_k = \text{supp}\{b_k\}$, then define the related space locally by $X_h(\omega_k) := \{b_j|_{\omega_k} : b_j \in \mathcal{S}_0^{0,1}(\Gamma_h)\}$. Let Q_h^k denote the L^2 -Projection onto the local trial space $X_h(\omega_k)$, such that for $u \in L^2(\omega_k)$

$$\langle Q_h^k u, v_h \rangle_{L^2(\omega_k)} = \langle u, v_h \rangle_{L^2(\omega_k)}, \quad \forall v_h \in X_h(\omega_k), h \in \mathbb{H}. \tag{C.7}$$

As it is shown in (Steinbach, 2003, Section 1.5), we have the stability estimate as well as the quasi optimal error estimate

$$\|Q_h^k u\|_{L^2(\omega_k)} \leq \|u\|_{L^2(\omega_k)}, \quad \text{for all } u \in L^2(\omega_k), \quad (\text{C.8})$$

$$\|(\text{Id} - Q_h^k)u\|_{L^2(\omega_k)} \leq c_{st}^{loc} \hat{h}_k |u|_{H^1(\omega_k)}, \quad \text{for all } u \in H^1(\omega_k). \quad (\text{C.9})$$

Furthermore, local quasi-uniformity gives us the following stability estimate

$$\|Q_h^k u\|_{H^1(\omega_k)} \leq \tilde{c}_{st}^{loc} \hat{h}_k \|u\|_{H^1(\omega_k)} \quad \text{for all } u \in H^1(\omega_k). \quad (\text{C.10})$$

Then, it is possible to define a quasi interpolation operator by

$$(P_h u)(x) = \sum_{k=1}^{N-2} (Q_h^k u)(x_k) \cdot b_k(x), \quad (\text{C.11})$$

which is also a projection onto $S_0^{0,1}(\Gamma_h)$. Moreover, P_h has properties which will be key pieces for the proof of Proposition 2.2. We introduce these results in the following two lemmas.

Lemma C.1 (Extension of Lemma 1.9 (Steinbach, 2003)). *Let $u \in H_0^1(\Gamma)$. Then, there exists a positive constant c_{p1} independent of h such that*

$$\|(\text{Id} - P_h)u\|_{L^2(\Gamma)} \leq c_{p1} \sum_{k \in J(l)} \hat{h}_k |u|_{H^1(\omega_k)}, \quad l = 1, \dots, N-1. \quad (\text{C.12})$$

Moreover,

$$\|P_h u\|_{H^1(\Gamma)} \leq c_{p1} \|u\|_{H^1(\Gamma)}, \quad \text{for all } u \in H_0^1(\Gamma), \quad (\text{C.13})$$

and

$$\sum_{k=1}^{N-2} \hat{h}_k^{-2} \|(\text{Id} - P_h)u\|_{L^2(\omega_k)}^2 \leq c_{p1} \|u\|_{H^1(\Gamma)}, \quad \text{for all } u \in H_0^1(\Gamma). \quad (\text{C.14})$$

Since the only difference with the original Lemma is due to the endpoints, where the arguments involved also hold, proof follows from (Steinbach, 2003, Lemma 1.9).

Lemma C.2 (Extension of Lemma 2.3 (Steinbach, 2003)). *Let condition (2.23) be satisfied and $q_k \in \mathcal{S}^{-1,0}(\hat{\Gamma}_h)$, $k = 1, \dots, N-2$. Then*

$$\sum_{l=1}^{N-1} h_l^{-2} \|v_h\|_{L^2(\tau_l)}^2 \leq c_{p2} \sum_{k=1}^{N-2} \left[\frac{\langle v_h, q_k \rangle_{L^2(\Gamma)}}{\hat{h}_k \|q_k\|_{L^2(\Gamma)}} \right]^2, \quad (\text{C.15})$$

for all $v_h \in \mathcal{S}_0^{0,1}(\Gamma_h)$ with a positive constant c_{p2} .

PROOF. This proof can be derived by adapting Steinbach's original proof (similarly to what it was shown in (Bramble, Pasciak, & Steinbach, 2002)). Therefore, we introduce his notation for the following two index sets: $I(k) := \{l \in \{1, \dots, N-1\} : \tau_l \cap \omega_k \neq \emptyset\}$ (indices of elements τ_l where b_k is not zero) and $J(l) := \{k \in \{1, \dots, N-2\} : \omega_k \cap \tau_l \neq \emptyset\}$ (indices of hat functions that do not vanish on τ_l). Since $v_h = \sum_{k=1}^{N-2} v_k b_k \in \mathcal{S}_0^{0,1}(\Gamma_h)$ we can write

$$\begin{aligned} \sum_{l=1}^{N-1} h_l^{-2} \|v_h\|_{L^2(\tau_l)}^2 &\leq c_p \sum_{l=1}^{N-1} h_l^{-2} \sum_{k \in J(l)} v_k^2 \|b_k\|_{L^2(\tau_l)}^2 \\ &\leq c_p \sum_{k=1}^{N-2} v_k^2 \sum_{l \in I(k)} h_l^{-2} \|b_k\|_{L^2(\tau_l)}^2 = c_p \sum_{k=1}^{N-2} v_k^2 \gamma_k^2, \end{aligned}$$

where $\gamma_k := \sqrt{\sum_{l \in I(k)} h_l^{-2} \|b_k\|_{L^2(\tau_l)}^2}$. Setting $x_k := v_k \gamma_k$ this gives

$$\sum_{l=0}^{N-1} h_l^{-2} \|v_h\|_{L^2(\tau_l)}^2 \leq c_p \|\mathbf{x}\|_2^2.$$

On the other hand,

$$\begin{aligned} \sum_{k=1}^{N-2} \left[\frac{\langle v_h, q_k \rangle_{L^2(\Gamma)}}{\hat{h}_k \|q_k\|_{L^2(\Gamma)}} \right]^2 &= \sum_{k=1}^{N-2} \left[\sum_{j=1}^{N-2} v_j \frac{\langle b_j, q_k \rangle_{L^2(\Gamma)}}{\hat{h}_k \|q_k\|_{L^2(\Gamma)}} \right]^2 \\ &= \sum_{k=1}^{N-2} \left[\sum_{j=1}^{N-2} x_j \frac{\langle b_j, q_k \rangle_{L^2(\Gamma)}}{\gamma_j \hat{h}_k \|q_k\|_{L^2(\Gamma)}} \right]^2 = \|\mathbf{A}\mathbf{x}\|_2^2, \end{aligned}$$

where \mathbf{A} is a matrix given by

$$A := D_q^{-1} \tilde{G}_h D_\gamma^{-1}, \quad D_q := \text{diag}(\hat{h}_k \|q_k\|_{L^2(\omega_k)}), \quad D_\gamma := \text{diag}(\gamma_k).$$

Let $\bar{G}_h = H^{-1}\tilde{G}_hH$. Define for any $\mathbf{y} \in \mathbb{R}^{N-2}$

$$u_h := \sum_{k=1}^{N-2} h_k y_k b_k \in \mathcal{S}_0^{0,1}(\Gamma_h), \quad \phi_h := \sum_{k=1}^{N-2} h_k^{-1} y_k q_k \in \mathcal{S}^{-1,0}(\hat{\Gamma}_h).$$

Then, using

$$(H_l^{-1}\tilde{G}_lH_l\mathbf{x}_l, \mathbf{x}_l) \geq c_0(D_l\mathbf{x}_l, \mathbf{x}_l) \quad \text{for all } \mathbf{x}_l \in \mathbb{R}^{M_l}, \quad l = 1 \dots N-1, \quad (\text{C.16})$$

which is transposed to (2.23), we derive the following bound:

$$\begin{aligned} (\bar{G}_h\mathbf{y}, \mathbf{y}) &= (H^{-1}\tilde{G}_hH\mathbf{y}, \mathbf{y}) = (\tilde{G}_hH\mathbf{y}, H^{-1}\mathbf{y}) = \langle u_h, \phi_h \rangle_{L^2(\Gamma)} = \sum_{l=1}^{N-1} \langle u_h, \phi_h \rangle_{L^2(\tau_l)} \\ &= \sum_{l=1}^{N-1} (H_l^{-1}\tilde{G}_lH_l\mathbf{y}_l, \mathbf{y}_l) \geq c_0 \sum_{l=1}^{N-1} (D_l\mathbf{y}_l, \mathbf{y}_l) = c_0(D\mathbf{y}, \mathbf{y}). \end{aligned}$$

Now, set $D_h^{1/2} := \text{diag}(\|b_k\|_{L^2(\omega_k)})$. From

$$\begin{aligned} c_0 \left\| D_h^{1/2} \mathbf{y} \right\|_2^2 &= c_0(D\mathbf{y}, \mathbf{y}) \leq (\bar{G}_h\mathbf{y}, \mathbf{y}) = (D_h^{-1/2}\bar{G}_h\mathbf{y}, D_h^{1/2}\mathbf{y}) \\ &\leq \left\| D_h^{-1/2}\bar{G}_h\mathbf{y} \right\|_2 \left\| D_h^{1/2}\mathbf{y} \right\|_2, \end{aligned}$$

we conclude that

$$c_0 \left\| D_h^{1/2} \mathbf{y} \right\|_2 \leq \left\| D_h^{-1/2}\bar{G}_h\mathbf{y} \right\|_2.$$

Taking $\mathbf{z} := D_\gamma\mathbf{y}$, this is equivalent to

$$c_0 \left\| D_h^{1/2} D_\gamma^{-1} \mathbf{z} \right\|_2 \leq \left\| D_h^{-1/2} D_q D_q^{-1} \bar{G}_h D_\gamma^{-1} \mathbf{z} \right\|_2.$$

From (C.4) and (C.5), the definition of \hat{h}_k , and local quasi-uniformity, the ratio of the diagonal entries satisfies

$$\frac{D_h^{1/2}[k, k]}{D_\gamma[k, k]} = \frac{\|b_k\|_{L^2(\Gamma)}}{\sqrt{\sum_{l \in I(k)} h_l^{-2} \|b_k\|_{L^2(\tau_l)}^2}} \geq \hat{c} \hat{h}_k,$$

due to

$$\begin{aligned} \frac{D_h^{1/2}[k, k]}{D_\gamma[k, k]} &= \frac{\sqrt{\frac{h_{k-1}+h_k}{3}}}{\sqrt{h_{k-1}^{-2} \frac{h_{k-1}}{3} + h_k^{-2} \frac{h_k}{3}}} = \frac{\sqrt{\frac{h_{k-1}+h_k}{3}}}{\sqrt{\frac{h_{k-1}+h_k}{3h_k h_{k-1}}}} = \sqrt{h_k h_{k-1}} \\ &\geq \sqrt{\frac{1}{c_L} h_k^2} = \sqrt{\frac{1}{c_L}} h_k \geq c_Q \sqrt{\frac{1}{c_L}} \hat{h}_k, \quad \text{for } k = 1..N-2, \end{aligned}$$

and

$$\frac{D_q[k, k]}{D_h^{1/2}[k, k]} = \frac{\hat{h}_k \|q_k\|_{L^2(\Gamma)}}{\|b_k\|_{L^2(\Gamma)}} \leq c \hat{h}_k.$$

We derive this last result from

$$\begin{aligned} \frac{D_q[k, k]}{D_h^{1/2}[k, k]} &= \frac{\hat{h}_k \|q_k\|_{L^2(\Gamma)}}{\|b_k\|_{L^2(\Gamma)}} = \sqrt{\frac{1}{6}} (h_{k-1} + h_k) = 3\sqrt{\frac{1}{6}} \hat{h}_k, \quad \text{for } k = 2, \dots, N-2, \\ \frac{D_q[k, k]}{D_h^{1/2}[k, k]} &= \frac{\hat{h}_k \|q_k\|_{L^2(\Gamma)}}{\|b_k\|_{L^2(\Gamma)}} \leq \sqrt{\frac{1}{3}} (h_{k-1} + h_k) = 3\sqrt{\frac{1}{3}} \hat{h}_k, \quad \text{for } k = 1, N-2. \end{aligned}$$

Thus, by taking $\mathbf{x} = H\mathbf{z}$

$$c_p \|\mathbf{x}\|_2 = c_p \|H\mathbf{z}\|_2 \leq \|HD_q^{-1} \tilde{G}_h D_\gamma^{-1} \mathbf{z}\|_2 = \left\| HD_q^{-1} H^{-1} \tilde{G}_h H D_\gamma^{-1} H^{-1} \mathbf{x} \right\|_2 = \|A\mathbf{x}\|_2.$$

□

Proof of Proposition (2.2). With the above, we can finally show

$$\begin{aligned}
& \|\tilde{Q}_h u\|_{H^1(\Gamma)}^2 \leq 2 \left\{ \|P_h u\|_{H^1(\Gamma)}^2 + \|(\tilde{Q}_h - P_h)u\|_{H^1(\Gamma)}^2 \right\} \\
\text{(C.13)} \quad & \leq 2 \left\{ c_{p1} \|u\|_{H^1(\Gamma)}^2 + \|(\tilde{Q}_h - P_h)u\|_{H^1(\Gamma)}^2 \right\} \\
& \leq 2 \left\{ c_{p1} \|u\|_{H^1(\Gamma)}^2 + \sum_{l=1}^{N-1} h_l^{-2} \|(\tilde{Q}_h - P_h)u\|_{L^2(\tau_l)}^2 \right\} \\
\text{(Lemma C.1)} \quad & \leq 2 \left\{ c_{p1} \|u\|_{H^1(\Gamma)}^2 + c_{p2} \sum_{k=1}^{N-2} \left[\frac{\langle (\tilde{Q}_h - P_h)u, q_k \rangle_{L^2(\Gamma)}}{\hat{h}_k \|q_k\|_{L^2(\Gamma)}} \right]^2 \right\} \\
& \leq 2 \left\{ c_{p1} \|u\|_{H^1(\Gamma)}^2 + c_{p2} \sum_{k=1}^{N-2} \left[\frac{\langle (\text{Id} - P_h)u, q_k \rangle_{L^2(\omega_k)}}{\hat{h}_k \|q_k\|_{L^2(\Gamma)}} \right]^2 \right\} \\
& \leq 2 \left\{ c_{p1} \|u\|_{H^1(\Gamma)}^2 + c_{p2} \sum_{k=1}^{N-2} \hat{h}_k^{-2} \|(\text{Id} - P_h)u\|_{L^2(\omega_k)}^2 \right\} \\
\text{(C.14)} \quad & \leq \tilde{c}_{st} \|u\|_{H^1(\Gamma)}^2. \tag{C.17}
\end{aligned}$$

References

- Andriulli, F., Cools, K., Bagci, H., Olyslager, F., Buffa, A., Christiansen, S., et al. (2008). A multiplicative Calderon preconditioner for the electric field integral equation. *IEEE Trans. Antennas and Propagation*, 56(8), 2398-2412.
- Bagci, H., Andriulli, F., Cools, K., Olyslager, F., & Michielssen, E. (2009, oct.). A Calderón multiplicative preconditioner for the combined field integral equation. *Antennas and Propagation, IEEE Transactions on*, 57(10), 3387 -3392.
- Bramble, J. H., Pasciak, J. E., & Steinbach, O. (2002). On the stability of the l_2 projection in h_1 (). *Math. Comp.*, 71(237), 147–156.
- Bruno, O. P., & Lintner, S. K. (2012, December). Second-kind integral solvers for TE and TM problems of diffraction by open arcs. *Radio Science*, 47, 6006.
- Buffa, A., & Christiansen, S. (2007). A dual finite element complex on the barycentric refinement. *Math. Comp.*, 76(260), 1743-1769.
- Cools, K., Andriulli, F., & Olyslager, F. (2009, Sept.). A Calderón preconditioned PMCHWT equation. In *Proceedings of the international conference on electromagnetics in advanced applications, 2009, torino, italy. iceaa '09*. (p. 521 -524).
- Costabel, M., & Dauge, M. (2002). Crack singularities for general elliptic systems. *Mathematische Nachrichten*, 235(1), 29–49.
- Costabel, M., Dauge, M., & Duduchava, R. (2003). Asymptotics without logarithmic terms for crack problems. *Communications in Partial Differential Equations*, 28(5-6), 869-926. Available from <http://www.tandfonline.com/doi/abs/10.1081/PDE-120021180>

- Ervin, V. J., & Stephan, E. P. (1990). A boundary element Galerkin method for a hypersingular integral equation on open surfaces. *Math. Methods Appl. Sci.*, 13(4), 281–289. Available from <http://dx.doi.org/10.1002/mma.1670130402>
- Gross, D., & Seelig, T. (2011). *Fracture mechanics with an introduction to micromechanics* (2nd ed.). Springer.
- Hiptmair, R. (2006). Operator preconditioning. *Computers and Mathematics with Applications*, 52(5), 699-706.
- Hsiao, G. C., & Wendland, W. L. (2008). *Boundary integral equations* (Vol. 164). Berlin: Springer-Verlag. Available from <http://dx.doi.org/10.1007/978-3-540-68545-6>
- Jerez-Hanckes, C., & Nédélec, J. (2012). Explicit variational forms for the inverses of integral logarithmic operators over an interval. *SIAM Journal on Mathematical Analysis*, 44(4), 2666-2694. Available from <http://epubs.siam.org/doi/abs/10.1137/100806771>
- Jerez-Hanckes, C., & Nédélec, J.-C. (2011). Variational forms for the inverses of integral logarithmic operators over an interval. *C. R. Math. Acad. Sci. Paris*, 349(9-10), 547–552. Available from <http://dx.doi.org/10.1016/j.crma.2011.01.016>
- Kelley, C. T. (1999). *Iterative methods for optimization* (Vol. 18). Philadelphia, PA: Society for Industrial and Applied Mathematics (SIAM). Available from <http://dx.doi.org/10.1137/1.9781611970920>
- Lintner, S., & Bruno, O. (2012, April). *A generalized calderon formula for open-arc diffraction problems: theoretical considerations* (Preprint No. arXiv:1204.3699 [math.AP]). arXiv.

- Lions, J., & Magenes, F. (1972). *Nonhomogeneous boundary value problems and applications*. Springer-Verlag, Berlin.
- Mardal, K.-A., & Winther, R. (2011). Preconditioning discretizations of systems of partial differential equations. *Num. Lin. Alg. Appl.*, 18(1), 1-40.
- McLean, W. (2000). *Strongly elliptic systems and boundary integral equations*. Cambridge, UK: Cambridge University Press.
- McLean, W., & Steinbach, O. (1999). Boundary element preconditioners for a hyper-singular integral equations on an interval. *Adv. Comp. Math.*, 11(4), 271–286.
- Meixner, J. (1972). The behavior of electromagnetic fields at edges. *IEEE Trans. Antennas and Propagation*, AP-20(4), 442-444.
- Moiseiwitsch, B. L. (1977). *Integral equations*. London: Longman. (Longman Mathematical Texts)
- Nicaise, S., & Sändig, A.-M. (1994a). General interface problems I. *Mathematical Methods in Applied Sciences*, 17(6), 395–429.
- Nicaise, S., & Sändig, A.-M. (1994b). General interface problems II. *Mathematical Methods in Applied Sciences*, 17(6), 431–450.
- Sauter, S., & Schwab, C. (2010). *Boundary element methods* (Vol. 39). Heidelberg: Springer.
- Shestopalov, Y., Smirnov, Y., & Chernokozhin, E. (2000). *Logarithmic integral equations in electromagnetics*. Berlin, Boston: De Gruyter.
- Steinbach, O. (2001). On the stability of the L_2 projection in fractional Sobolev spaces. *Numer. Math.*, 88(2), 367–379. Available from <http://dx.doi.org/10.1007/PL00005449>

- Steinbach, O. (2002). On a generalized L_2 projection and some related stability estimates in Sobolev spaces. *Numer. Math.*, 90(4), 775–786. Available from <http://dx.doi.org/10.1007/s002110100329>
- Steinbach, O. (2003). *Stability estimates for hybrid coupled domain decomposition methods* (Vol. 1809). Berlin: Springer-Verlag. Available from <http://dx.doi.org/10.1007/b80164>
- Steinbach, O. (2008). *Numerical approximation methods for elliptic boundary value problems: Finite and boundary elements*. New York: Springer. Available from <http://dx.doi.org/10.1007/978-0-387-68805-3> (Finite and boundary elements, Translated from the 2003 German original)
- Steinbach, O., & Wendland, W. (1998). The construction of some efficient preconditioners in the boundary element method. *Adv. Comput. Math*, 9, 191–216.
- Stephan, E. (1987). Boundary integral equations for screen problems in \mathbb{R}^3 . *Integral Equations and Operator Theory*, 10(2), 236–257.
- Stephan, E. P., & Wendland, W. L. (1984). An augmented Galerkin procedure for the boundary integral method applied to two-dimensional screen and crack problems. *Applicable Anal.*, 18(3), 183–219. Available from <http://dx.doi.org/10.1080/00036818408839520>
- Tran, T. (1995). The K -operator and the Galerkin method for strongly elliptic equations on smooth curves: local estimates. *Math. Comp.*, 64(210), 501–513. Available from <http://dx.doi.org/10.2307/2153436>
- Wendland, W. L., & Stephan, E. P. (1990). A hypersingular boundary integral method for two-dimensional screen and crack problems. *Arch. Rational Mech. Anal.*, 112(4), 363–390. Available from <http://dx.doi.org/10.1007/BF02384079>